CRANFIELD UNIVERSITY

YONGLIANG DU

DEVELOPMENT OF REAL-TIME FLIGHT CONTROL SYSTEM FOR LOW-COST VEHICLE

SCHOOL OF ENGINEERING

MSc by Research Thesis

January 2011

Cranfield University

School of Engineering

MSc by Research Thesis

Academic Year 2010 - 2011

YONGLIANG DU

DEVELOPMENT OF REAL-TIME FLIGHT CONTROL SYSTEM FOR LOW-COST VEHICLE

Supervisor: HUAMIN JIA

January 2011

ABSTRACT

In recent years, more and more light aircraft enter our daily life, from Agricultural applications, emergency rescue, flight experiment and training to Barriers to entry, light aircraft always have their own advantages. Thus, they have become more and more popular.

However, in the process of GDP research about Flight Control System design for the Flying Crane, the author read a lot of literature about Flight Control System design, then noticed that the research in Flight Control System have apparently neglected to Low-cost vehicles. So it is necessary to do some study about Flight Control System for this kind of airplane. The study will more concern the control law design for ultra-light aircraft, the author hopes that with an ‘intelligence’ Flight Control System design, this kind of aircraft could sometimes perform flying tasks according to a prearranged flight path and without a pilot.

As the Piper J-3 cub is very popular and the airframe data can be obtained more easily, it was selected as an objective aircraft for the control law design. Finally, a ¼ scale Piper J-3 cub model is selected and the aerodynamics coefficients are calculated by DATCOM and AVL. Based on the forces and moments acting on the aircraft, the trim equilibrium was calculated for getting proper dynamics coefficients for the selected flight conditions. With the aircraft aerodynamics coefficients, the aircraft dynamics characteristics and flying qualities are also analyzed. The model studied in this thesis cannot answer level one flying qualities in the longitudinal axis, which is required by MIL-F-8785C. The stability augment system is designed to improve the flying qualities of the longitudinal axis.

The work for autopilot design in this thesis includes five parts. First, the whole flight profile is designed to automatically control aircraft from takeoff to landing. Second, takeoff performance and guidance law is studied. Then, landing performance and trajectory is also investigated. After that, the control law

design is decoupled into longitudinal axis and later-directional axis. Finally, simulation is executed to check the performance for the auto-controller.

Keywords:

Classical control, modern control, Root locus, ultra-light aircraft, autopilot, takeoff, landing, Pole placement, PID, flight simulation

ACKNOWLEDGEMENTS

Sincere thanks to my supervisor Dr. Huamin Jia for his devoted instruction not only in the group design project (GDP) but especially in the individual research project (IRP). With his encouragement and urging I have made one after another progress. My gratitude also gives to all the staff of the department of Aerospace Vehicle Design at Cranfield University, they gave a lot of help in GDP and some of the courses they teach really helped me a lot, like Flight Dynamics.

I am also particularly grateful to my classmates for each other's support and encouragement, with a great teamwork, flight simulation became an exciting moment of GDP final presentation.

I cannot forget to express appreciation to all the staff who work in library, just because their rich patience and enthusiasm make library became a good place.

Thanks Mike for much help when I live in this strange country, and many people in this nation are quite warm hearted. So, my feelings of this country are increasing each day.

Acknowledge AVIC and FAI for giving me the opportunity of studying in the UK.

Without the support of my family, study life would become tougher or even having the opportunity would become impossible. I owe my parents a lot for their help and my wife by looking after my daughter nearly all the time and without any complaint. My grateful heart goes to my wife for her continued support and the close family relationships she has constructed.

Love is great!

TABLE OF CONTENTS

LIST OF FIGURES

LIST OF TABLES

NOMENCLATURE

Of the considerable number of notations are used in this thesis, some have more than one significance. In general, the meaning is explicit in the using context.

A	Coefficient matrix
B	driving matrix
b	wingspan
b_a	Aileron span
b_e	Elevator span
b_h	Horizontal tail span
b_r	Rudder span
b_v	Vertical tail span
C	Output matrix
CAP	Control anticipation parameter
$C_{l\beta}$	rolling-moment derivative coefficient with respect to sideslip angle
C_m	Pitch moment derivative coefficient
$C_{m\alpha}$	pitching-moment derivative coefficient with respect to alpha
cg	Center of gravity
$\bar{c}$	Mean aerodynamic chord
$\bar{c}_a$	Aileron chord

$\bar{c}_e$	Elevator chord
$\bar{c}_h$	Horizontal tail chord
$\bar{c}_r$	Rudder chord
$\bar{c}_v$	Vertical tail chord
D	Direct matrix
FCS	Flight control system
h	Altitude
I_x	Moment of inertia in roll
I_y	Moment of inertia in pitch
I_z	Moment of inertia in yaw
K	Gain
m	Mass of aircraft
n_α	aircraft acceleration sensitivity
p	roll rate
q	pitch rate
r	yaw rate
s	Laplace operator
STOL	Short take-off and landing
u	velocity in body axis x-direction
u	Control vector

X_h	Longitudinal location of theoretical horizontal tail apex
X_w	Longitudinal location of theoretical wing apex
X_v	Longitudinal location of theoretical vertical tail apex
x	input vector
x_{cg}	X position of centre of gravity
y	Output vector
y_{cg}	Y position of centre of gravity
z_{cg}	Z position of centre of gravity

Greek letter

α	Angle of attack
α_e	Angle of attack for trim condition
β	Sideslip angle
γ	Flight path angle
Γ	Wing dihedral angle
δ_a	Aileron deflection angle
δ_e	Elevator deflection angle
δ_r	Rudder deflection angle
ζ_{sp}	Short period damping ratio
ζ_p	Phugoid damping ratio

τ	Engine thrust
ϕ	Roll angle
ψ	Yaw angle
ω_d	Dutch roll undamped natural frequency
ω_p	Phugoid undamped natural frequency
ω_{sp}	Short period pitching oscillation undamped natural frequency
Δ	Increment

1 INTRODUCTION

1.1 Background

A kind of Low-Cost aircraft was developed from the 1970s, which generally is less than 150kg. According to MIL-F-8785C, they belong with Class I aircraft because they have light weight, so they are also called ultralight aircraft. There are some advantages of this kind of airplane, including: Low operating cost, Short take-off and landing (STOL), Good performance at Low-altitude and low-speed, Maintenance friendly.

Because of their strong points, they are popular in agriculture applications; aerial photography and news reporting; geological exploration; aerial surveys; Communication and emergency transportation; Sports flights; Air tours; Traffic control; Anti smuggling operations.

1) Agriculture applications

   For example, China, a big agriculture country has about 1.45 billion Chinese acres (0.1646 acre) of arable land, 4.79 billion Chinese acres of grassland, 1.73 billion Chinese acres of forest, 1.29 billion Chinese acres of barren mountains, and 18000km coastline. In such an expansive source field, there is a need for the support of general aviation. Currently, the areas using aircraft to work in agriculture only take account of 0.6% in China, but up to 70% in the USA. The only reason for agricultural aviation lagging behind is because the Low-Cost Vehicle is not popular. So the ultra light aircraft has a widely developing place in agriculture.

2) Aerial photography & news reports

   Compared with other airplanes or helicopters, they have three obvious advantages in this field. Low cost: roughly about 20% of other aircraft; High quality: ultra light aircraft have a good performance at low altitude and at low speed and have a small turn radius. They are highly manoeuvrable; they can be convenient for landing and takeoff without the support of an airport. So

they can be very adaptable in work, can landing and take-off according to people’s demands, and cooperate with the process of photography.

3) Geological exploration

Using ultra light aircraft with low altitude and low speed characteristics, for underground exploration is like the reconnaissance of a human being on the spot, but the efficiency is very high.

4) Aerial surveys

In many civil economic departments, in order to maintain safety conditions, there is a need to carry out long distance patrols or checks. For example, forestry prevention and cure of plant diseases and insect pests, checking fire situations, water and soil conservation, high pressure oil transport pipework and coastal population inspection, etc.

5) Communication and emergency transportation

In hinterland areas and traffic inconvenience belts, ultra light aircraft can take on little emergency transport tasks. Between many islands in the world, people already use light aircraft to maintain contact.

6) Sports flight

Flying is a dream for many, but in the past relatively few people have this privilege, the light aircraft will make it become possible to ordinary people.

7) Air tour

Many mountainous regions, have a great deal of interesting and beautiful scenery, Visitors in the air can see this human heritage, a gift of nature. It must be fun enough to arouse people's imagination to create new enthusiasm.

8) Traffic control

There are many police agencies flying ultra-light aircraft patrols, especially in the provinces to view traffic conditions and inform road drivers with a traffic information service, check for irregularities, and render first aid. The cost and benefits are even better than the using of highway patrol police car.

9) Anti smuggling

The United States used to use ultra-light aircraft to monitor the vessels over the water, and cooperate with patrol boats to prevent smuggling. If necessary, they would direct descent near the water surface and to get intervention.

With bright market prospects, the study and design of a low-cost flight control system for this kind of aircraft is necessary and timely.

1.2 Research objectives

The thesis makes an attempt to design Flight Control System (FCS) for ultra-light aircraft, and the work focuses on a typical aircraft and meets the following objectives:

- Obtain the airplane aerodynamics coefficients and check the aircraft stability
- Design a Stability Augmentation System (SAS) if the aircraft cannot meet the level one flying qualities requirements
- Study and design a representative flight profile and design control law to implement automatic control during the whole flight phases
- Simulate the aircraft performance with the designed control law

In order to achieve the above objectives, the research should be based on a certain aircraft. For there is no available light-aircraft aerodynamics data, and to get a certain aircraft geometry is also difficult. In [17], David Jensen analyzed a ¼ scale Piper J-3 Cub aerodynamics based on the aircraft geometry and inertial

data, and then designed the control law. For the detailed geometry and inertial data, the ¼ scale Piper J-3 Cub model is also selected in this thesis for the control law study reason. It is a high-wing monoplane with two tandem seats, which was generally produced in the 1940s and the number of piper J-3 Cub exceeded 20,000 until 1947. During the Second World War, it was mainly used in air detection and as a travel tool to carry senior generals. By far, it's simple design and safety quality made it famous. Almost in every place of the world, people can always find the trace of the Piper J-3 cub. So it is selected to do the research work. The flight control surfaces of the Piper J-3 cub are elevator, aileron and rudder, which will be used to control the aircraft in the later chapters. Figure 1-1 shows a picture of the Piper J-3 Cub in 2007 Camarillo Air show.

Figure 1-1 Piper J-3 Cub in 2007 Camarillo Air show [1]

1.3 Arrangement

The contents of this thesis are arranged as follows: Chapter 2 reviews some research in FCS design, and then gives the methodology which will be used in this thesis. In Chapter 3, two estimated methods are used to calculate the aircraft dynamics of a ¼ scales Piper J-3 cub model. The flying qualities of model are analyzed in Chapter 4 based on the requirements of MIL-F-8785C and MIL-HDBK-1797. The analysis results show that the flying qualities of the

longitudinal axis cannot meet the level one requirements, so in order to guarantee the aircraft has level one flying qualities in longitudinal axis, a Stability Augmentation System (SAS) is designed in Chapter 5. Next the autopilot design for longitudinal axis and lateral-directional axis is studied in Chapters 6 and 7. The flight simulation is described in Chapter 8. Finally, in Chapter 9 a conclusion of the work is discussed and some suggestions are given to future work.

2 LITERATURE REVIEW

2.1 Acquiring Aircraft's aerodynamics characteristics

There are several methods which can be used to acquire the aerodynamics characteristics of an aircraft. Directly measure the forces and moments of aerodynamics which act on the aircraft is thought to be one of the most accurate techniques. This method needs to build a prototype of the aircraft and flying it, so it is very expensive. Another well known method is wind tunnel, which needs a wind tunnel model and operating a wind tunnel also costs a lot of money. But both of them are an essential part of vehicle design. In order to minimize cost, some prediction methods were always used before flight testing and wind tunnel testing methods. The prediction methods can give concept of the induced performance of aircraft geometry which can satisfy requirements or not, and in this way the number of iteration of running wind tunnel can be reduced, thus reduce the spending.

Several programs exist for predication methods, and can be directly obtained from the internet for free, and the aircraft aerodynamics coefficients and control derivatives can be quickly acquired with them. DATCOM, which was developed by the U.S. Air Force, and AVL, which was developed by Dr Drela and his students of Massachusetts Institute of Technology, are better known software for analytical methods. In [2], the author analyzed a Light-weight aircraft longitudinal aerodynamics coefficient with DATCOM, and then designed an altitude hold control law to analyze the aircraft performance. In [3], the AVL method was used to get aerodynamics coefficients and then that data was used to design control law.

In conclusion, although predicated methods are not as accurate as wind tunnel and flight testing, it is a very convenient and efficient way to be used to obtain the approximate aircraft characteristics. At the same time, without any cost. So it is always used in aircraft concept design and preliminary design to reduce the expensive and time consuming wind tunnel cost. Because of the advantages of these methods, they are also very popular in the research field.

2.2 Control law design

Over the past three decades, many methodologies have been developed to design Flight Control laws. Some of them are reviewed in this part are according to the division of classical control and modern design theories.

a) Classical control methods:

By far, many aircraft FCS were designed by using classical frequency domain or root locus method. These techniques are simple and practical, with a transparent design processes, engineers can clearly see the performance of the system dynamics and how they are modified. Furthermore, most of the existing flying qualities requirements are based on classical control theory, so design consignments are sufficient, designers based on their own experiences, through the use of multi-mode control law and gain scheduling techniques, a flight control system with satisfactory performance can be achieved easily.

Of the classical control methods, only the Root Locus Method is mentioned here, for the root locus way has the most advantage methods in classical control design. Root Locus Method is a graphical technique to analyze linear and time-invariant systems. It depicts when a certain parameter changes from 0 to infinity, how the root trajectories of characteristic equation changes. The necessary term for the closed-loop system is stable which are all poles of the plant must locate in the left half of complex plane. The bigger distance the poles from the imaginary axis, the more stable the system. Thus, the system performance can be improved by adjusting the poles position. In [4], the inner loop of roll autopilot is designed in root locus way, PID algorithms is employed for outer loop design. In [5], because only by selecting a proper close-loop gain cannot adjust all the poles to idea region, in order to achieve this objective, the author designed a lead compensator by using root locus method.

Classical control techniques like root locus are excellent at single input single output (SISO) system design. However, with more complex performance requirements of a control system, using classical control methods to design the control law becomes very difficult, slow and even unattainable. The main reason

is: the classical methods are difficult to handle and coordinate multi-input and multi-output (MIMO) system characteristics. Therefore, design methods to handle a complex flight control system are needed.

b) Modern control methods

For the limitation of classical control design, the designs based on state-variable model techniques of modern control theory have made great progress.

Pole Placement/Eigenvector Assignment: System performances are decided by the poles locations and eigenvectors. Pole placement approach is a method by using signal feedback to change the poles position of the plant. Root locus gives an easy way to assign the pole location of single input single output (SISO) system, but to multi input multi output (MIMO) systems root locus way has many difficulties. Fortunately, a modern design of pole placement technique for MIMO systems has been described in the literatures. In [6], an ideal close-loop characteristic equation is achieved by a full state feedback pole placement method. In [7], the author introduced the eigenstructure assignment technique and gives an example of it using the L-1011 aircraft lateral axis to control law design.

Linear Quadratic Regulator: The full name of LQR is Linear Quadratic Regulator. Its object is linear system which gives out in state space format, but target function is quadratic function of the object state and control input. LQR optimum design means that the designed feedback K should make quadratic object function J minimized. However, the value of K is only decided by Q and R, so the selection of Q and R is especially important. LQR theory is the earliest developed and the most mature state-space design method in modern control theory. In [8], LQR method is used to assure the aircraft stability. In [9], the author used Dynamic Inversion (DI) for inner-loop plus LQR for outer-loop control strategy in longitudinal control, the inner loop and the outer loop account for the system dynamic changes with flying conditions and achieving the designed flying qualities respectively. However, when used in flight control law design, there are still many practical problems, some of these issues have been resolved, such as varying state feedback to the output feedback, thus making

the feedback variables become some of the measured state variables of aircraft. But, there are still some problems difficult to solve, for example, the problems of how to transfer flight control system performance requirements into performance index of design. What is the principle of selecting weighting coefficients, robustness and other issues.

H_∞ Mixed Sensitivity: Many control problems can be attributed to the H_∞ norm problem. In the actual control system, disturbance and control objective uncertainty always exist simultaneously. Suppressing disturbance and control object uncertainty is called the mixed sensitivity H_∞ control problem.

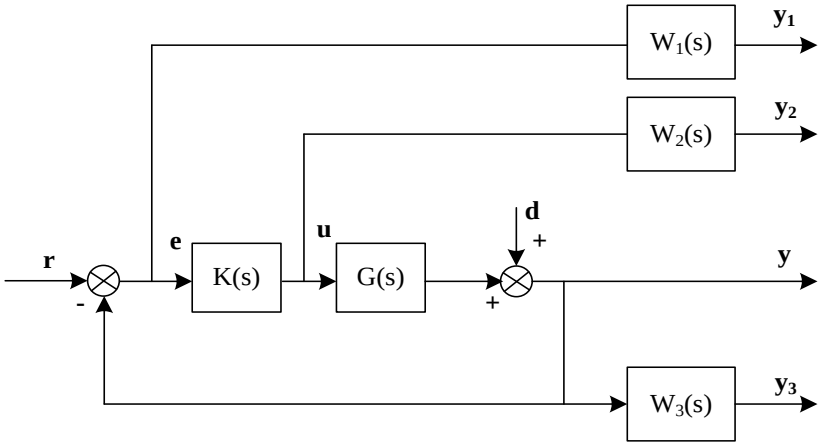

Figure 2-1 Structure of mixed sensitivity problem

As shown in Figure 2-1, G(s) is the control object, which is selected with weighting function (W1(s), W2(s) and W3(s)); K(s) is controller; y is system output signal; u is control input; r is reference input; e is tracking error; d is the disturbance input; y1, y2 and y3 are evaluate signals for weighting augmented system.

The close-loop transfer functions from r to y, u and e, respectively, are

$$T = GK(1 + GK) = 1 - S \quad \textbf{(2-1)}$$

$$R = K(I + GK) = 1 - S \quad \textbf{(2-2)}$$

$$S = (I + GK)^{-1} \quad \textbf{(2-3)}$$

Where: S is the sensitivity function; R for the input sensitivity function; T for the complementary sensitivity function.

Mixed sensitivity optimization problem is to seek the controller K, which improves the stability of the close-loop system, and meets the requirements of the norm that is

$$\min\|\Phi\|_\infty = \left\| \begin{matrix} W_1 S \\ W_2 R \\ W_3 T \end{matrix} \right\|_\infty \quad \textbf{(2-4)}$$

(2-4) is called H_∞ optimization problem. If $\|\Phi\|_\infty<1$, is called the H_∞ standard problem. $\|S\|_\infty$ is the measurement for system tracking and disturbance suppression ability; $\|R\|_\infty$ is the measurement of permit of perturbation amplitude for the additive perturbation of a system, and also the constraints on the controller output; $\|T\|_\infty$ is the measurement for multiplicative perturbation of the system which allows the size of perturbation amplitude. The corresponding weighting function for performance is W1(s), the function for controller output amplitude limitation is W2(s), and the robust weighting function is W3(s).

Mixed sensitivity method is one of the most useful design methods in optimal control area, but it is not easy to solve problems like multi-variable mutual coupling, and also may cause undesirable zero-pole cancellation between the H_∞ controller and system model.

H_∞ Loop Shaping: Loop shaping design idea is to construct a loop transfer function to meet the close loop system performance requirements. Generally, system low-frequency and high-frequency characteristics can be directly assigned according to performance requirements and bandwidth. Specifically, it is to make systems have the required characteristics by adding series compensation. For MIMO systems, the transfer function matrices multiplication has two divisions: left-handed and right-handed. Therefore, the compensation part of series compensation are also divided into anterior (W1) and posterior (W2), the compensated object is called the shaped object (Gs),

$$K = W_1 K_\infty W_2 \quad \textbf{(2-5)}$$

To ensure the stability of shaping design, at first H_∞ is used to design for Gs, which produces a K_∞ controller. K_∞ with the compensation of Gs together make up the final controller

$$Gs = W_2 G W_1 \quad \textbf{(2-6)}$$

The shape design is called H_∞ loop shaping design, which could generate none pole-zero cancellations between the controller and system model and relax the restrictions on the number of right-half plane poles. Moreover, H_∞ loop shaping design succeeds to classical loop shaping notions and modern control concepts.

μ-Synthesis: In order to overcome the conservative caused by H_∞ robust control small gain theorem, Doyle first proposed the 'structure singular value' concept, which has gradually become an important way in modern robust control theory, i.e. μ-synthesis method. Structure singular value μ-synthesis analysis of the structure dynamic caused the robust stability. A more important aspect is that stability and performance can be involved, thereby reducing the robust control system design conservative. But using this method, the designer should know structured uncertainly very well, the optimum solution requires iterative repetition. Using this method always produces a high-order controller than using H∞ optimum control way.

2.3 FCS architecture and software design

FCS architecture: Boeing and Airbus are all quite successful in Flight Control System design, but the system hardware they developed is fairly complex and expensive, so to minimise the FCS hardware cost, another methods should be found. References [10][11][12][13][14] come up with distributed ideas to FCS architecture, by introducing 'intelligent' sensors and actuators, the workload of centre the Flight Control Computers (FCCs), which are always the bottleneck for the traditional FCS, are reduced and thus simplified. The centralized risk can be dispersed and minimised by designing a distributed structure suitably.

The challenge of designing FCS for a low cost vehicle is in the process of reducing costs, adequate reliability must be maintained. Using the idea of

‘Centralized management, decentralized control’ of a distributed control system in industry for reference, distributed flight control system architecture is suggested in this thesis for the low cost aircraft.

FCS software: The software of control law in [15] accounts for 47% of the whole software, which means except for the software of the control law other software also should be designed, such as Executive software, software for fault detection and isolation, etc. also should be developed. In [16], the author gives an overview of the C-17 FCS software and also illustrates that the control law software is only one part of the FCS software. Summarised from many individual references, FCS software architecture is shown in figure 2-2, which is divided into three categories: operational software, application software and BIT software.

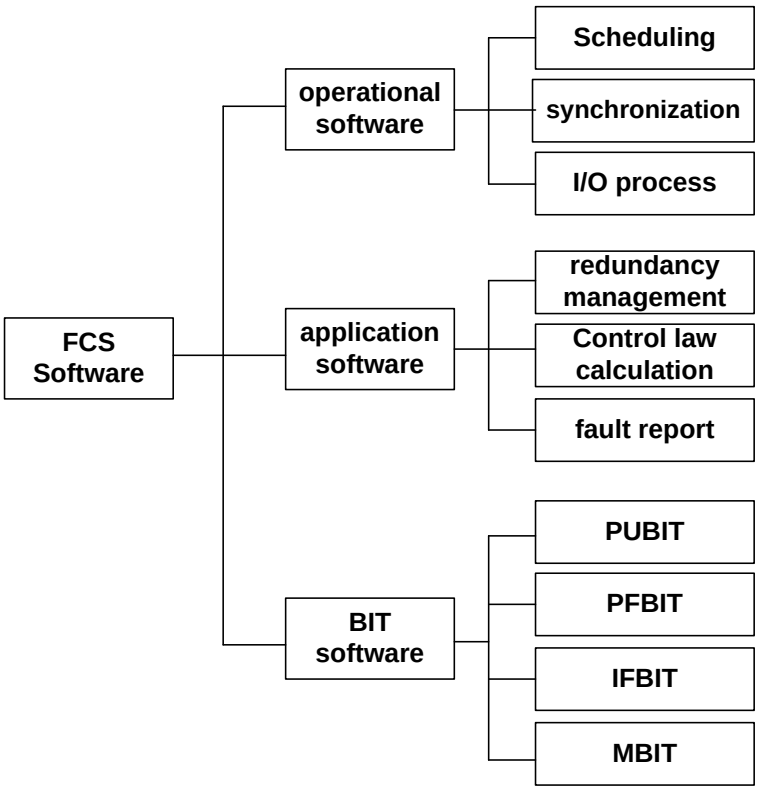

Figure 2-2 FCS architecture software construction

2.4 Methodology selection

This thesis assumes FCS hardware and other software has been done already, and only focuses on flight control law design, for it is the most important part of FCS. As there is no available light-aircraft aerodynamics data at hand, the DATCOM and AVL are selected to estimate the aerodynamic coefficients for a selected Piper J-3 Cub model. To control law design, it is hard to say which method is the best one. Pole placement method is easy to correspondence to flying qualities requirements, so it was selected for stability augmentation system design. For PID controller has simple structure, stable performance and high reliability, so it is selected for autopilot design.

3 AIRCRAFT AERODYNAMICS

3.1 Introduction

Each aircraft has specifically dynamics characteristics which are dependent on its geometric configuration and wing airfoil. Again, the system coefficients matrix A and driving matrix B are determined by the dynamics characteristics. It is difficult to get enough authoritative aerodynamics data of any one aircraft to support this study, thus the aerodynamics coefficients and control derivatives are calculated from attainable software which is based on a target aircraft model: the Piper J-3 cub. The main parameters of the Piper J-3 Cub model come from [17], which are given in table 3-1.

Table 3-1 Specifications of the Piper J-3 Cub aircraft model

Parameters	Value	Parameters	Value
$\mathbf{X_w}$	0.33m	$\mathbf{b_v}$	0.10m
$\bar{\mathbf{c}}$	0.3491m	$\bar{\mathbf{c}}_\mathbf{v}$	0.30m
$\mathbf{b}$	2.34m	$\mathbf{b_r}$	0.10m
$\mathbf{b_a}$	0.61m	$\bar{\mathbf{c}}_\mathbf{r}$	0.27m
$\bar{\mathbf{c}}_\mathbf{a}$	0.07m	$\mathbf{m}$	7.62kg
$\mathbf{X_h}$	1.47m	$\mathbf{I_x}$	0.5528 $\mathrm{kg.m^2}$
$\mathbf{b_h}$	0.7m	$\mathbf{I_y}$	0.6335 $\mathrm{kg.m^2}$
$\bar{\mathbf{c}}_\mathbf{h}$	0.28m	$\mathbf{I_z}$	1.0783 $\mathrm{kg.m^2}$
$\mathbf{b_e}$	0.7m	$\mathbf{x_{cg}}$	0.46m
$\bar{\mathbf{c}}_\mathbf{e}$	0.11m	$\mathbf{y_{cg}}$	0.0m
$\mathbf{X_v}$	1.47m	$\mathbf{z_{cg}}$	-0.18m

3.2 ASCC estimation

Therefore, based on the geometry data, the aerodynamics stability and control coefficients (ASCC) of a special Piper J-3 Cub model was estimated by two programs, AVL and DATCOM, in the following parts. DATCOM and AVL are better known software for analytical methods. AVL as a main tool to obtain

aerodynamics in this thesis and DATCOM as a complement only be used to estimate dynamics derivatives which cannot be estimated by AVL. Except for those data listed in table 3-1, the wing shape is also crucial in determining the aircraft aerodynamics characteristics. According to [17], NACA 2314 type airfoil is selected to the main wing of the aircraft and NACA 0002 is selected for the empennage. Ultra-light aircraft flight envelops is small, it is only used at low height range, so only sea level altitude is selected to get aerodynamics derivatives and control coefficients of the Piper J-3 Cub model.

AVL analysis: Athena Vortex Lattice (AVL) was developed by Dr. Drela and his students of Massachusetts Institute of Technology. It can be used to analyze the aerodynamics stability and control characteristics of subsonic aircraft.

The aircraft geometry and inertial data should be depicted in three type files in the AVL program, i.e. Geometry Input File, Mass input File and Run-Case File. The Geometry input file describes the vortex lattice geometry and aerodynamics section properties. Mass input file contain the mass and inertia properties of the configuration. It also defines units to be used to run case setup. These units may want to be different from those used to define the geometry. The analysis flight conditions are defined in the Run-Case File. The coordinate system used in these files is X downstream, Y out the right-wing and Z up. The Geometry input file of the Piper J-3 Cub model is given in Appendix A.

With the input files, the analyzed results can be obtained by running the AVL program. The most important input files to generate the output files are Geometry Input File and Run-Case File. With these files, aerodynamics output and trim condition can be calculated, and it can also be used to output the aircraft geometry model. The trim condition mentioned here is different from the trim condition to be introduced later, for the AVL program only can calculate the moments balance. The trim in the later section is means aircraft in forces and moments balance.

The modelled aircraft in AVL is presented in Figure 3-1.

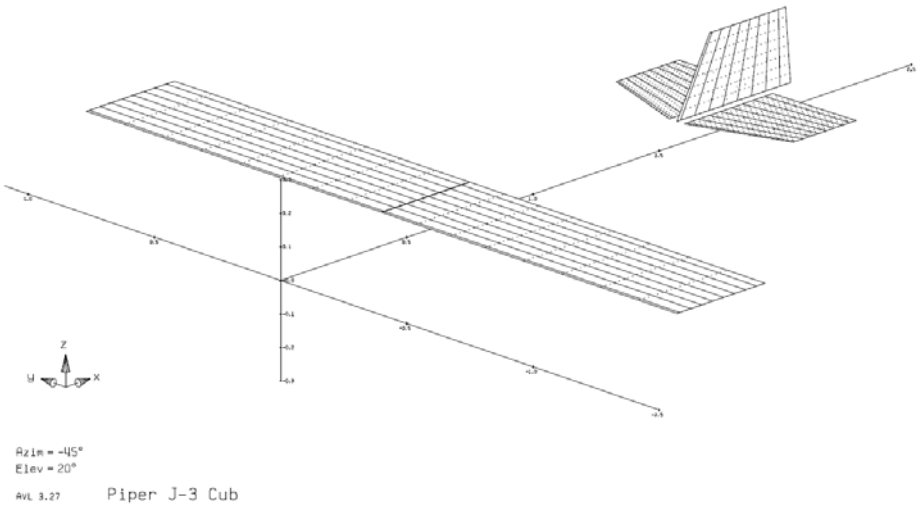

Figure 3-1 Geometry model calculated by AVL

Aerodynamics coefficients and control derivatives can also be obtained by running the input files in AVL. In order to use the software to produce the linearized coefficients, specific flight conditions should be set beforehand. Operating points like Cruise, Climb and Descent are specified in this thesis, and the obtained coefficients are given in Appendix B according to different velocities.

DATCOM methods: DATCOM is developed by the U.S. Air Force, adopting a component combination method with modularity ideas, etc. The estimation method it uses is a theory, semi-empirical and Empirical mixed way. It can provide the recipient accurate degree data to different flight conditions to various airplanes. The DATCOM input file includes four parts, which defines flight conditions and geometric characteristics about wings, fuselage, horizontal and vertical stabilizer, aileron, elevator, flap and slat, etc.[18]. Therefore, in order to create an input file to DATCOM, aircraft geometry should be acquired first. Once the input file has been created, then it can be run in DATCOM to get the output files. The output files contain a 3D geometry model, estimated stability and control coefficients and derivatives for the appointed airplane geometry and flight conditions. It shows that in the process of the programming that if the aircraft main body data was not defined in the input file, it means if only wing plus empennage configuration were specified, the DATCOM would

not calculate the dynamics derivatives. So the aircraft body data has to be defined in the DATCOM input file which was obtained by estimation based on the picture from some websites. Figure 3-2 gives the 3-D model described by the input file.

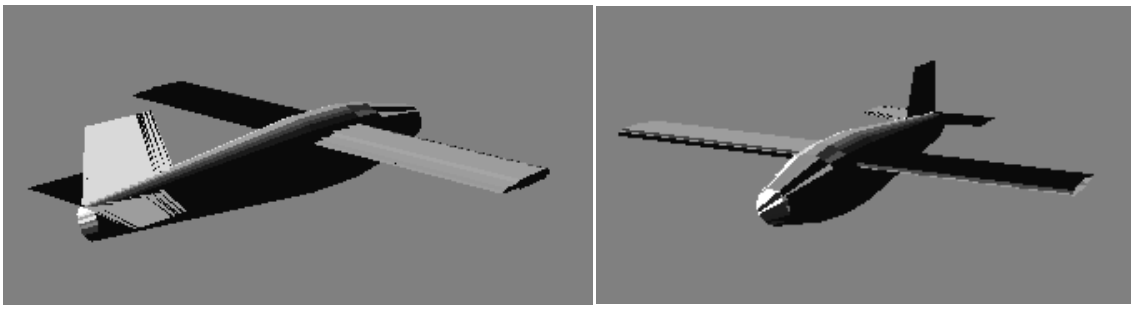

Figure 3-2 Geometry model calculated by DATCOM

3.3 Trim

The trim condition here means the aircraft is in steady flight, which is also simply shorthand for saying that it is in rotational equilibrium and the forces balance. It is obvious that in trim condition the aircraft speed and altitude are constants. Steady flight is studied in this thesis including horizontal flight, climbing flight and descending flight, to simplify the aircraft in individual cruise, take off and landing phases. The main difference among these phases is flight path angle.

Because an aeroplane is symmetric, the forces and moments for lateral-direction are supposed to keep in balance throughout, and then the equilibrium problem is confined to the longitudinal balance only.

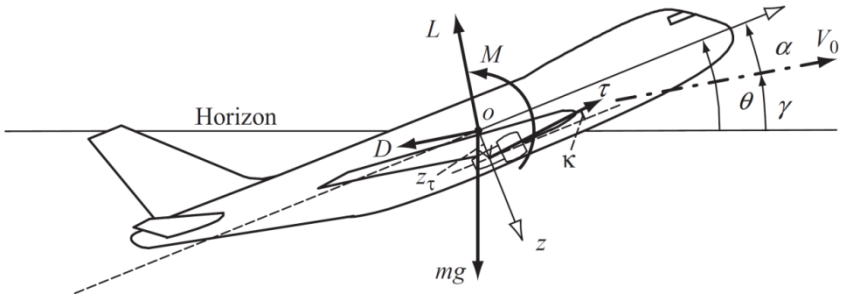

Figure 3-3 Sketch map of plane longitudinal moments and forces

As can be seen from figure 3-3, the total force in X axis can be derived by analyzing the component of total aerodynamics forces L, D and the thrust τ.

$$X = Lsin\alpha + \tau cos\kappa - Dcos\alpha - mgsin(\alpha + \gamma) \quad \textbf{(3-1)}$$

α, γ and κ are angle of attack, steady flight path angle and engine thrust line angle respectively. Similarly, the total force in Z axis is expressed in equation 3-2.

$$Z = mgcos(\alpha + \gamma) - Lcos\alpha - Dsin\alpha - \tau sin\kappa \quad \textbf{(3-2)}$$

The aerodynamics coefficients were calculated by AVL is in rotational equilibrium. When given a certain speed and certain AoA, AVL can calculate the corresponding elevator deflection angle which to balance the pitch moment. The thrust is assumed through the centre of gravity, so it does not contribute to the aircraft moment. Based on those conditions, a MATLAB program was made to calculate the trim conditions only used (3 - 1) and (3 - 2), which is listed in appendix C. Figure 3-4 illustrates the relationship of the angle of attack and elevator deflection in trim conditions. Table 3-2 shows the results of the calculation.

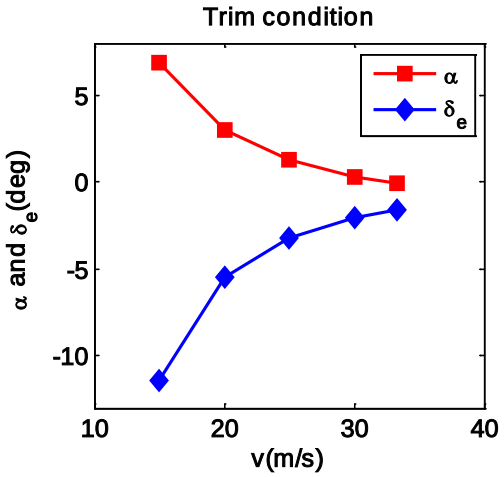

Figure 3-4 α vs δ_e in different velocity

Table 3-2 Sea level horizontal steady flight coefficients

	V (m/s)	15	20	25	30	33.33
Trim condition	**AOA**	6.8593	3.0007	1.2531	0.3127	-0.0916
	δ_e	-11.3963	-5.4733	-3.2017	-2.0851	-1.6281
Longitudinal Aerodynamic Derivatives & Control coefficients	C_L	0.6594	0.3723	0.2387	0.1660	0.1346
	C_D	0.0430	0.0284	0.0245	0.0231	0.0226
	$C_{L\alpha}$	4.7205	4.7998	4.8228	4.8333	4.8383
	$C_{D\alpha}$	0.3041	0.1878	0.1373	0.1073	0.0904
	$C_{m\alpha}$	-2.0327	-1.6559	-1.4803	-1.3846	-1.3432
	$C_{L\dot{\alpha}}$	2.3394	2.3591	2.2901	2.2122	2.1767
	$C_{m\dot{\alpha}}$	-8.1059	-8.1751	-7.9352	-7.6661	-7.5420
	C_{Lq}	7.3859	7.8822	8.1078	8.2312	8.2857
	C_{mq}	-12.9568	-12.6926	-12.5668	-12.4990	-12.4707
	C_{m_u}	-0.0036	-0.0038	-0.0036	-0.0027	-0.0020
	$C_{L_{\delta e}}$	0.3232	0.3267	0.3275	0.3277	0.3278
	$C_{m_{\delta e}}$	-1.1982	-1.2035	-1.2032	-1.2025	-1.2022
Lateral-directional Aerodynamic Derivatives & Control coefficients	C_{y_β}	-0.1373	-0.1362	-0.1355	-0.1351	-0.1349
	$C_{l\beta}$	-0.0782	-0.0494	-0.0358	-0.0285	-0.0253
	$C_{n\beta}$	0.0710	0.0631	0.0608	0.0599	0.0596
	C_{yp}	0.1434	0.0657	0.0299	0.0105	0.0022
	C_{lp}	-0.5095	-0.5200	-0.5233	-0.5248	-0.5255
	C_{np}	-0.0531	-0.0237	-0.0106	-0.0036	-0.0006

	V (m/s)	15	20	25	30	33.33
	C_{yr}	0.1311	0.1429	0.1447	0.1448	0.1447
	C_{lr}	0.1969	0.1221	0.0874	0.0686	0.0605
	C_{nr}	-0.0899	-0.0825	-0.0797	-0.0784	-0.0779
	$C_{l\delta a}$	-0.3421	-0.3474	-0.3489	-0.3496	-0.3499
	$C_{n\delta a}$	-0.0137	-0.0071	-0.0040	-0.0024	-0.0017
	$C_{y\delta r}$	-0.0926	-0.0933	-0.0933	-0.0933	-0.0933
	$C_{l\delta r}$	-0.0130	-0.0134	-0.0136	-0.0137	-0.0137
	$C_{n\delta r}$	0.0562	0.0566	0.0566	0.0565	0.0565

3.4 Chapter Summary

DATCOM and AVL programs have been used to estimate aerodynamics coefficients for a ¼ scales Piper J-3 cub model. DATCOM does not have rudder performance, so the main aerodynamics and control coefficients are estimated by AVL, but the dynamic derivatives cannot be calculated by AVL, thus the DATCOM is still used as a supplement to find this data.

Of course, neither of them is as accurate as wind tunnel and flight testing, but they are very effective ways for preliminary design, and also the best method just for research purpose. After the coefficients were calculated, a MATLAB program was made to calculate the trim points of selected flight conditions.

4 FLYING QUALITIES OF THE PIPER J-3 CUB

4.1 Longitudinal flying qualities

Longitudinal static stability

Without any input, if the changes by disturbance can be restored to its original condition by aircraft itself, it means the aircraft is statically stable.

Longitudinal static stability is the ability of aircraft when suffering an angle-of-attack disturbance to return to pitch equilibrium. This is a crucial characteristic to an aircraft when determining if it will be able to fly as intended or not.

A positive pitch disturbance follows the increase of α, the resulting pitching moment should be restored in a static stable aircraft. It means positive disturbance should result in a pitching down moment, and vice versa. In other words, the term for longitudinal static stability determined by the relationship between M (C_m) and α at the trim value α_e, and the slope of the C_m vs α should be negative. Thus, the condition for stable trim at incidence α_e, may be expressed:

$$C_m = 0, \frac{dC_m}{d\alpha} < 0 \qquad \textbf{(4-1)}$$

Longitudinal dynamic stability

The dynamic stability of an aircraft is how the motion of an aircraft behaves after it has been disturbed from steady non-oscillating flight. Longitudinal axis has two dynamic stability modes, the short period pitching oscillation and the phugoid.

a) Short-period pitch oscillation(SPPO)

This mode generally has a high frequency and is usually damped over a period of a few seconds. A short, sharp pull back on the control column may be used, and will generally lead to oscillations about the new trim condition. If the oscillation is poorly damped the aircraft will take a long period of time to settle to

the new condition, potentially leading to Pilot-induced oscillation. If the short period mode is unstable it will generally be impossible for the pilot to safely control the aircraft for any period of time.

b) Phugoid

If the stick is fixed, the aircraft will not maintain straight and level flight, but will start to dive, level out and climb again. It will repeat this cycle until pilot intervenes. This long period oscillation in speed and height is called the phugoid mode. This is analyzed by assuming that the SSPO performs its proper function and maintains the angle of attack near its nominal value.

Longitudinal stability analysis

Static stability: Aircraft longitudinal always connects with trim condition; the aerodynamics coefficients given in Table 3-2 are all based on trim conditions. So, when analyzing longitudinal static stability, the parameter $C_{m\alpha}$ is just used here. As it is illustrated by Figure 4-1, to the Level Flight conditions that $C_{m\alpha}$ are all negative, which means the aircraft longitudinal is static stable in given flight conditions.

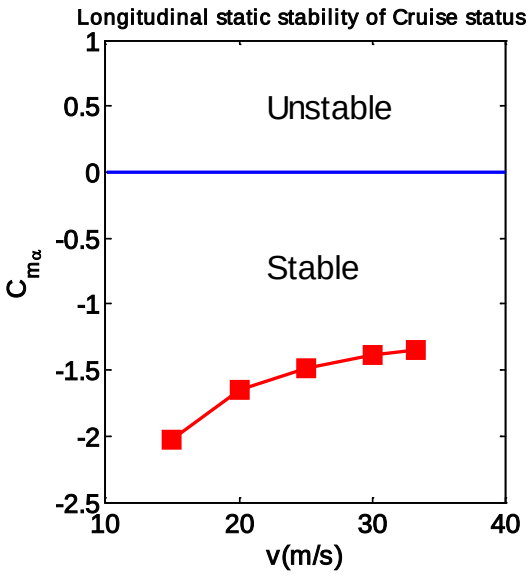

Figure 4-1 horizontal steady flight static stability

Dynamic stability: In this thesis, dynamics stability analysis based on aircraft dynamics model, which is calculated by use of the aerodynamics coefficients and they will be introduced in a later chapter. These models represent aircraft kinematic characteristics, so MATLAB software is used to examine the roots of the Matrices in these models and thus check the longitudinal dynamic stability of the Piper J-3 Cub. The Program of MATLAB is listed in Appendix C, this function is not only used to create a state-space model within the MATLAB environment, but also eigenvalues of Matrices 'As', which representation of longitudinal aircraft dynamics. The analysis results are that the Piper J-3 Cub is dynamically stable at all given flight conditions.

Longitudinal Flying Qualities criterion

The flying qualities criterion of this section and the section below of lateral-directional flying qualities are all based on the MIL-HDBK-1797 and MIL-F-8785C. According to MIL-HDBK-1797, the Piper J-3 Cub belongs to class I and include two phases mission phases: B & C. Phase B includes Cruising (CR) and Phase C includes take-off (TO) and Landing (L).

a) Short period response

ζ_{sp} and $\frac{\omega_{sp}}{n_\alpha}$ are important factors in assessing aircraft flying qualities. ζ_{sp} is the short period damping ratio, ω_{sp} is the short period frequency and n_α is the acceleration sensitivity of the aircraft. $\frac{\omega_{sp}}{n_\alpha}$ is the control anticipation parameter (CAP), which is the ratio of the aircraft's pitch acceleration to change in steady state load factor.

$$CAP = \frac{\omega_{sp}}{n_\alpha} = \frac{W{\omega_{sp}}^2}{qsC_{L\alpha}} \quad \textbf{(4-2)}$$

The requirements of ζ_{sp} are shown in the table 4-1, and the requirements of CAP are given by table 4-2.

Table 4-1 ζ_{sp}requirements

Flight Phases	Level 1		Level 2		Level 3	
	Min.	Max.	Min.	Max.	Min.	Max.
B	0.3	2.0	0.20	2.0	0.15	-
C	0.35	1.30	0.25	2.0	0.15	-

Table 4-2 CAP requirements

Flight Phases	Level 1		Level 2	
	Min.	Max.	Min.	Max.
B	0.085	3.6	0.038	10
C	0.16	3.6	0.096	10

b) Phugoid Response

Longitudinal long-term pitch damping ratio ζ_p should satisfy the following requirements.

Level 1 ----- ζ_p at least 0.04

Level 2 ----- ζ_p at least 0

Level 3 ----- T_2 at least 55 seconds

Bare airframe longitudinal Flying Qualities

With an appropriate approximation, for a conventional aircraft the short period pitching oscillation and the phugoid mode can be treated completely separate from each other.

a) Short-Period approximation

Normally $\Delta u = 0$ is assume to be the short-period mode of motion approximation, the equation of motion of longitudinal state-space would reduce to two orders. The approximation short-period damping and frequency in this way is listed as follows.

$$\omega_{n_{sp}} = \sqrt{M_q \frac{Z_\alpha}{u_0} - M_\alpha} \quad \textbf{(4-3)}$$

$$\zeta_{sp} = -\frac{M_q + M_{\dot{\alpha}} + \frac{Z_\alpha}{u_0}}{2\omega_{n_{sp}}} \quad \textbf{(4-4)}$$

b) Long-Period (phugoid) Approximation

Phugoid mode or long-period mode is about the slow change in altitude and airspeed. It is characterized by changes in pitch attitude, altitude, and velocity at a nearly constant angle of attack. So the approximation to the phugoid mode is neglecting the pitching moment equation and assuming no change in the angle of attack (AOA). Long-period frequency and damping ratio are listed follows.

$$\omega_{n_p} = \sqrt{\frac{-Z_u g}{u_0}} \quad \textbf{(4-5)}$$

$$\zeta_p = -\frac{X_u}{2\omega_{n_p}} \quad \textbf{(4-6)}$$

c) The Piper J-3 cub Flying qualities analysis

The Piper J-3 cub longitudinal flying qualities are analyzed in figure 4-2~4. These curves show that the damping ratios of two modes meet the level one flying qualities requirements, but short period frequency and CAP cannot satisfy the higher requirements. It means an SAS is needed to improve the flying qualities of longitudinal mode.

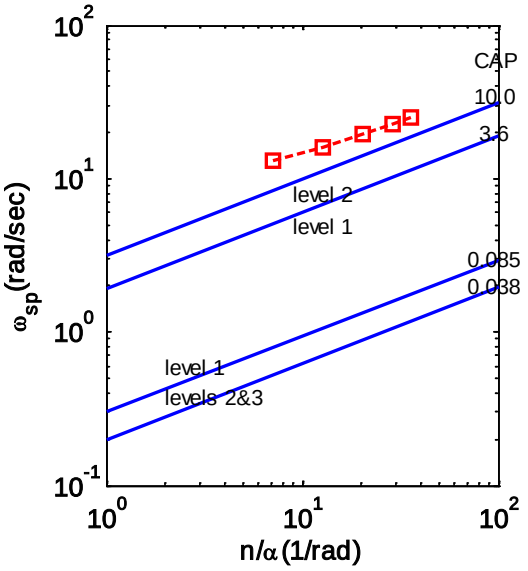

Figure 4-2 short period frequency

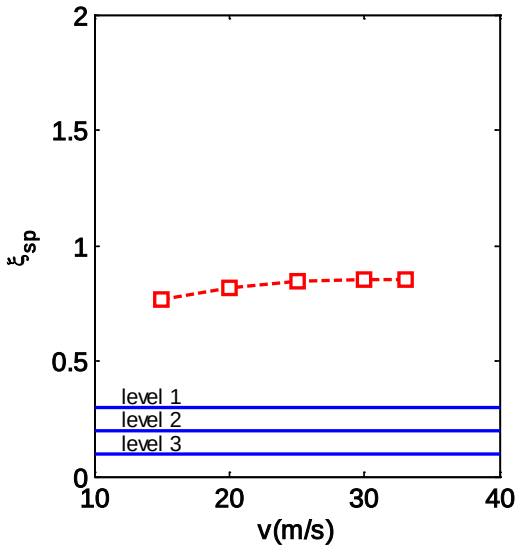

Figure 4-3 short period damping ratio

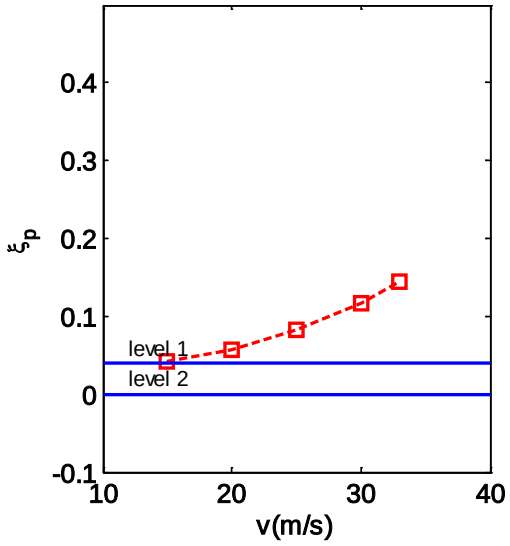

Figure 4-4 Phugoid damping ratio

4.2 Lateral-Directional Flying Qualities

Lateral-directional static stability

Lateral-directional static stability includes lateral static stability and directional static stability.

Lateral static stability, or rolling stability, is the ability to maintain its wing level condition during the roll transfer. Wing dihedral has a significant effect on aircraft lateral static stability, generally speaking the bigger the dihedral angle, the more stable the aircraft. In aerodynamics terms it is always described by derivatives for rolling moment, $C_{l\beta}$, if this parameter is positive, the aircraft is rolling stable.

Directional static stability, stability in yaw, is the ability of aircraft to yawing disturbance and maintaining directional equilibrium. The most contributing factor to directional static stability is the tail fin. If an aircraft is directional static stable, it means a positive yaw should cause a negative directional moment. So the condition for an aircraft to be directionally stable is $\frac{dC_n}{d\psi} < 0$ or, equivalently, $\frac{dC_n}{d\beta} > 0$.

Lateral-directional dynamic stability

Lateral-directional equation includes three degree-of-freedom of motion, roll, yaw and sideslip. The roll, or bank angle, ϕ, describes aircraft turn around body axis x, when body axis y moves towards body z axis, the movement is positive. p denotes the rate of roll. Yaw, or heading angle, ψ, is the angle between the aircraft body axis x and the direction of flight(positive nose right). Yaw rate is denoted by r. Sideslip angle, or angle of sideslip (AoS, β), is the angle between aircraft centreline and airflow(positive nose left).

Lateral-Directional dynamic stability can be divided into three modes, Roll mode, Spiral mode and Dutch roll mode. Roll mode, or roll subsidence mode, is a non-periodicity motion where rolling angle and rolling angle rate reduce very quickly. In Lateral-Directional state space equation, it is described by a bigger single real root. Spiral mode is also called as spiral dive mode, like roll mode it is also without oscillatory and determined by the little real root in state space equation. Dutch roll mode is a complex interaction between yaw, roll and sideslip, it is described by a pair of complex roots in the state space equation and is a high frequency oscillatory periodicity motion.

Lateral directional stability analysis

a) Static stability

Based on the above description, the Piper J-3 cub's lateral directional stability is analyzed in this section. Table 4-3 lists the static stability parameters of different flight conditions.

Table 4-3 Lateral directional static stability analysis（sea level）

v (m/s)	15	20	25	30	33.33
$C_{l\beta}$	-0.0782	-0.0494	-0.0358	-0.0285	-0.0253
$C_{n\beta}$	0.0710	0.0631	0.0608	0.0599	0.0596

The parameters in the table all satisfy the static stability requirement, in one word, the Piper J-3 cub is lateral-directional static stable in all the flight conditions listed above.

b) Dynamic stability

In this thesis, dynamic stability is judged by the eigenvalues of state-space matrices for the motion, the same as the longitudinal part. If the eigenvalues have positive real part, it means the system is dynamic unstable. The next chapter gives the details of how to calculate the state-space matrices, and Appendix C lists a program to calculate the matrices and analyzes the dynamic stability of Lateral-directional motions. The dynamics mode of 15m/s flight condition was calculated to have the following eigenvalues.

$$\lambda_{\mathrm{DR}} = -1.0988 \pm 4.4827\mathrm{i} \quad \lambda_{\mathrm{roll}} = -18.7011 \quad \lambda_{\mathrm{spiral}} = 0.1035 \qquad \textbf{(4-7)}$$

As can be found from the eigenvalues above, the Piper J-3 cub has an unstable spiral mode at 15m/s flight condition, others are also the case. This should not be a great concern, for many airplanes have an unstable spiral mode, and it can be stabilized use a feedback gain controller.

Lateral-directional Flying Qualities

a) Dutch roll mode requirements

Dutch roll mode may be compared to short period pitching oscillation (SPPO). Because I_z is much bigger than I_y, the periodic time is greater than the SPPO period time. The requirements of the frequency, ω_{nd}, and the damping ratio, ζ_d, of the lateral-directional oscillations are given in table 4-4.

Table 4-4 least Dutch Roll and ζ_d, requirements

Level	Min ζ_d,	Min $\zeta_d\omega_{nd}$ rad/sec.	Min ω_{nd} rad/sec.
1	0.08	0.15	0.4
2	0.02	0.05	0.4
3	0	--	0.4

b) Spiral mode requirements

Just as the Dutch roll mode is compared to the SPPO, the Spiral mode can be thought similar to a longitudinal phugoid mode. Table 4-5 lists the spiral mode double amplitude time minimum value requirements.

Table 4-5 Spiral stability - minimum time to double amplitude

Level 1	Level 2	Level 3
20	8	4

c) Roll mode requirements

As the foregoing text describes, Roll reduces very quickly because generally large producing moment produced by the wing. The roll-mode time constant, R, shall be less than Table 4-6 listed.

Table 4-6 Maximum roll-mode time constant, seconds

Level 1	Level 2	Level 3
1.4	3	10

Bare airframe lateral directional flying Qualities

a) Dutch Roll Approximation

When analyzing the Dutch roll mode, we can consider that it consists primarily of side slipping and yawing motions, and can neglect the rolling moment equation. Then we get the approximations as follows [19].

$$\omega_{nDR} = \sqrt{\frac{Y_\beta N_r - N_\beta Y_r + u_0 N_\beta}{u_0}} \quad \textbf{(4-8)}$$

$$\zeta_{DR} = -\frac{1}{2\omega_{nDR}}\left(\frac{Y_\beta + u_0 N_r}{u_0}\right) \quad \textbf{(4-9)}$$

b) Roll Approximation

This motion can be approximated by the single degree of freedom rolling motion

$$\lambda_{roll} = -\frac{1}{\tau} = L_p \quad \textbf{(4-10)}$$

τ is the roll time constant. The magnitude of the roll damping L_p is dependent on the size of the wing and tail surfaces.

c) Spiral Approximation

The spiral mode is characterized by changes in the bank angle ϕ and the heading angle. The sideslip angle usually is quite small, but cannot be neglected. Because aerodynamic moments do not depend on the roll angle ϕ or the heading angle, but depend on the sideslip angle, roll rate p, and yawing rate r.

The aerodynamics contributions due to β and r usually are in the same order of magnitude. Therefore, to obtain an approximation of the spiral mode the side force equation and $\Delta\phi$ should be neglected. With these assumptions, the eigenvalue for the spiral mode is

$$\lambda_{spiral} = \frac{L_\beta N_r - L_r N_\beta}{L_\beta} \quad \textbf{(4-11)}$$

d) Flying qualities analysis

Based on this description and the aerodynamics coefficients given in Chapter 3, the bare airframe lateral directional flying Qualities are as follows.

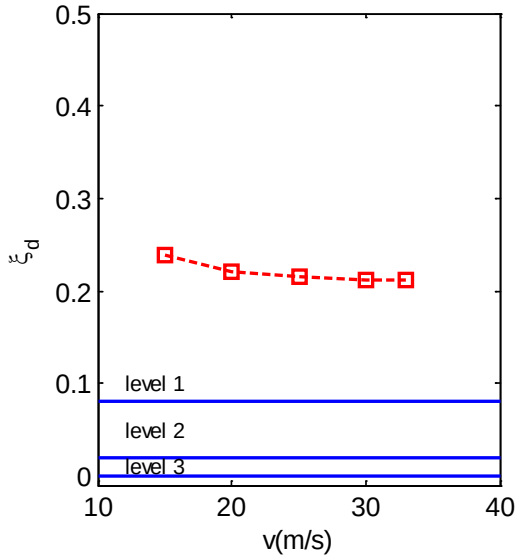

Figure 4-5 Dutch Roll damping ratio

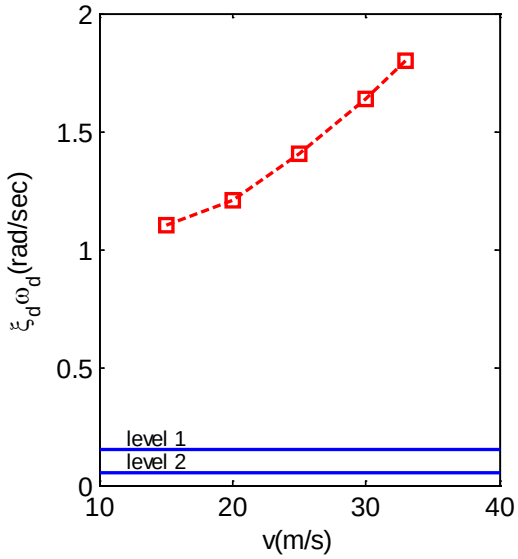

Figure 4-6 Dutch Roll Damping

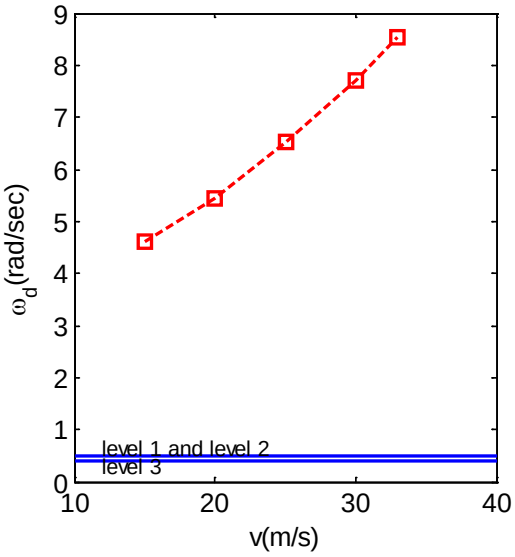

Figure 4-7 Dutch Roll natural frequency

According to Figure 4-5~7, the Dutch roll stability characteristics of the Piper J-3 Cub at given flight conditions meet the flying quality requirements.

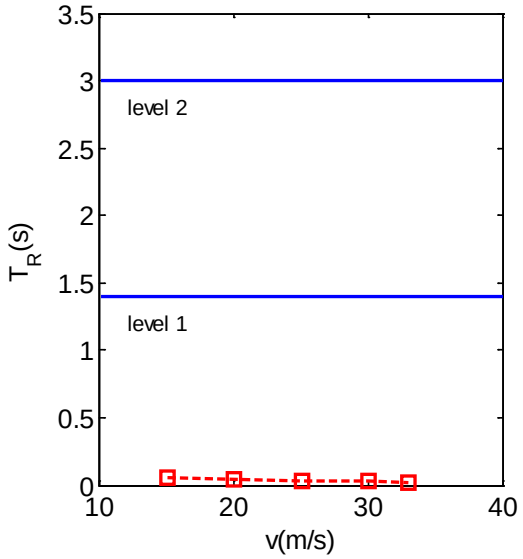

Figure 4-8 Roll time constants

Similarly, roll mode time constants of the aircraft can also meet the level 1 flying qualities requirement.

4.3 Chapter Summary

Using the aerodynamics coefficients calculated in Chapter 3, the Piper J-3 Cub static stability, dynamic stability and flying qualities are discussed in this Chapter. The investigation results show that the Piper J-3 Cub is static stable in longitudinal axis and lateral-directional axis, which also has a longitudinal dynamic stable characteristic. Except for an unstable spiral mode, it is also stable in other lateral-directional dynamic movement. The flying qualities are analyzed based on the requirements of MIL-HDBK-1797 and MIL-F-8785C. The Piper J-3 Cub meets the Level 1 lateral-directional flying qualities but needs to be improved in its longitudinal flying qualities.

5 AIRCRAFT MODELING AND SAS DESIGN

5.1 Aircraft state space model

The equations of aircraft motion are based on Newton's second law for the behaviour of a free body in three dimensional spaces under the influence of external forces; the summation of all external forces acting on the aircraft is equal to the time derivative of its momentum, it can be described by a set of non linear differential Equations. To simplify the design, it becomes necessary to linearize the equations. The linearization is based on perturbation theory with the assumption that aircraft is flying in an equilibrium condition. The mathematical model of aircraft dynamics is described by differential equations, which are usually given in the following state-space form:

$$\dot{x} = Ax + Bu \quad \textbf{(5-1)}$$

$$y = Cx + Du \quad \textbf{(5-2)}$$

Where x is the state vector, u is the control vector, y is the output vector, and A, B, C and D is state, input, output and feed through matrices.

Depending on the assumed flight conditions the complete set of linearised equations of aircraft motion can be De-coupled into two independent sets: longitudinal and lateral set of equations. The equations of longitudinal aircraft motion are obtained by assuming symmetric reference flight condition.

Longitudinal state space equation

The following are the given state-space matrices for the longitudinal motions:

$$\begin{bmatrix}\Delta\dot{u}\\ \Delta\dot{w}\\ \Delta\dot{q}\\ \Delta\dot{\theta}\end{bmatrix}=\begin{bmatrix}X_u & X_w & 0 & -g\\ Z_u & Z_w & u_0 & 0\\ M_u+M_{\dot{w}}Z_u & M_w+M_{\dot{w}}Z_w & M_q+M_{\dot{w}}u_0 & 0\\ 0 & 0 & 1 & 0\end{bmatrix}\begin{bmatrix}\Delta\mathrm{u}\\ \Delta\mathrm{w}\\ \Delta\mathrm{q}\\ \Delta\theta\end{bmatrix}+\begin{bmatrix}\mathrm{X}_{\delta_\mathrm{e}} & \mathrm{X}_{\delta_\mathrm{T}}\\ \mathrm{Z}_{\delta_\mathrm{e}} & \mathrm{Z}_{\delta_\mathrm{T}}\\ \mathrm{M}_{\delta_\mathrm{e}}+\mathrm{M}_{\dot{\mathrm{w}}}\mathrm{Z}_{\delta_\mathrm{e}} & \mathrm{M}_{\delta_\mathrm{T}}+\mathrm{M}_{\dot{\mathrm{w}}}\mathrm{Z}_{\delta_\mathrm{T}}\\ 0 & 0\end{bmatrix}\begin{bmatrix}\Delta\delta_e\\ \Delta\delta_T\end{bmatrix} \quad \textbf{(5-3)}$$

Where the state vector x and control vector u are given by

$$x=\begin{bmatrix}\Delta\mathrm{u}\\ \Delta\mathrm{w}\\ \Delta\mathrm{q}\\ \Delta\theta\end{bmatrix},u=\begin{bmatrix}\Delta\delta_e\\ \Delta\delta_T\end{bmatrix} \quad \textbf{(5-4)}$$

And the matrices A and B are given by

$$A=\begin{bmatrix}X_u & X_w & 0 & -g\\ Z_u & Z_w & u_0 & 0\\ M_u+M_{\dot{w}}Z_u & M_w+M_{\dot{w}}Z_w & M_q+M_{\dot{w}}u_0 & 0\\ 0 & 0 & 1 & 0\end{bmatrix} \quad \textbf{(5-5)}$$

$$B=\begin{bmatrix}\mathrm{X}_{\delta_\mathrm{e}} & \mathrm{X}_{\delta_\mathrm{T}}\\ \mathrm{Z}_{\delta_\mathrm{e}} & \mathrm{Z}_{\delta_\mathrm{e}}\\ \mathrm{M}_{\delta_\mathrm{e}}+\mathrm{M}_{\dot{\mathrm{w}}}\mathrm{Z}_{\delta_\mathrm{e}} & \mathrm{M}_{\delta_\mathrm{T}}+\mathrm{M}_{\dot{\mathrm{w}}}\mathrm{Z}_{\delta_\mathrm{T}}\\ 0 & 0\end{bmatrix} \quad \textbf{(5-6)}$$

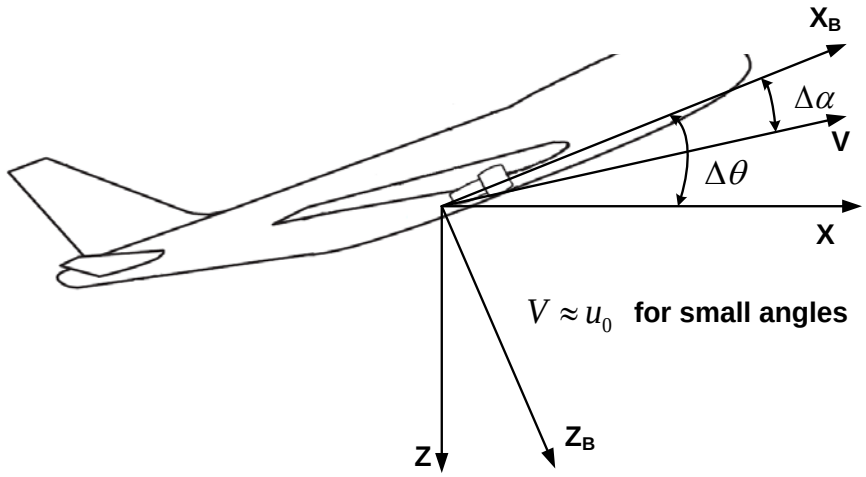

Figure 5-1 Velocity with AOA and pitch angle

From figure 5-1, the following expression can be obtained.

$$\Delta\dot{h} = u_0 \sin(\Delta\theta - \Delta\alpha) \tag{5-7}$$

For small angles change, may be written:

$$\Delta\dot{h} = u_0(\Delta\theta - \Delta\alpha) = u_0\Delta\theta - \Delta w \tag{5-8}$$

By combining equation (5-7) with equation (5-3), the altitude variable can be included as formula (5-9).

$$\begin{bmatrix} \Delta\dot{u} \\ \Delta\dot{w} \\ \Delta\dot{q} \\ \Delta\dot{\theta} \\ \Delta\dot{h} \end{bmatrix} = \begin{bmatrix} X_u & X_w & 0 & -g & 0 \\ Z_u & Z_w & u_0 & 0 & 0 \\ M_u + M_{\dot{w}}Z_u & M_w + M_{\dot{w}}Z_w & M_q + M_{\dot{w}}u_0 & 0 & 0 \\ 0 & 0 & 1 & 0 & 0 \\ 0 & -1 & 0 & u_0 & 0 \end{bmatrix} \begin{bmatrix} \Delta u \\ \Delta w \\ \Delta q \\ \Delta\theta \\ \Delta h \end{bmatrix} + \begin{bmatrix} X_{\delta_e} & X_{\delta_T} \\ Z_{\delta_e} & Z_{\delta_T} \\ M_{\delta_e} + M_{\dot{w}}Z_{\delta_e} & M_{\delta_T} + M_{\dot{w}}Z_{\delta_T} \\ 0 & 0 \\ 0 & 0 \end{bmatrix} \begin{bmatrix} \Delta\delta_e \\ \Delta\delta_T \end{bmatrix} \tag{5-9}$$

The short-period motion is characterized by heavily-damped longitudinal motion (lasting several seconds) where the assumptions of constant speed and zero thrust are incorporated. The long period, which lasts 30 or more seconds, is characterized as being only slightly damped (compared to the short period) and the assumption of a constant angle of attack is made.

Equation (5-10) illustrates short period state-space matrices.

$$\begin{bmatrix} \Delta\dot{w} \\ \Delta\dot{q} \end{bmatrix} = \begin{bmatrix} Z_w & u_0 \\ M_w + M_{\dot{w}}Z_w & M_q + M_{\dot{w}}u_0 \end{bmatrix} \begin{bmatrix} \Delta w \\ \Delta q \end{bmatrix} + \begin{bmatrix} Z_{\delta_e} \\ M_{\delta_e} + M_w Z_{\delta_e} \end{bmatrix} [\Delta\delta_e] \tag{5-10}$$

Table 5-1 the Piper J-3 Cub Longitudinal state-space matrices

V (m/s)	A	B
15	$\begin{bmatrix} -0.0848 & 0.3500 & 0 & -9.8100 & 0 \\ -1.2995 & -4.6940 & 15.0070 & 0 & 0 \\ 0.4920 & -6.5798 & -15.2126 & 0 & 0 \\ 0 & 0 & 1.0000 & 0 & 0 \\ 0 & -1.0000 & 0 & 15.0070 & 0 \end{bmatrix}$	$\begin{bmatrix} 0 & 32.1224 \\ -4.7787 & 0 \\ -72.5369 & 0 \\ 0 & 0 \\ 0 & 0 \end{bmatrix}$
20	$\begin{bmatrix} -0.0748 & 0.2424 & 0 & -9.8100 & 0 \\ -0.9783 & -6.3436 & 20.0093 & 0 & 0 \\ 0.3637 & -6.6397 & -20.0957 & 0 & 0 \\ 0 & 0 & 1.0000 & 0 & 0 \\ 0 & -1.0000 & 0 & 20.0093 & 0 \end{bmatrix}$	$\begin{bmatrix} 0 & 32.1224 \\ -8.5881 & 0 \\ -129.4836 & 0 \\ 0 & 0 \\ 0 & 0 \end{bmatrix}$
25	$\begin{bmatrix} -0.0804 & 0.1665 & 0 & -9.8100 & 0 \\ -0.7840 & -7.9608 & 25.0116 & 0 & 0 \\ 0.2749 & -7.1682 & -24.6793 & 0 & 0 \\ 0 & 0 & 1.0000 & 0 & 0 \\ 0 & -1.0000 & 0 & 25.0116 & 0 \end{bmatrix}$	$\begin{bmatrix} 0 & 32.1224 \\ -13.4512 & 0 \\ -202.3972 & 0 \\ 0 & 0 \\ 0 & 0 \end{bmatrix}$
30	$\begin{bmatrix} -0.0909 & 0.1157 & 0 & -9.8100 & 0 \\ -0.6543 & -9.5709 & 30.0139 & 0 & 0 \\ 0.2193 & -7.9271 & -29.1286 & 0 & 0 \\ 0 & 0 & 1.0000 & 0 & 0 \\ 0 & -1.0000 & 0 & 30.0139 & 0 \end{bmatrix}$	$\begin{bmatrix} 0 & 32.1224 \\ -19.3841 & 0 \\ -291.5276 & 0 \\ 0 & 0 \\ 0 & 0 \end{bmatrix}$
33.3	$\begin{bmatrix} -0.0989 & 0.0969 & 0 & -9.8100 & 0 \\ -0.5895 & -10.6442 & 33.3488 & 0 & 0 \\ 0.1958 & -8.4871 & -32.1205 & 0 & 0 \\ 0 & 0 & 1.0000 & 0 & 0 \\ 0 & -1.0000 & 0 & 33.3488 & 0 \end{bmatrix}$	$\begin{bmatrix} 0 & 32.1224 \\ -23.9377 & 0 \\ -359.9664 & 0 \\ 0 & 0 \\ 0 & 0 \end{bmatrix}$

Lateral directional state space equation

Lateral directional state space is given below.

$$\begin{bmatrix} \Delta\dot{\beta} \\ \Delta\dot{p} \\ \Delta\dot{r} \\ \Delta\dot{\phi} \end{bmatrix} = \begin{bmatrix} \frac{Y_\beta}{u_0} & \frac{Y_p}{u_0} & -(1-\frac{Y_r}{u_0}) & \frac{gcos\theta_0}{u_0} \\ L_\beta & L_p & L_r & 0 \\ N_\beta & N_p & N_r & 0 \\ 0 & 1 & 0 & 0 \end{bmatrix} \begin{bmatrix} \Delta\beta \\ \Delta p \\ \Delta r \\ \Delta\phi \end{bmatrix} + \begin{bmatrix} 0 & \frac{Y_{\delta_r}}{u_0} \\ L_{\delta_a} & L_{\delta_r} \\ N_{\delta_a} & N_{\delta_r} \\ 0 & 0 \end{bmatrix} \begin{bmatrix} \Delta\delta_a \\ \Delta\delta_r \end{bmatrix} \quad \textbf{(5-11)}$$

Where the state vector x and control vector u are given by

$$x = \begin{bmatrix} \Delta\beta \\ \Delta p \\ \Delta r \\ \Delta\phi \end{bmatrix}, u = \begin{bmatrix} \Delta\delta_a \\ \Delta\delta_r \end{bmatrix} \quad \textbf{(5-12)}$$

And the matrices A and B are given by

$$A = \begin{bmatrix} \frac{Y_\beta}{u_0} & \frac{Y_p}{u_0} & -(1-\frac{Y_r}{u_0}) & \frac{gcos\theta_0}{u_0} \\ L_\beta & L_p & L_r & 0 \\ N_\beta & N_p & N_r & 0 \\ 0 & 1 & 0 & 0 \end{bmatrix} \quad \textbf{(5-13)}$$

$$B = \begin{bmatrix} 0 & \frac{Y_{\delta_r}}{u_0} \\ L_{\delta_a} & L_{\delta_r} \\ N_{\delta_a} & N_{\delta_r} \\ 0 & 0 \end{bmatrix} \quad \textbf{(5-14)}$$

Table 5-2 the Piper J-3 Cub Lateral directional state-space matrices

V (m/s)	A	B
15	$\begin{bmatrix} -0.1353 & 0.0110 & -0.9899 & 0.6537 \\ -37.3233 & -18.9477 & 7.3234 & 0 \\ 17.3510 & -1.0122 & -1.7142 & 0 \\ 0 & 1.0000 & 0 & 0 \end{bmatrix}$	$\begin{bmatrix} 0 & -0.0912 \\ -163.1868 & -6.1872 \\ -3.3561 & 13.7423 \\ 0 & 0 \end{bmatrix}$
20	$\begin{bmatrix} -0.1790 & 0.0050 & -0.9890 & 0.4903 \\ -41.8525 & -25.7815 & 6.0544 & 0 \\ 27.4244 & -0.6031 & -2.0964 & 0 \\ 0 & 1.0000 & 0 & 0 \end{bmatrix}$	$\begin{bmatrix} 0 & -0.1226 \\ -294.6034 & -11.3813 \\ -3.0887 & 24.6005 \\ 0 & 0 \end{bmatrix}$

25	$\begin{bmatrix} -0.2226 & 0.0023 & -0.9889 & 0.3922 \\ -47.4856 & -32.4338 & 5.4201 & 0 \\ 41.2909 & -0.3376 & -2.5326 & 0 \\ 0 & 1.0000 & 0 & 0 \end{bmatrix}$	$\begin{bmatrix} 0 & -0.1533 \\ -462.3071 & -17.9954 \\ -2.7460 & 38.4331 \\ 0 & 0 \end{bmatrix}$
30	$\begin{bmatrix} -0.2663 & 0.0008 & -0.9889 & 0.3268 \\ -54.3352 & -39.0351 & 5.1055 & 0 \\ 58.5813 & -0.1378 & -2.9890 & 0 \\ 0 & 1.0000 & 0 & 0 \end{bmatrix}$	$\begin{bmatrix} 0 & -0.1839 \\ -667.0126 & -26.0586 \\ -2.3301 & 55.3009 \\ 0 & 0 \end{bmatrix}$
33.33	$\begin{bmatrix} -0.2955 & 0.0002 & -0.9889 & 0.2942 \\ -59.5831 & -43.4274 & 5.0024 & 0 \\ 71.9461 & -0.0257 & -3.2989 & 0 \\ 0 & 1.0000 & 0 & 0 \end{bmatrix}$	$\begin{bmatrix} 0 & -0.2042 \\ -824.2131 & -32.2450 \\ -2.0120 & 68.2441 \\ 0 & 0 \end{bmatrix}$

5.2 Stability Augmentation System design

Because the Piper J-3 Cub, the model studied in this thesis, has an undesirable flying characteristic, it needs to have a Stability Augmentation System (SAS) designed.

Longitudinal Stability Augmentation system

ζ_{sp} at 0.707 is an ideal value for aircraft, according to the requirement the middle value 0.45 was select for CAP, based on this condition, the pole placement method is used to design a longitudinal Stability Augmentation System, the feedback signal to relocate the poles are shown in figure 5-2. The designed parameters for each flight conditions are given in table 5-3.

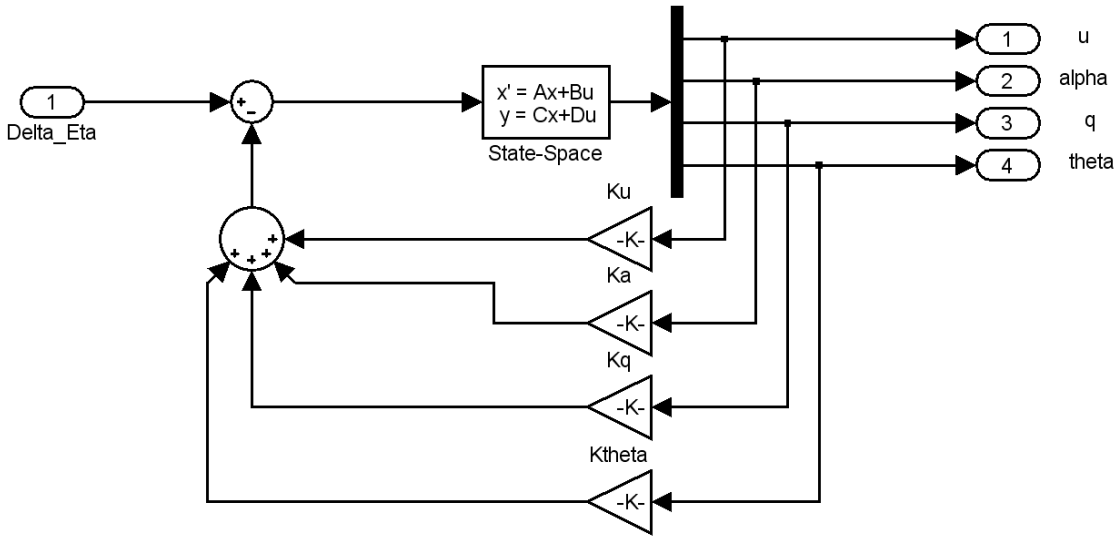

Figure 5-2 Longitudinal full state feedback to elevator

Table 5-3 Longitudinal SAS control law gains

Speed(m/s)	K_u	K_α	K_q	K_θ
15	-0.0088	1.2374	0.2294	-0.0106
20	-0.0037	0.8838	0.1719	-0.0034
25	-0.0019	0.7364	0.1360	-0.0013
30	-0.0010	0.6631	0.1119	-0.0005
33.33	-0.0008	0.6317	0.1001	-0.0002

Longitudinal Flying Qualities of Augmented System

Figure 5-3~5 illustrated with the SAS in longitudinal axis, the flying qualities of the Piper J-3 Cub: the studied model aircraft, obviously improved.

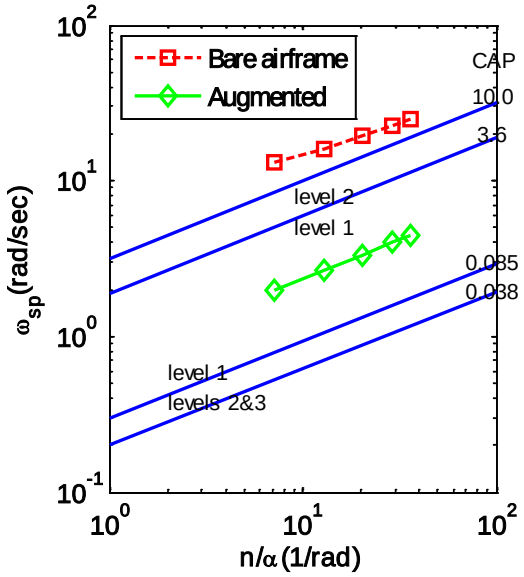

Figure 5-3 Short period frequency and CAP

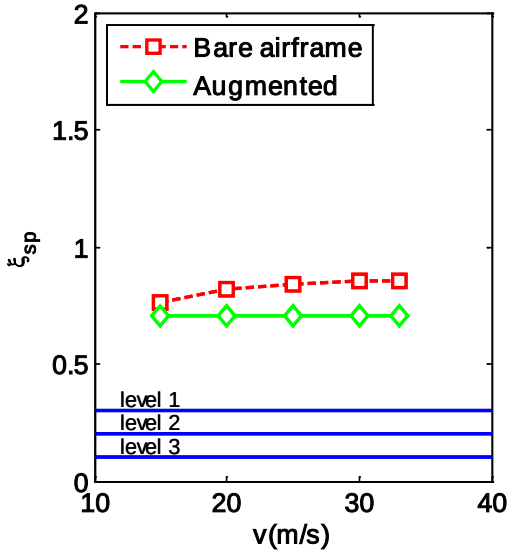

Figure 5-4 Short period damping ratio

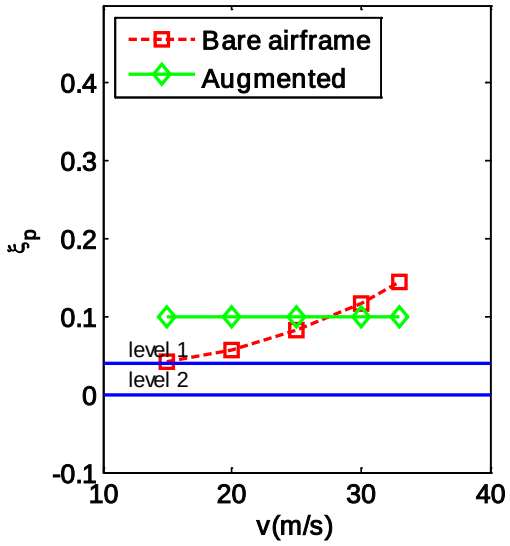

Figure 5-5 Phugoid damping ratio

5.3 Chapter Summary

Most aircraft are not perfect in flying qualities to some extent, so Stability Augmentation System is always needed. This chapter briefly introduced aircraft state space model and also gave the selected flight conditions in state space models, then these models are used to design the longitudinal SAS by using

pole placement method, for the longitudinal flying qualities cannot satisfy level one flying qualities requirements of MIL-F-8785C. Finally, the comparison is made between the augmented and unaugmented aircraft, and the result shows that with the SAS, the flying qualities of the Piper J-3 Cub model are greatly improved.

6 LONGITUDINAL AUTOPILOT DESIGN

6.1 Introduction

The SAS investigated in the preceding chapter actually is also a kind of autopilot, with it the aircraft's handing qualities would be improved so the pilots can fly the aircraft easily. Other styles of autopilot will be investigated in this chapter and next chapter, which aim to lessen the airmen's workload during the whole flying process.

The flying qualities criteria do not serve to pilot-relief autopilot modes. Specifications are mainly focused on steady-state error and transient responses. The requirements are given in next section for autopilot performance of the aircraft studied in this thesis.

6.2 Performance index (PI) requirements

Autopilot performance index specifications discussed in this section including operational constraint, steady-state error e_{ss} and transient response. Setting time is not researched here for the proper regulations have not been found, but it does not mean this parameter is less important, the automatic flight control system is still needed to respond as quickly as possible.

- Operational constraint and steady-state error

  Pitch angle $\theta \in [-3^\circ +30^\circ]$, $e_{ss} \in [-1^\circ + 1^\circ]$

  Roll angle $\phi \in [-60^\circ +60^\circ]$, $e_{ss} \in [-0.5^\circ + 0.5^\circ]$

  Speed control stability should be confined in less than 1 m/s

  Altitude hold stability should be less than 10m in cruise phase, and confined into 1m in takeoff and landing phases.

- Transient response

Altitude and velocity of aircraft change should be smooth and rapid, and the overshoot should be no more than 20%. Namely, to pitch angle θ, when it is intended to change to 5°, the overshoot return to initial state should be less than 1°; to heading angle ψ, when it was changed to 10°, the overshoot return to its original value should be maintained within 2°.

6.3 Flight profile

Full automatic control of an aircraft from take off to landing phase requires that the airplane be designed to track a certain defined path. The flight profile designed and studied here is just a vertical section plane, which is shown in figure 6-1. From the original ground park point, it includes takeoff, climb, cruise and landing. When compared with other phases, cruise is to some extent simpler. Autonomous take-off and landing phases have to be controlled more precisely over the flight path which is more closely connected with safety, and they will be studied later. Every phase also contains several sub-phases; more details can be seen in the following sections.

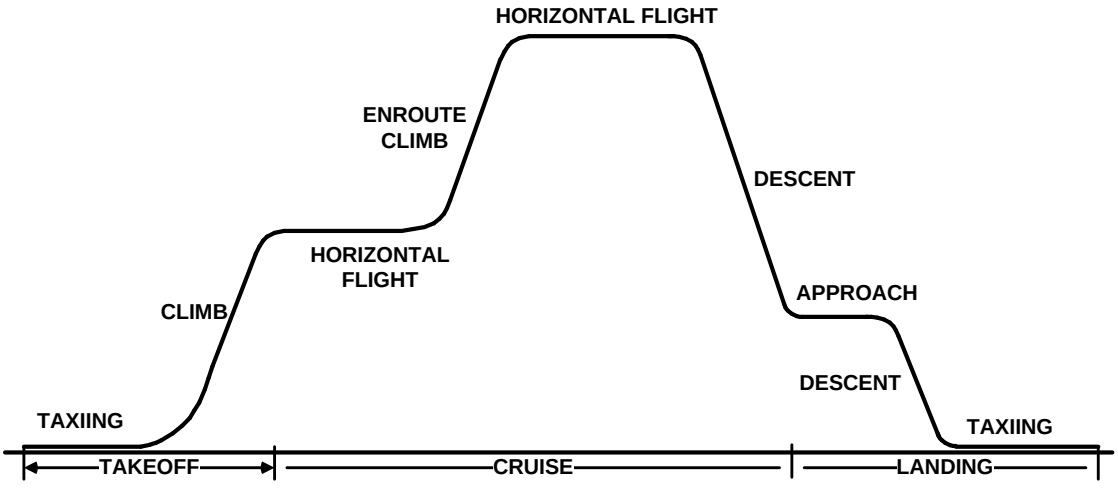

Figure 6-1 Flight profile for automatic control Takeoff phase

6.4 Takeoff

6.4.1 Stages of take off

Generally, the phases of aircraft takeoff is the process of the aircraft from ground run and leave the ground to get to the screen height (10.7m or 15.2m). The take-off is assumed to be divided into three stages as shown in figure 6-2, which include ground run, transition and climb to the screen height [20].

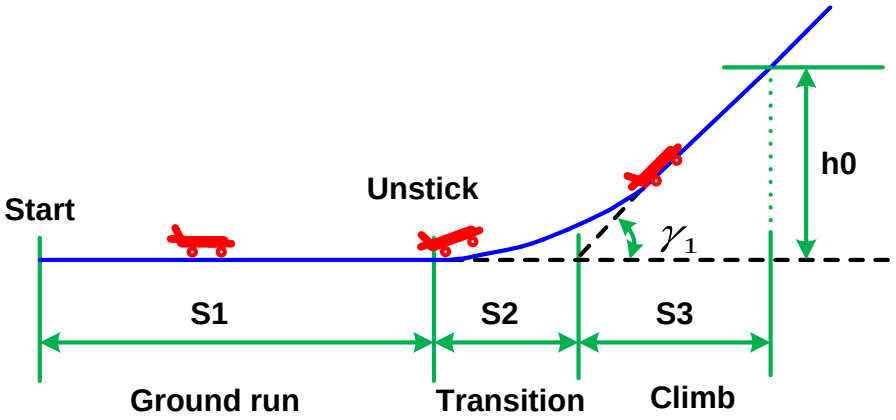

Figure 6-2 Take-off stages

Ground roll stage

The purpose of the ground run is to increase the speed of aircraft until it gets the rotation speed and eventually the lift off speed. The more the engine thrust, the more residual thrust. This means the speed of aircraft can increase more quickly. Normally, to increase the velocity as quickly as possible, the power lever of aircraft should be pushed to maximum position.

a) Lift up nose wheel or tail wheel

Nose wheel aircraft: The aircraft with nose wheel ground angle is relatively small, if the three point attitude is maintained throughout the whole take-off roll stage, the angle of attack and lift coefficient is small, and thus the speed must be increased to generate sufficient lift for the aircraft to leave the ground. So the ground run distance is bound to much longer. Therefore, to reduce the lift off

speed and shorten the roll distance, the nose wheel should be pulled up when the speed has increased sufficiently to a certain extent to increase the angle of attack and lift coefficient.

The time of lifting the nose wheel should not be too early or too late. To put up the front wheel, the horizontal tail or elevator must generate a greater pitch moment. If a premature uplift the nose wheel, because the velocity is still small, lift and drag are also small and the induced upward torque is also small, so the horizontal tail or elevator produces low additional aerodynamics power. Thus more deflection of the control surfaces is needed to generate enough pitch up torque. As a result, with the increase of the roll speed, the pitching moment augments rapidly, thus a larger amount of the reciprocating manipulation is needed to maintain the balance of the lift of the nose wheel, which makes some difficulty to manoeuvre the aircraft. At the same time, the drag is increased with the early nose wheel lift and the takeoff distance will be increased. If the front wheel is lifted too late by a man operated aircraft, not only the ground roll distance would be increased, but also because the liftoff time is very short, it is not easy for the pilot to amend the height of the nose wheel to maintain the appropriate angle of attack of liftoff, even can result in a sudden increase in lift and cause a sudden uprising. Every type of aircraft has a specification for lifting the nose wheel. The height for the front wheel lifting off from the ground should be required just to maintain the aircraft's angle of attack of liftoff, if the front wheel is lifted too low, it would be bound to make the small angle of attack and lift coefficient, the liftoff speed and ground run distance would be increased. If the front wheel is lifted too high, although the roll distance might be shortened, the drag and the takeoff distance for aircraft would be increased, and a too large angle of attack and lift coefficient, it would inevitably result in a low-speed high angle of attack on leaving the ground, which can induce lower handing and stability qualities. Too large an elevation angle also may cause the tail to swipe the ground. So from the standpoint of ensuring safety and reducing roll distance, every aircraft is given a special nose wheel lift up height.

Tail wheel aircraft: The Piper J-3 Cub is a tail wheel aircraft, which needs to lift up the tail wheel during the ground run. Different from a nose wheel aircraft, the

tail wheel aircraft ground angle is fairly large. The angle of attack of a three wheel ground run is close to the critical angle of attack. If the three point run was kept during the entire roll stage, lift coefficient is relatively big, an aircraft at low speed can generate sufficient lift to lift itself leave the ground. Although having a very short roll distance, but with a very low speed and high angle of attack when leaving the ground, the aircraft handing stability are poor and may even cause a stall. For tail wheel aircraft, when the roll speed increases to some extent, the pilot or autopilot should push forward joystick, to raise aircraft tail for a two point roll and thus reduce the angle of attack. The same as nose wheel aircraft, the tail should be raised at a proper time for the safety and reduce the ground run. It the tail is lifted too early or too late, too high or too low, not only will the roll distance and take off distance be increased, but also flight safety would be endangered. The speed and the height of lifting the tail are different in different aircraft.

b) Maintain the ground run direction

For propeller-driven aircraft, the main reason for aircraft yawing is due to the propeller side effects. During the ground roll, the reaction torque of the propeller is trying to make the aircraft tilt towards the opposite direction of propeller rotation, which causes the different forces of the two main wheels to ground, and thus induce different friction, the difference again causing the deflection torque to cg.

The slipstream of the propeller acts on the vertical tail also produces the deflection torque. When the front wheel or after wheel are lifted the propeller precession also causes aircraft deflexion. The rougher use of the throttle, the greater the side effects from the propeller. So to alleviate the secondary action of the propeller, the operation of throttling up the engine and pushing or pulling the joystick should be soft and appropriate. At the initial stage of rolling, due to the poor effectiveness of the rudder, the generally available methods to the running of travel direction are steering the nose wheel and difference braking the main wheel. In the last stage of the ground run the rudder should be used to

keep the roll direction of roll. With the increasing of the roll speed, the effectiveness of the rudder is also increased.

It is easy to maintain the ground run direction of jet aircraft, the reasons are: First, the jet airplane is also a nose wheel aircraft, while the front wheel aircraft has good directional stability during the ground run. Second, without the secondary action of the propeller, so in the process of throttling up the engine and lift up the nose wheel, the aircraft does not produce relative deflection.

Transition and climb stages

When the speed of aircraft is increased to a certain value, inducing the lift which is slightly larger than gravity, the aircraft can take off from the ground. Of the forces acting on the aircraft, the lift is greater than gravity and the pull of thrust is larger than drag.

The control actions to the nose wheel and tail wheel aircraft are different. To the aircraft which has front wheels, it is due to the pilot or autopilot's pulling action to produce a pitching moment which makes the aircraft running at two points. As the roll speed increases, the angle of attack and the pitching moment also increase. While pilot continues to push forward the stick to maintain the two points' attitude, the balance of original pitching moment is always destroyed with the speed increase. When getting to liftoff velocity, the angle of attack also has a tendency for increasing automatically. Therefore, it is generally to better to wait for the aircraft to lift off the ground automatically for aircraft which has a front wheel.

But it is not the case for those ones which have a tail wheel. When the aircraft gets to liftoff speed, it is generally required to increase the angle of attack and then lift from the ground. This is because the two points of running is made by pushing the stick forward, then the result of the down deflection of the elevator for tail wheel aircraft, the pitch downward moment increases with the augmented velocity, and it induces the decreases of the angle of attack. The pilot continually manipulates the stick to keep the two points running, but when

the liftoff speed is attained, the angle of attack also tends to decrease. Therefore, the stick should be pulled backward to increase the angle of attack to make the aircraft lift off the ground. It is important to know the correct liftoff time for tail wheel aircraft. Too early or too late off from the ground will all cause negatives to the flight. The friction of the wheel disappears after liftoff from the ground, the airplane will have a pitch up tendency, so the stick should be pushed forward to stop it. For propeller aircraft, the torque caused by wheel friction also disappears; the aircraft has a tendency of rolling towards the direction of propeller rotation, which should be suppressed by control surfaces.

The climb stage just after the transition stage, in which the thrust balances with the component of gravity and drag, the aircraft gets the maximum of ascend rate to get to the screen height. And then the takeoff is complete.

6.4.2 Takeoff performance of the Piper J-3 Cub model

The first stage of takeoff is the ground run, and at the initiate time of it, controlling the throttle to the maximal position and releasing the brakes. The aircraft begins to accelerate. When it reaches the rotation speed V_R the aircraft nose comes up, the aircraft keeps running on ground until decision (lift off) speed V_1. It is permitted to use $V_1 = V_R$, so in order to simplify the process $V_1 = V_R$ is used here. The velocity of the aircraft always keeps parallel to the ground at this stage. The stage after the ground run is transition stage, in which the aircraft leaves the ground and transfers to obstacle clearance stage, which uses the maximum climb gradient. The obstacle clearance is also called the screen height, 10.7m is used in this thesis to calculate performance. It is completed just when the aircraft gets to the screen height.

For light aircraft, the takeoff and landing area selection should be flexible, so here the shortest distance for taxiing or ground run is used to the take-off phase. Aircraft takeoff speed and distance should be the minimum possible. The criteria that determine the minimum value of V_2 for any calculation it is usual to assume that [20]:

$$V_2 = 1.2V_{stall}\text{, or } C_{L_2} = \frac{C_{L_{stall}}}{1.44} \quad \textbf{(6-1)}$$

The relationship between C_L vs α of the Piper J-3 Cub model is shown in figure 6-3. The lift coefficient for V_{stall} is about 1.813, So $C_{L_2} = 1.26$.

$$L = \frac{1}{2}\rho V^2 C_L S \quad \textbf{(6-2)}$$

Based on this equation and the data found in the pervious chapter, V_2 here is 10.89m/s.

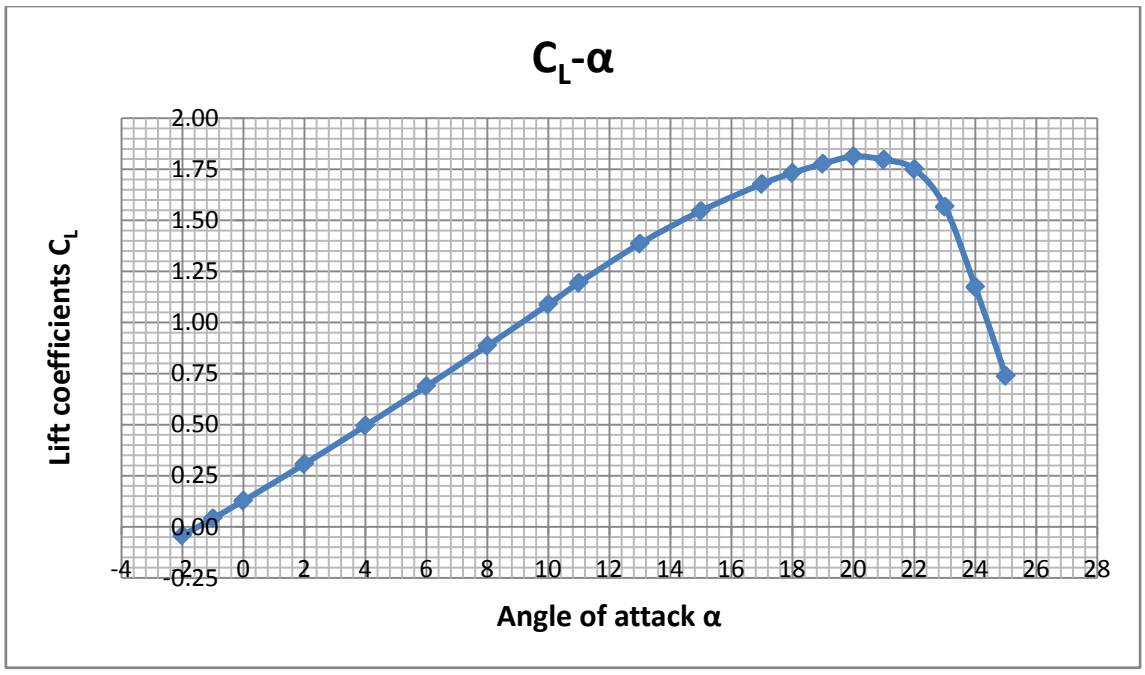

Figure 6-3 C_L vs α of the Piper J-3 Cub

The following formulae also come from [20] are used to calculate the distance for the stages of takeoff.

$$s_1 = \frac{W}{2g}\frac{V_1^2}{(F_N - D - \mu(W - L))} \quad \textbf{(6-3)}$$

$$s_2 = \frac{W}{2g}\frac{(V_2^2 - V_1^2)}{(F_N - D)} \quad \textbf{(6-4)}$$

$$s_3 = \frac{W}{2g}\frac{(V_2^2 - V_1^2)}{(F_N - D)} \quad \textbf{(6-5)}$$

$$\sin\gamma = \frac{F_N - D}{W} \quad \textbf{(6-6)}$$

The unknown parameters to calculate s_1 , s_2 and s_3 are F_N , D , L, μ and V_1. According to [21], thrust equal to 0.75mg for average transition speed is selected to estimate the take off distance (i.e. $F_N = 0.75mg$), and some hypothesis is taken here, for the difference between V_1 and V_2 is small, so $V_1 = 0.9V_2$ is used in the calculation, and the F_N is taken as a constant parameter in the calculation because the aircraft velocity is very low during takeoff. More details about D , L and μ selection can be found in [20]. The calculated distance value s_1 , s_2 and s_3 for the studied model are 6.82m, 1.80m and 12.73m individually, and the flight path during obstacle clearance stage is $\gamma_{1=}40.05^{\circ}$.

Table 6-1 Maximum takeoff flight path angle to different speed

V(m/s)	γ (degree)
15	44.2483
20	42.5947
25	34.4669
30	29.5626
33.33	25.9100

6.4.3 The following operations after screen height

For the small excess thrust piston propeller aircraft, the aircraft liftoff speed has still not attained the required climb speed, so it needs to accumulate the rate during level flight or shallow climb.

Therefore, a period of level flight or shallow climb may occur to some aircraft, it needs to push the stick forward to reduce the angle of attack after the screen

height, in order to make the airplane accelerate or climb. The aircraft should not climb with a larger angle of attack just after cleared off of the screen height. Too large a climb angle would affect the aircraft speed, and even endanger the safety. To reduce resistance and facilitate speedup, the aircraft should retract the gear as soon as possible, but the height for retracting the landing gear should not be less than screen height. To some high thrust to weight ratio aircraft which do not climb at maximum flight path angle should not be less than 5 meters because the aircraft may not climb at the maximum flight path angle and so may attain a larger speed when it reaches screen height. If too early, when the aircraft is near the ground, it could pitch down and may touch the ground again, thereby threatening security. If the pilot retracts the landing gear too late, as the aircraft speed is relatively high the landing gear will generate large drag, which causes difficulty to accumulate speed and may also cause landing gear retraction problems.

During the period of level flight or shallow climb, it is preferable to prevent aircraft sloping down because the low attitude of the aircraft and any small minus grade may cause aircraft slip down and crash into ground

When the aircraft has increased to the previously designated speed, the joystick should be moved smoothly to make the aircraft get into a steady state climb, which would not end until the aircraft has attained cruise altitude.

6.4.4 The takeoff stage design for the Piper J-3 Cub autopilot

In order to simplify the aircraft automatic control, the takeoff is divided into five stages in this thesis which includes ground run, liftoff, initial steady state climb, horizontal speedup and second steady state climb which will guide the aircraft climb to cruise altitude.

For the roll stage of the Piper J-3 cub, auto-throttle is used in the ground roll control, the given liftoff speed as an input and the throttle is controlled automatically by computer automatically. For getting a smooth liftoff, this stage is controlled by an altitude control loop and the altitude command changes as an exponential function to

a certain height, and then the aircraft climb with 25 degrees flight path angle to 50 meters. As can be seen from table 6-1, for different speeds the Piper J-3 has a good takeoff performance characters. For safety in automatic control, the maximum flight path angle is confined to 25 degrees for all speeds. After the airplane has climbed to 50 meters, then it would enter into level flight, the aim then of the level flight is to speedup. After the aircraft attained its predefined speed, it then enters into second steady state climb until it has obtained cruise altitude.

6.5 Landing

6.5.1 Stages of landing

Takeoff and landing always involves frequent changes of various parameters, but which also need accurate control. So they are not only challenging phases for the pilot the flying aircraft, but also for autopilot design. Compared with other flight phases, more accidents happen in the landing phase. According to a Boeing' report, 64.5% of the flight safety events are due to human factors and 3.2% is attributed to weather factors [22]. It is worth exploring automatic control for this phase.

The study in this thesis based on different GPS automatic landing. According to ICAO, the Instrument Landing System (ILS) is divided into three categories, and category **III** includes three subsections. The demands of Category III B are:

- Decision height lower than 15m
- Runway visual range between 75m and 200m

The differential GPS can satisfy the requirements of Category III B. Landing phase is divided into four stages in this thesis: approach, Descent (glide), flare, and taxiing. The full process of landing is showed in Figure 6-4.

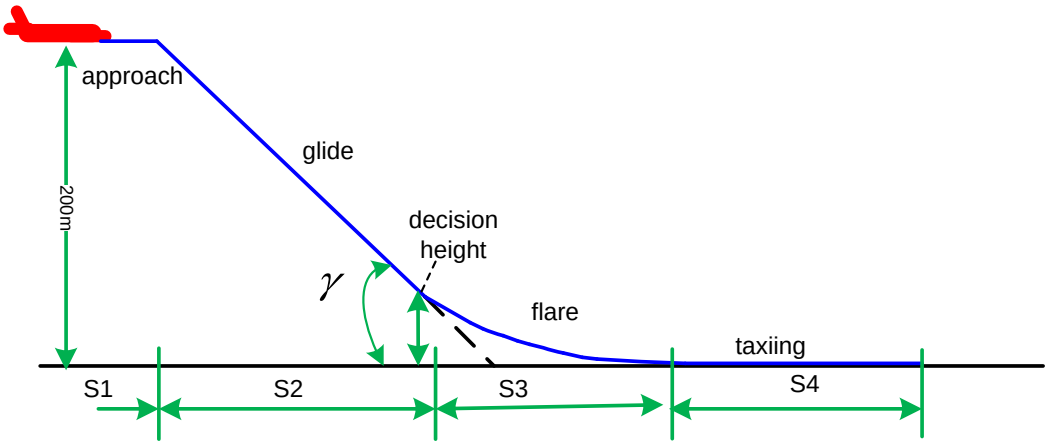

Figure 6-4 Procedure of landing

Approach stage

A good landing should be begun as a good approach. At the initial approach stage, aircraft from cruise altitude descend to the designated altitude (200m is used in this thesis), then fly at this height. The glide condition, when satisfied uses -2.5 to -6 degree to descend. Altitude hold control arithmetic is used at the beginning of this stage.

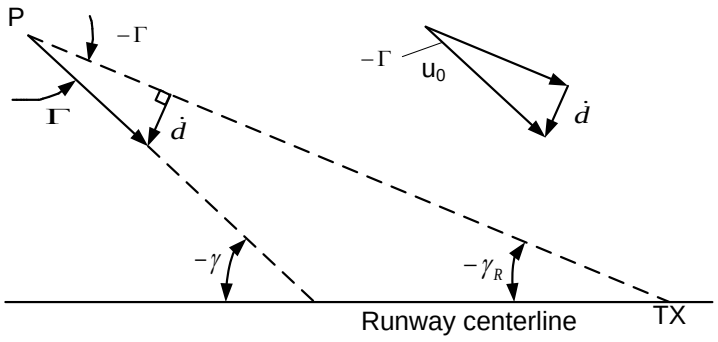

Figure 6-5 Glide slope control

$$\Gamma = \gamma - \gamma_R \quad \textbf{(6-7)}$$

$$\dot{d} = u_0 sin(\gamma_R - \gamma) \approx u_0(\gamma - \gamma_R) = u_0(\theta - \alpha - \gamma_R) \quad \textbf{(6-8)}$$

Along the glide gradient, pitch attitude and aircraft velocity must be controlled. The purpose of the autopilot is to follow the flight path and driven displacement back to zero. Equation (6-8) was joined to the aircraft model, with d as an additional state and γ_R as a model input, the final expression is given in equation (6-9).

$$\begin{bmatrix} \Delta\dot{u} \\ \Delta\dot{w} \\ \Delta\dot{q} \\ \Delta\dot{\theta} \\ \Delta\dot{h} \\ \Delta\dot{d} \end{bmatrix} = \begin{bmatrix} X_u & X_w & 0 & -g & 0 & 0 \\ Z_u & Z_w & u_0 & 0 & 0 & 0 \\ M_u + M_{\dot{w}} Z_u & M_w + M_{\dot{w}} Z_w & M_q + M_{\dot{w}} u_0 & 0 & 0 & 0 \\ 0 & 0 & 1 & 0 & 0 & 0 \\ 0 & -1 & 0 & u_0 & 0 & 0 \\ 0 & -1 & 0 & u_0 & 0 & 0 \end{bmatrix} \begin{bmatrix} \Delta\mathrm{u} \\ \Delta\mathrm{w} \\ \Delta\mathrm{q} \\ \Delta\theta \\ \Delta\mathrm{h} \\ \Delta\mathrm{d} \end{bmatrix} + \begin{bmatrix} \mathrm{X}_{\delta_e} & \mathrm{X}_{\delta_T} & 0 \\ \mathrm{Z}_{\delta_e} & \mathrm{Z}_{\delta_T} & 0 \\ \mathrm{M}_{\delta_e} + \mathrm{M}_{\dot{w}} \mathrm{Z}_{\delta_e} & \mathrm{M}_{\delta_T} + \mathrm{M}_{\dot{w}} \mathrm{Z}_{\delta_T} & 0 \\ 0 & 0 & 0 \\ 0 & 0 & 0 \\ 0 & 0 & -1 \end{bmatrix} \begin{bmatrix} \Delta\delta_e \\ \Delta\delta_T \\ \gamma_R \end{bmatrix} \quad \textbf{(6-9)}$$

Descent stage

When the descent command is given the altitude hold system is disconnected and the slide path tracking system is engaged in the same time. To control the aircraft at this stage, the velocity and glide slope need to be chosen and they should also be kept constant during the whole stage. A low value of aircraft speed can achieve a short distance landing. At a same time, a large angle of glide slope can reduce the landing time. Different from the cruise and climb phase, which control aircraft speed only by changing the thrust of engine, another possible way to control velocity in this stage is through adjusting the pitch angle. Even without the thrust of the engine, the airspeed might not be reduced greatly if it keeps a certain pitch angle. So the flight path angle needs to be selected beforehand, and then used it to decide appropriate aircraft velocity for descent at a certain thrust without stalling.

When the aircraft reaches a decision height, it checks for the state variables. If they are within an acceptable range, the decision is taken to continue with the

landing. Otherwise, the decision is taken to ‘go-around’. At the decision height, the control is switched over to altitude control for the flare.[24]

Flare stage

When the aircraft get to the decision height, the flight control system cuts the glide path tracking control system and enters into the flareout control system. When entering into this stage, the aircraft will increase angle of attack to reduce the descent rate, making the air speed vector parallel to ground then the flare stage finishes. The aim of this stage is to provide a smooth transition from the decision height to the runway. In this thesis, equation 6-10 is used to model the flare trajectory.

$$h_{com} = h_d e^{-\frac{t}{\tau}} \quad \textbf{(6-10)}$$

$$\dot{h}_{com} = -\frac{h_d}{\tau} e^{-\frac{t}{\tau}} \quad \textbf{(6-11)}$$

The initial of the flare sink rate is the same as the glideslope decent rate. It can be seen from the previous section that the straight line sink rate is $\dot{\mathrm{H}} = -1.05\mathrm{m/s}$, the time to achieve the exponential flare can be taken as 5τ, in order to confine the flare stage completed in about 20s, according to equation (6-10) and (6-11), 4 is selected for the time constant, thus the decision height h_d was selected as 4.2m. Flare trajectory profile is shown in figure 6-6.

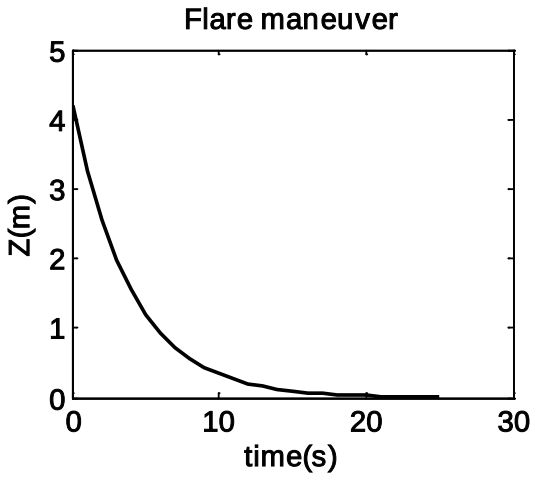

Figure 6-6 Flare trajectory profile

Taxiing stage

The final stage is taxiing, which begins just after flare. In this stage, the nose landing gear and rudder are used to control the heading; the throttle would be set in idle state.

The first three stages will be studied in this paper, and will design control law respectively.

6.5.2 Landing performance of the Piper J-3 cub

This section focuses on the performance of the Descent stage, and the boundary condition is just studied here. The forces acting on the aircraft with a full shut down of the engine would become the following.

$$\mathrm{F}_X = Lsin\alpha - Dcos\alpha - mgsin(\alpha + \gamma) \quad \textbf{(6-12)}$$

$$F_Z = mgcos(\alpha + \gamma) - Lcos\alpha - Dsin\alpha \quad \textbf{(6-13)}$$

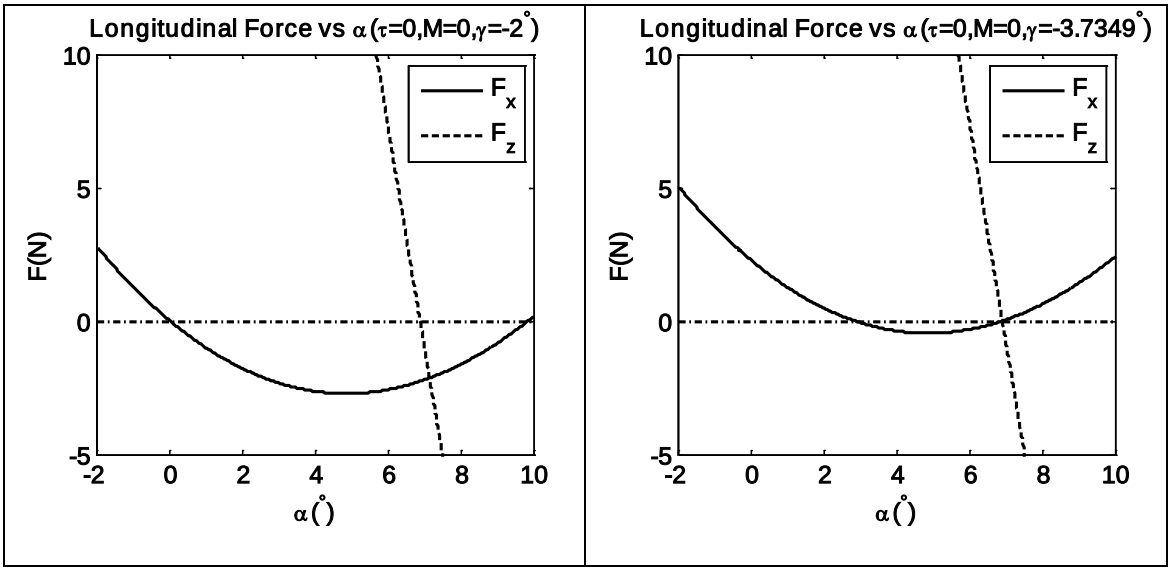

Figure 6-7 Longitudinal forces vs α

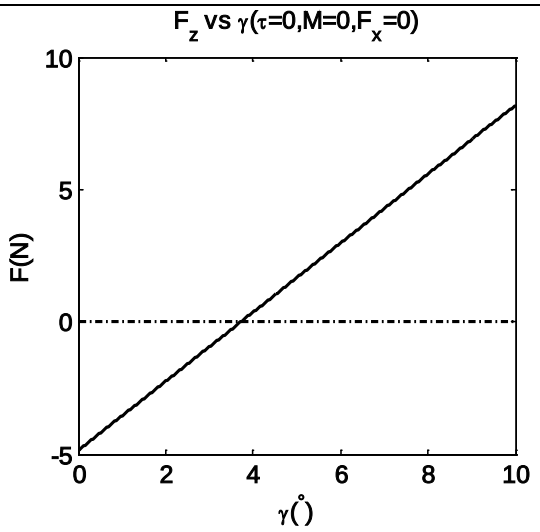

Figure 6-8 F_z vs γ at $F_z = 0$

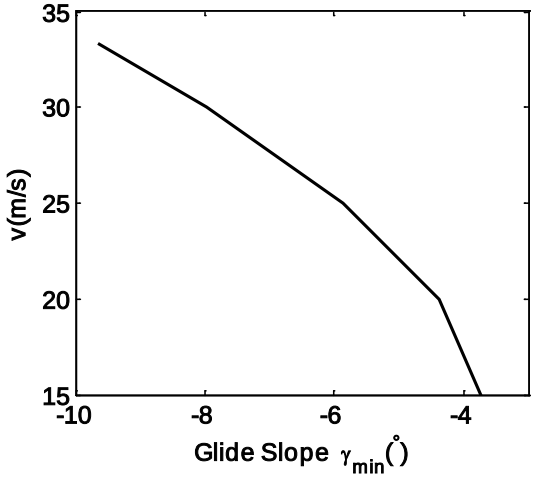

Figure 6-9 γ_{min} for different sink velocity

As can be seen from figure 6-9, the boundary of the flight path angle γ for zero thrust during descent are listed as follows: v=15m/s, $\gamma = -3.73^{\circ}$, v=20m/s $\gamma = -4.4^{\circ}$, v=25m/s $\gamma = -5.9^{\circ}$, v=30m/s $\gamma = -8.0^{\circ}$, v=33.33m/s s $\gamma = -9.7^{\circ}$.

For $\gamma = -4.0^{\circ}$, the corresponding speed is v=17.42m/s and when $\gamma = -5.0^{\circ}$, the speed is v=22.84m/s. So for safe reasons 20m/s velocity and -3 degrees flight path angle are selected for the descent stage, thus the downward speed is $\dot{H} = -1.05\mathrm{m/s}$.

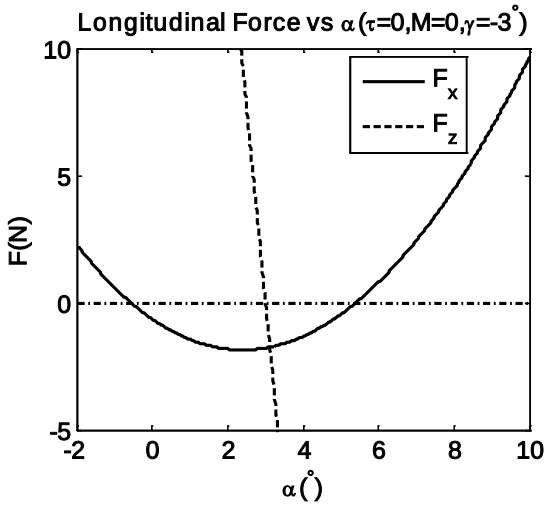

Figure 6-10 Longitudinal forces vs α (20m/s)

When $F_z = 0, \alpha = 3.0076^{\circ}, \delta_e = -5.4827^{\circ}, F_x = -1.7829N$

6.6 Control law design

With full throttle, the longitudinal takeoff controller needs mainly to control elevator deflection based on velocity and altitude. When the vehicle achieves the decision speed, controls the elevator deflection then control aircraft nose up and leaves the runway. It then tracks the ramp slope to climb to the screen height. The following stage controls aircraft climb with a certain flight path to get to a pre-specified altitude and then switches to an altitude controller. Altitude and velocity is the most important parameter in the cruise phase. During the landing descent stage aircraft should be exactly following the glide slope at a certain speed, so the flight path angle should be controlled, it is also true for the flight path angle control at the flare stage.

The basic control loops to longitudinal control are pitch angle control, altitude hold control and speed control. With these basic controllers, other kinds of more complex controller can be achieved easily. So in this part, pitch angle autopilot, altitude hold autopilot and auto-throttle are discussed and designed.

Pitch Attitude hold

Pitch attitude θ is a crucial variable in both the short and long period modes. Pitch-attitude-hold character can suppress the variations in velocity, height and pitch attitude, which is lightly damped and low-frequency. No matter in climb, level flight or descent, pitch attitude control system can be used to maintain aircraft at a given pitch attitude θ_c.

1) Pitch attitude controller design method one

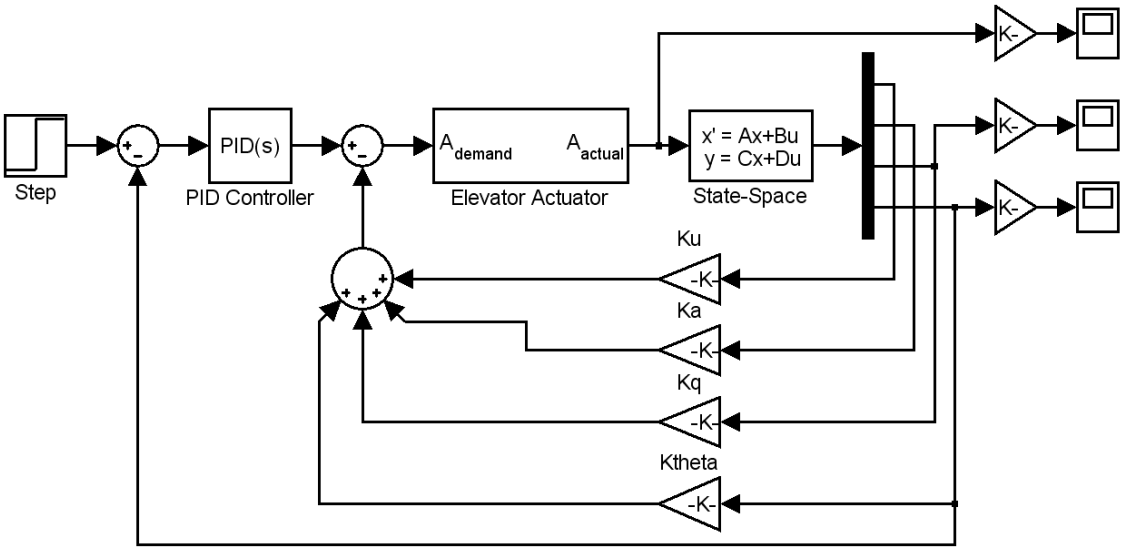

Figure 6-11 Pitch attitude Controller block one

As shown in Figure 6-11, the pitch attitude controller uses SAS as inner loop, PID controller as outer loop, thus the control law can be expressed as equation (6-14). Aircraft state-Space mode uses that data which havs been calculated by AVL and DATCOM. The elevator actuator uses a Second order Nonlinear actuator model from SIMULINK blocks, in which the Natural frequency is defined as 150hz, Damping ratio is 0.7 and the Maximum and Minimum deflection angle for elevators are 20 degrees and -20 degrees respectively. The simulation results of flight condition of 15m/s is given in figure 6-12. As the curves illustrates, the response of pitch angle of aircraft with slight overshoot and the setting time is about 10 seconds.

$$\delta_e = K_p(\theta_c - \theta) + K_I\frac{d(\theta_c - \theta)}{dt} + K_D\int(\theta_c - \theta)dt - K_u u - K_\alpha \alpha - K_q q - K_\theta \theta \quad \textbf{(6-14)}$$

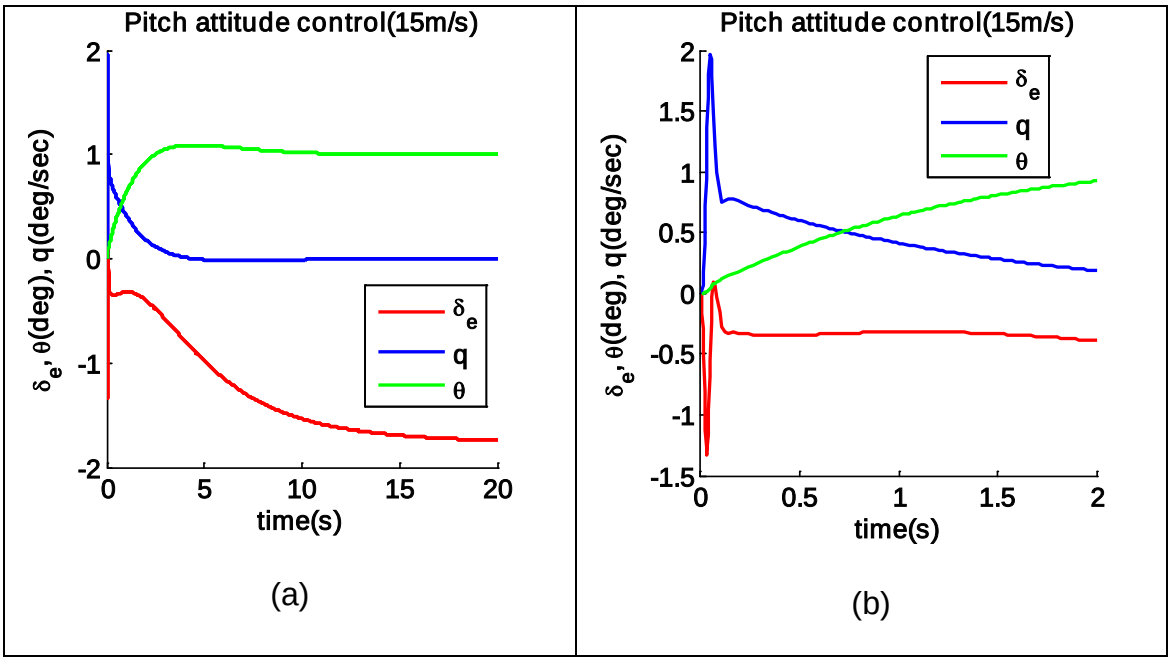

Figure 6-12 Unit step input response of Pitch attitude control

Controllers are also designed for other flight conditions, which include speed at 20 m/s, 25 m/s, 30 m/s and 33.33 m/s. The value for integral, proportional and rate control for choosing flight conditions are given in Table 6-2.

Table 6-2 Pitch attitude hold control law gains

Speed(m/s)	K_p	K_I	K_D
15	-0.3654	-0.0571	-0.3509
20	-0.1736	-0.0257	-0.2018
25	-0.1050	-0.0152	-0.1355
30	-0.0891	-0.0134	-0.0936
33.33	-0.0767	-0.0119	-0.0806

Figure 6-13 in curve form expresses changes of the parameters of the controller, which definitely illustrate that the controller changes with different flight conditions.

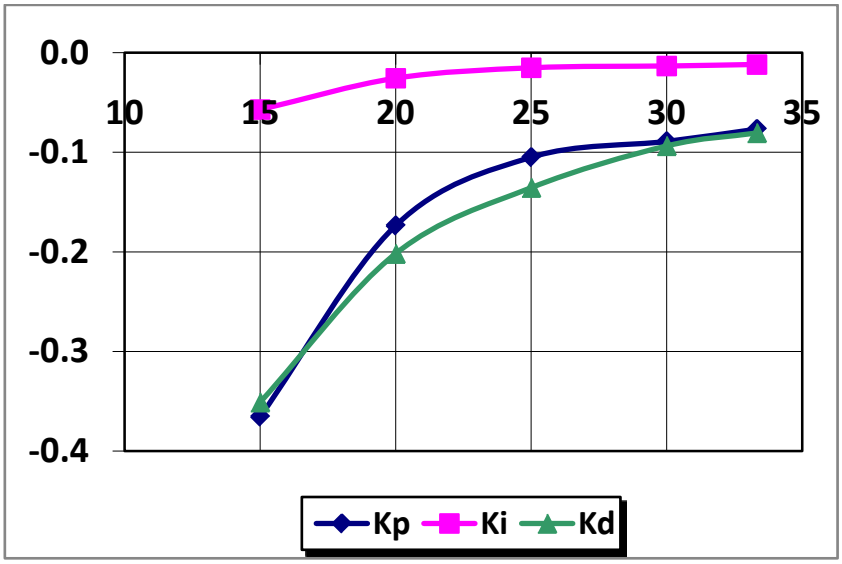

Figure 6-13 the change of gains with different speed

2) Pitch attitude controller design method two

The PID controller algorithm is only used for design of the pitch attitude control system, as shown in figure 6-14. Compared with the first method, it is without the inner loop so it only needs one signal feedback. Thus from the viewpoint of acquiring the full needed signal viewpoint, it has more reliability than the first one. The 15 m/s fight condition is designed here, the value for K_p, K_I and K_D are -1.2867, -0.0226 and 0.5462 respectively. As is shown in figure 6-15, this controller has a better performance than the previous one which with an acceptable overshoot and especially the setting time is about 3 seconds.

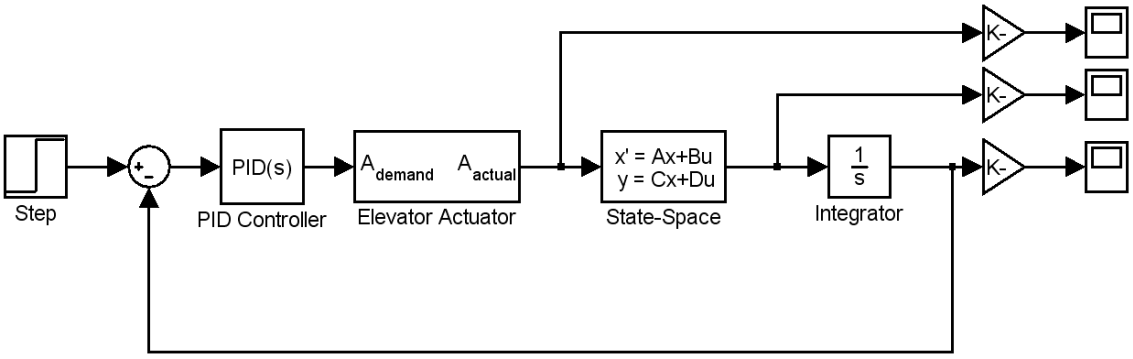

Figure 6-14 Pitch attitude Controller block two

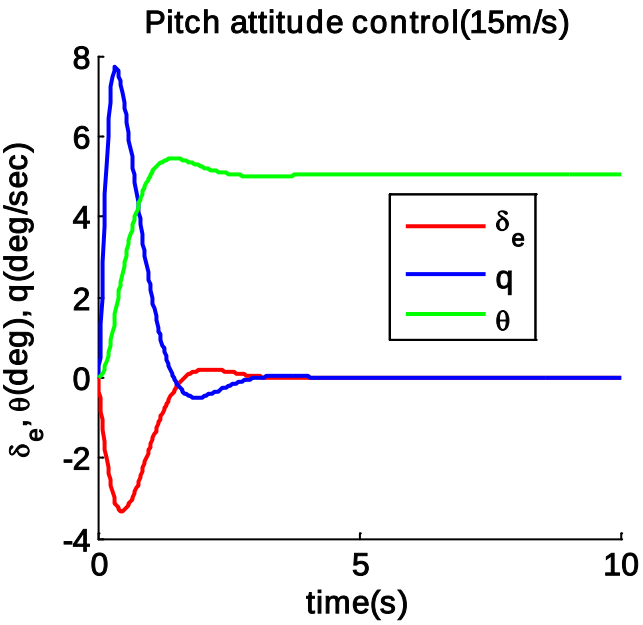

Figure 6-15 Responses to 5 degrees step command

Altitude hold control law design

The aim of altitude hold control is to control the aircraft flying at a certain given height. It has two operative modes: one is to automatically keep the aircraft at current altitude, called constant-level status; the other is automatically change the flying height until aircraft attains the pre-selected one, then keep flying at this height, called preselected altitude status. When the pilot inputs a height command to the autopilot, the aircraft automatically goes into climb (or glide) state. When closed to the commanded height, it then automatically maintains straight and level flight to keep the altitude.

Altitude hold and control cannot be achieved by pitch attitude hold and control algorithm. Pitch attitude control can be realized in the vertical wind, but the altitude would changes after seconds later. Deviation of the velocity vector would induce the drift of height. So generally altitude feedback should also be introduced to the longitudinal control loop. The pitch altitude hold control system is always used as the inner loop of the altitude hold control system, which will be seen in the next section.

An alternative way is used here in the case of missing height signal. The two methods can be used together to reduce faults in flight control system. The relationship between the velocity, pitch angle and angle of attack can be seen from figure 5-1. The function of height with these signals is built in the following equations.

$$\Delta\dot{h} = u_0 \sin(\Delta\theta - \Delta\alpha) \quad \textbf{(6-15)}$$

$$\Delta\dot{h} = u_0(\Delta\theta - \Delta\alpha) \quad \textbf{(6-16)}$$

$$s\Delta h(s) = u_0(\Delta\theta(s) - \Delta\alpha(s)) \quad \textbf{(6-17)}$$

$$\frac{\Delta h(s)}{\Delta\delta_e(s)} = \frac{u_0}{s}\left(\frac{\Delta\theta(s)}{\Delta\delta_e(s)} - \frac{\Delta\alpha(s)}{\Delta\delta_e(s)}\right. \quad \textbf{(6-18)}$$

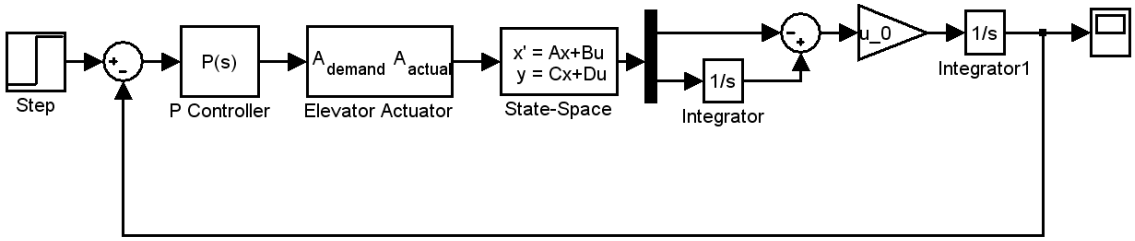

Figure 6-16 altitude hold control law 1

The transfer function form (not including elevator transfer function) is:

$$\frac{h}{\delta_e} = -\frac{72.54s^2 + 309s + 77.38}{s^4 + 19.91s^3 + 170.2s^2} \quad \textbf{(6-19)}$$

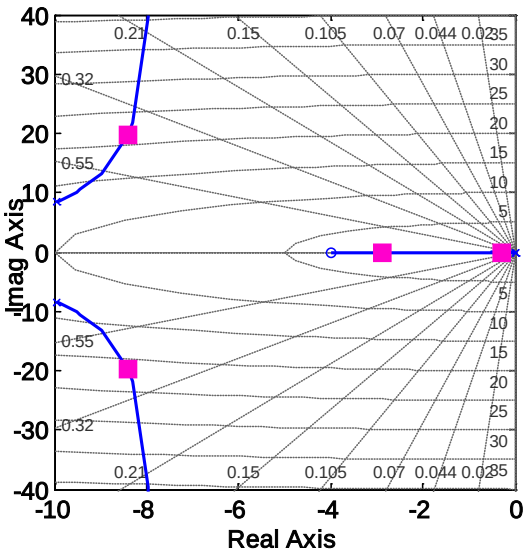

Figure 6-17 Root locus with K<0

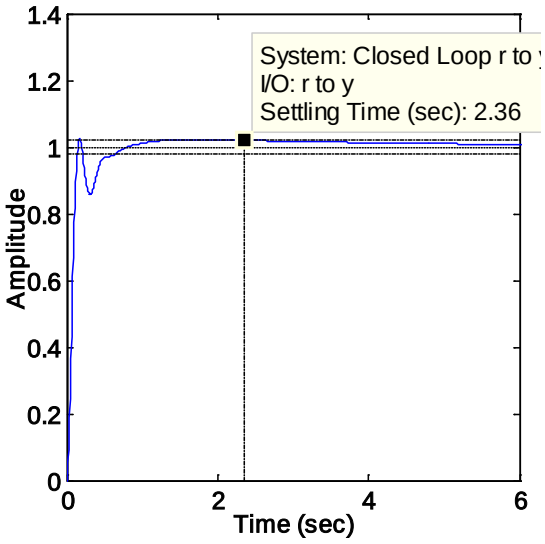

Figure 6-18 Unit step input response

The root locus design method is used here, which can be very easily achieved by the single input and single output toolbox of MATLAB. As figure 6-17 and figure 6-18 illustrate. By selecting the appropriate position of the close loop gains, the system response can also be adjusted, by this principle the parameter of controller P is selected. And as 6-18 describes, the controller has good response characteristics.

Longitudinal control law design integration

The above controller can achieve its own purpose very well, but with the process of achieving the predefined pitch angle or altitude, the speed of aircraft would also be changed. Of course, this phenomenon can be used for velocity control in some cases, but if one want to keep speed constant during or after this process, an auto-throttle should be introduced, which can also be used to adjust aircraft speed with the hold of altitude or attitude. The whole structure for the longitudinal controller designed in this thesis is shown in figure 6-19. The pitch controller can be used alone for the pitch hold control system or as an inner loop for the altitude hold control system. The auto-throttle is designed to

control the aircraft velocity, which can be used together with the pitch hold or altitude hold controller.

The dynamics of the elevator and throttle would typically be approximated by the first-order transfer function $\frac{1}{(1+\tau s)}$, the characteristic time for elevator and throttle are selected for 0.1s and 3s respectively. Elevator deflection rate confined in 60 degrees per second and the deflection range is restricted between plus-minus 20 degrees, the input for the inner loop of the altitude is also limited in [-3 25] degrees. The response speed of elevator and elevator are all confined in between plus-minus 20 degrees.

Based on those models above, the control law is designed for 15m/s flight condition, and the parameters of controller were finally selected as follows.

Pitch altitude PID controller, $\mathrm{K_P} = 3.491, \mathrm{K_I} = 2.0, \mathrm{K_D} = 0.3.$

Altitude hold P controller, $\mathrm{K_P} = 0.1317$

Auto-throttle PID controller, $\mathrm{K_P} = 0.0206, \mathrm{K_I} = 0.0001, \mathrm{K_D} = 0.0535.$

The flight simulation condition is as follows: 5 degrees step input signal to pitch altitude hold control, 10 meters height change to altitude hold control and confined the altitude hold in 5 degrees, they all simulated with the speed hold loop respectively; 1 m/s velocity changes step input to Auto-throttle control and with Altitude hold system works.

The simulation results for the performance of pitch angle hold controller, auto-throttle controller and altitude hold controller are shown in figure 6-20~22 respectively. As figure 6-20 illustrated, the overshoot of pitch attitude hold control is about 10%, and the setting time is about 7 seconds. With a bigger pitch angle, the aircraft would ascend so it needs more lift; As a result the angle of attack is also changed 1 degree, which results in the increase of lift coefficients, the elevator also deflects to a new position, which is used to keep a new pitch moment balance. Figure 6-21 clarifies the altitude change with the step command input, after receiving the command aircraft pitch quickly to get pitch boundary given previously, then to climb at a certain rate of ascent to the command altitude. When close to or having attained the desired height, to hold

at that altitude, the pitch angle changed fairly smoothly during the whole process. The elevator is deflected during the climb time and is retracted to its original position when the desired altitude is attained, aircraft velocity is also changed during the climb range and is also recovered. Figure 6-22 shows with the change of speed during certain altitudes, the changes of other parameters. With the increase of speed, the aerodynamic pressure is also increased, which means it needs less lift coefficients to support its weight to keep the flight level, so the aircraft adjust angle of attack as shown in figure 6-22 (c). And the elevator changed to keep the moment balance. But it can also be seen that after attaining the new speed, the throttle nearly returns to its original position, which means the drag is not changed obviously between the two speeds.

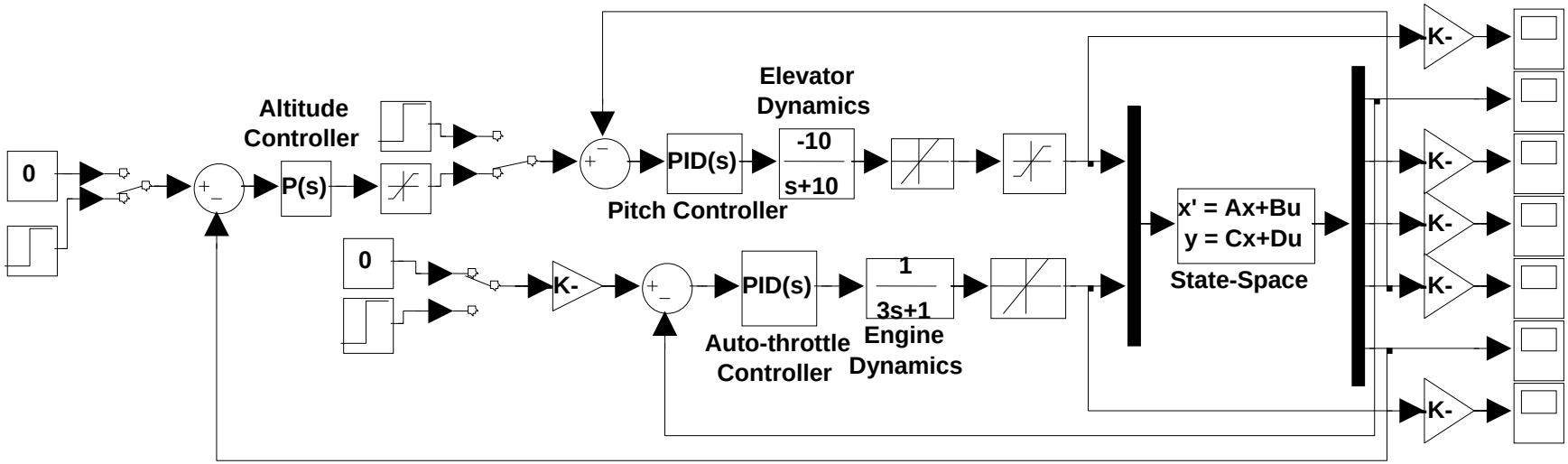

Figure 6-19 the Piper J-3 Cub longitudinal control block diagram

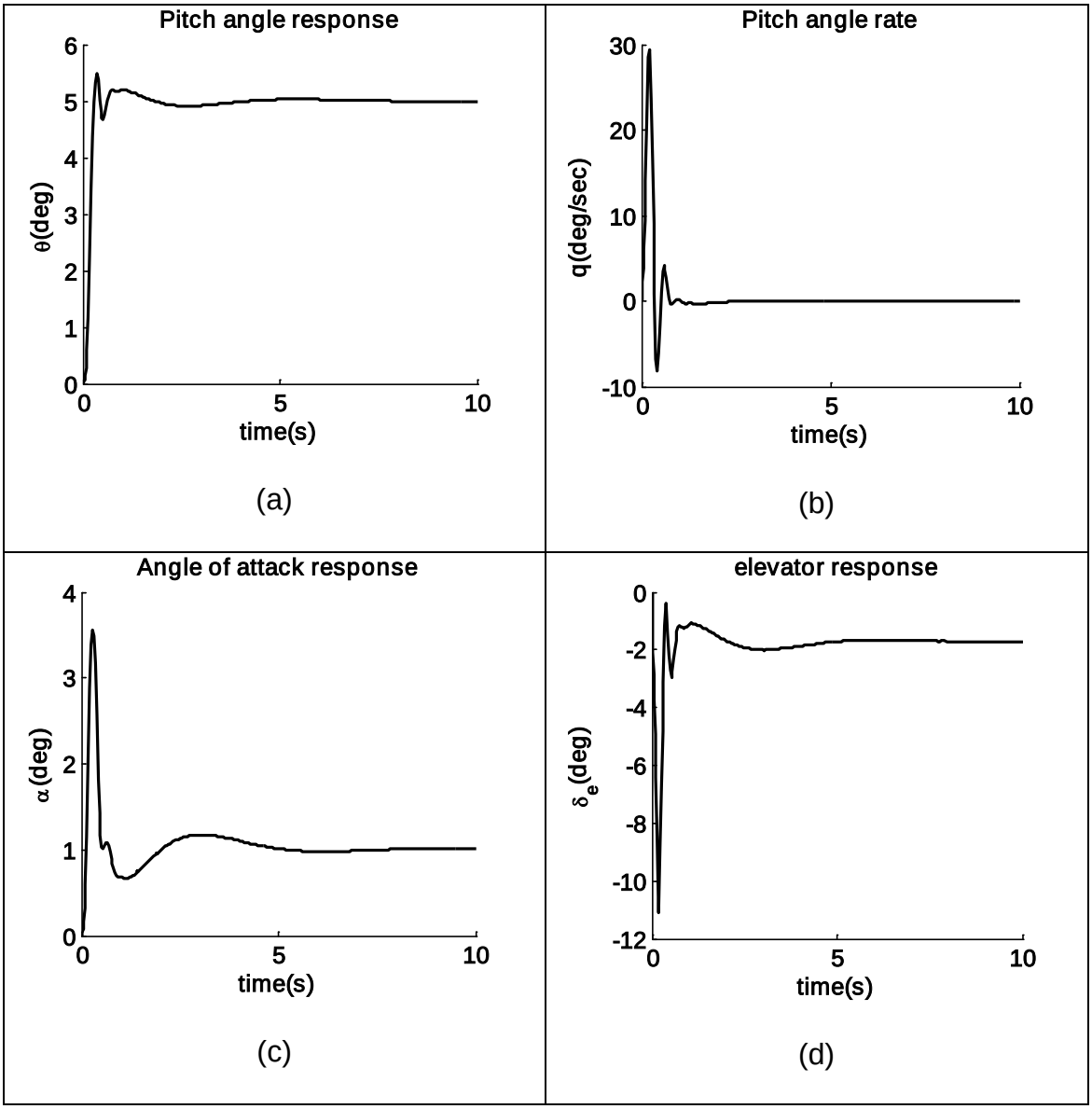

Figure 6-20 Pitch angle control

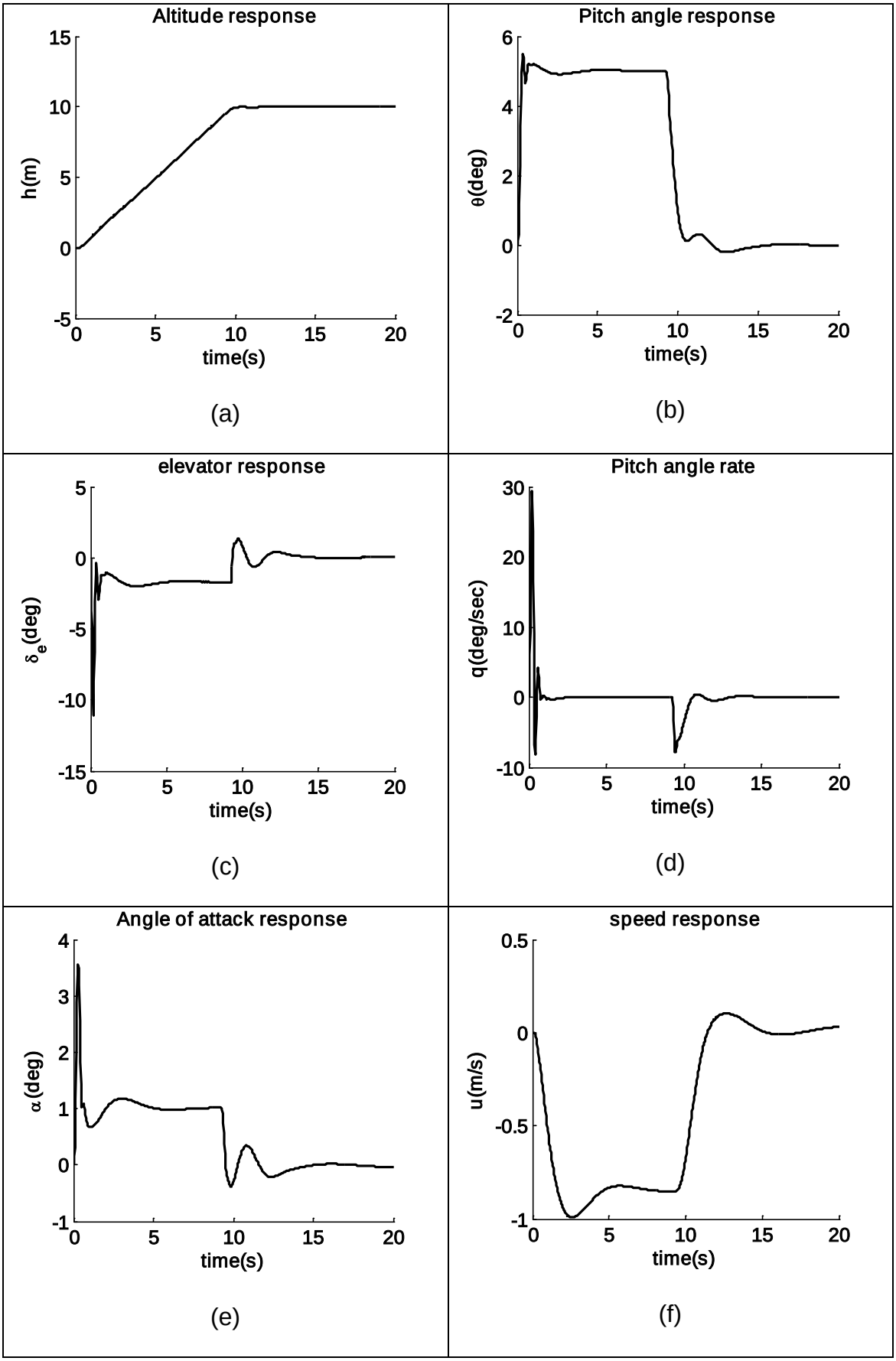
Altitude response
h(m)
time(s)
(a)
Pitch angle response
θ(deg)
time(s)
(b)
elevator response
δe(deg)
time(s)
(c)
Pitch angle rate
q(deg/sec)
time(s)
(d)
Angle of attack response
α(deg)
time(s)
(e)
speed response
u(m/s)
time(s)
(f)

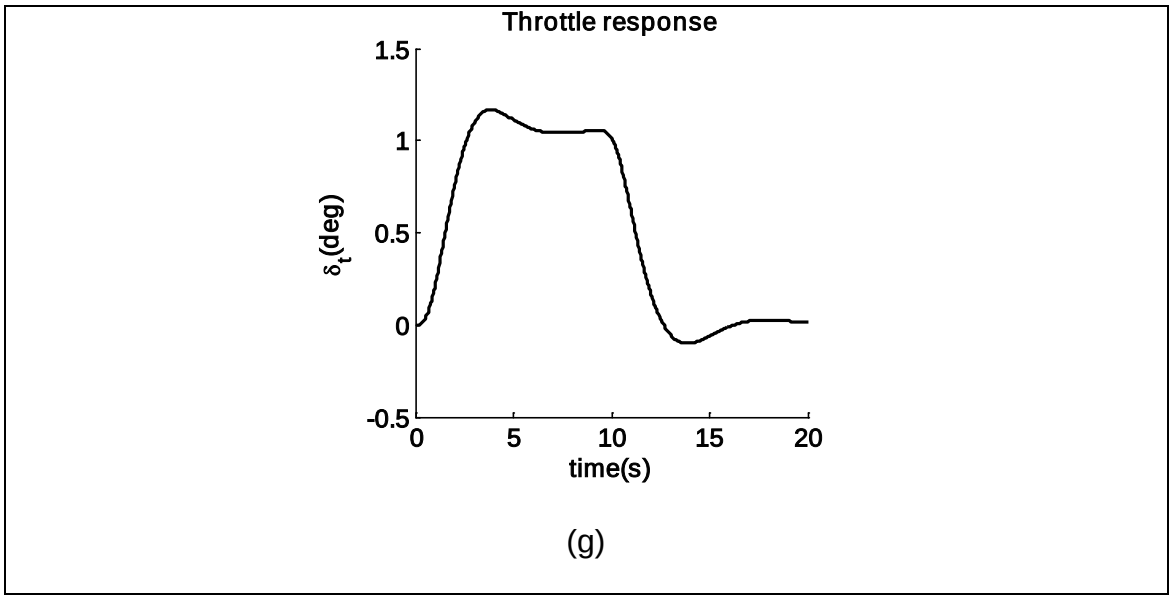

(g)

Figure 6-21 Altitude Control

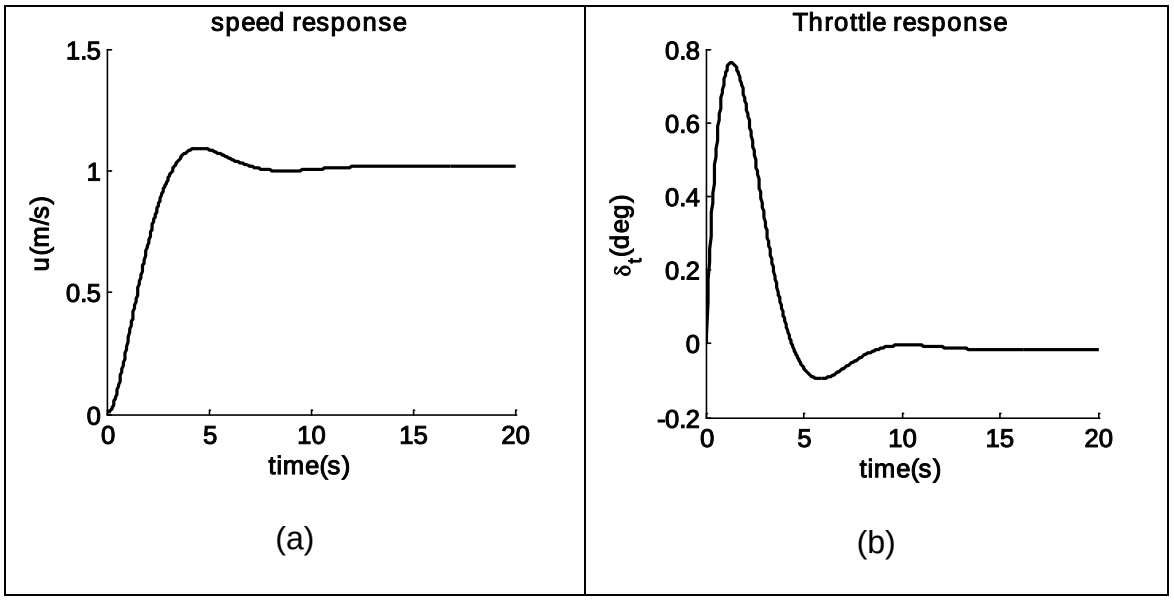

(a) (b)

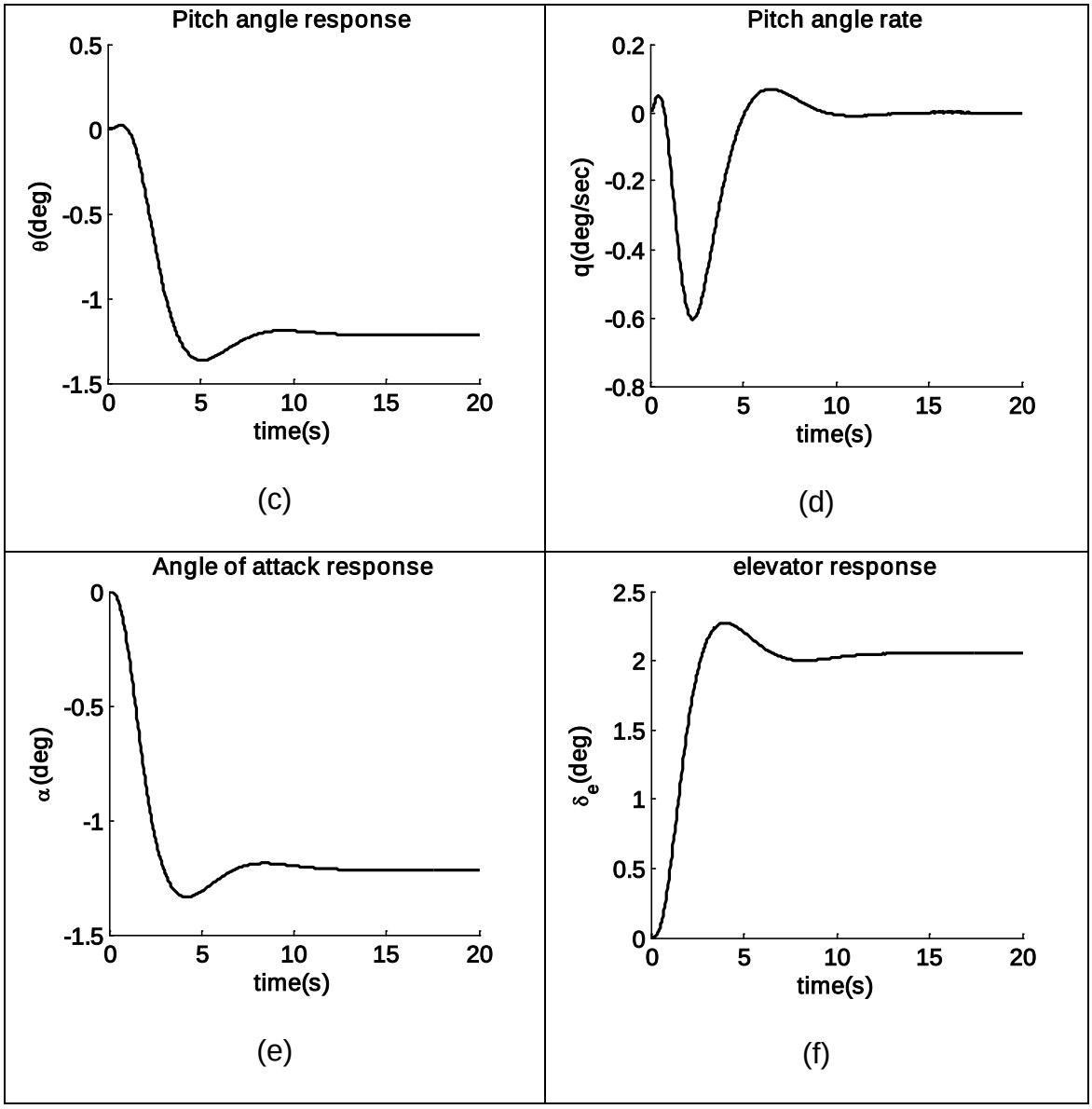

Figure 6-22 Speed control

6.7 Chapter Summary

This Chapter starts with performance index requirements of the Automatic Flight Control System, and then designs a flight profile for the Piper J-3 Cub autopilot. The aircraft's takeoff and landing phases need to be controlled with high accuracy, so the trajectory characteristics of these two phases and the guidance law is studied in details. The takeoff and landing are divided into several stages, the control strategy is invested according to the special characteristics of each stage, in order to safely control and make the utmost of

the Piper J-3 Cub performance, it takeoff and landing performance are also calculated. Finally, research of control law design is done in longitudinal axis to control the aircraft automatically. Multi-design method used to design pith hold and altitude hold autopilot, and the results have been compared. They are then integrated and combined with speed control to illustrate the effectiveness of combined control. The simulation in MATLAB shows that the overshoot of pitch control response, altitude control response and speed control response are all much less that 20%, and the system has rapid response and high precision. Therefore, the design satisfies the PI requirements.

7 LATERAL DIRECTIONAL AUTOPILOT DESIGN

The longitudinal control law is discussed and designed in chapter 6, by assuming aircraft only move up, down and forward in its symmetry plane. For the symmetrical characteristics of these motions, it is very convenient to put to one side in any situation where this is not the case. In this chapter, lateral-directional control is studied, which involves rotations about two axes at once, as well as movement of the centre of gravity away from the undisturbed flight path.

7.1 Ground trajectory guidance algorithm

The track following strategy that is similar to [23] is adopted in this thesis for ultra-light aircraft lateral track control, as shown in figure 7-1. The desired flight path for aircraft is from P1 to P2, the current relative distance of vehicle is known as (X_{track}, Y_{track}). The control algorithm is aimed to control the aircraft ground velocity direct toward the point C. A parameter k is predefined in order to decide the intercept point C, which is equal to $(1-k)X_{track}$ at any instant time. So, in order to fly the ideal trajectory according to the given strategy, the aircraft must always follow the heading (k=0.2 is selected in this thesis):

$$\psi = \psi_0 + \operatorname{atan}\left(\frac{kX_{track}}{Y_{track}}\right) \qquad \textbf{(7-1)}$$

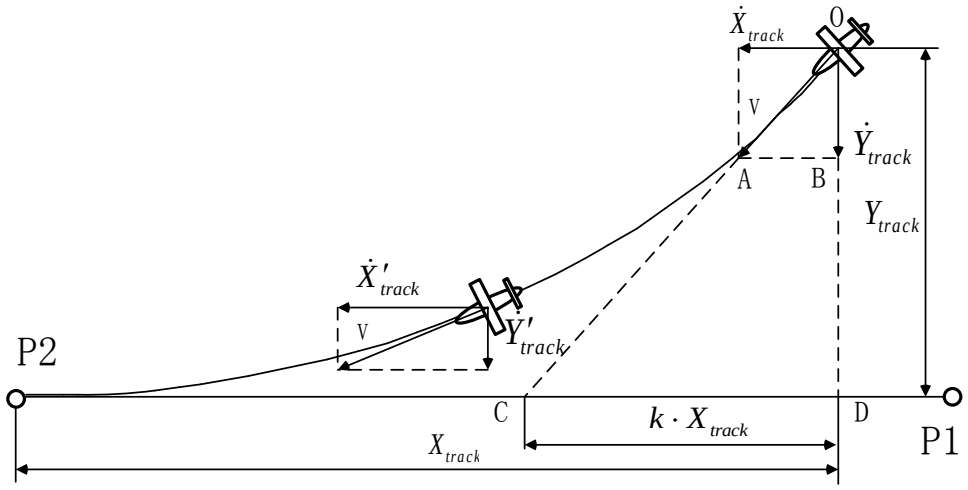

Figure 7-1 ground trajectory following

7.2 Decrab control

Control of aircraft landing in crosswind is a challenging job, for airplane is impressionable to the direction of the wind during flight. Aircraft should employ a yaw action to keep the flying direction in the case of crosswind. This pose may cause safety problems when landing an aircraft, for the safe handling of the landing gear demands the alignment of the body and the speed of the airplane involving Sideslip, Crab and Decrab. The Decrab maneuver will be discussed in this thesis.

Aircraft flying position and flying direction during to a crosswind is maintained to some extent crabbing pose during approach and glide stage, so it would be a little inclined to the runway centreline. Thus, just ahead of the flare, the rudder should be used to reduce the skew, and at the same time aileron should be used to keep a wings-level attitude, thus to align the airframe, bank angle and aircraft speed with the runway.

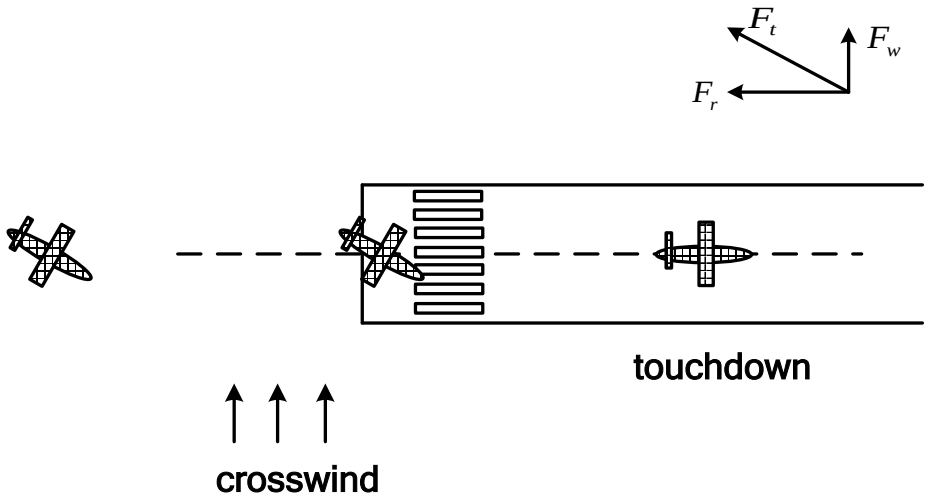

Figure 7-2 Decrab manoeuvre during landing

7.3 Control law design

7.3.1 Coordinated turn

Coordinated turn is aircraft changing flight direction in horizontal plane, assuring $\beta = 0$ to minimize the coupling between roll and yaw, and holding constant

altitude. In fact, aircraft roll and yaw is not independent, but has a close relationship, and couples each other. Therefore, aircraft longitudinal axis is different with velocity vector during aircraft turn maneuver, much sideslip would occur. The existence of sideslip angle would not only increase drag, but also makes pilot feel uncomfortable. Coordinated turn is a method which guarantees aircraft safety, softness and comfort.

The condition of coordinated turn

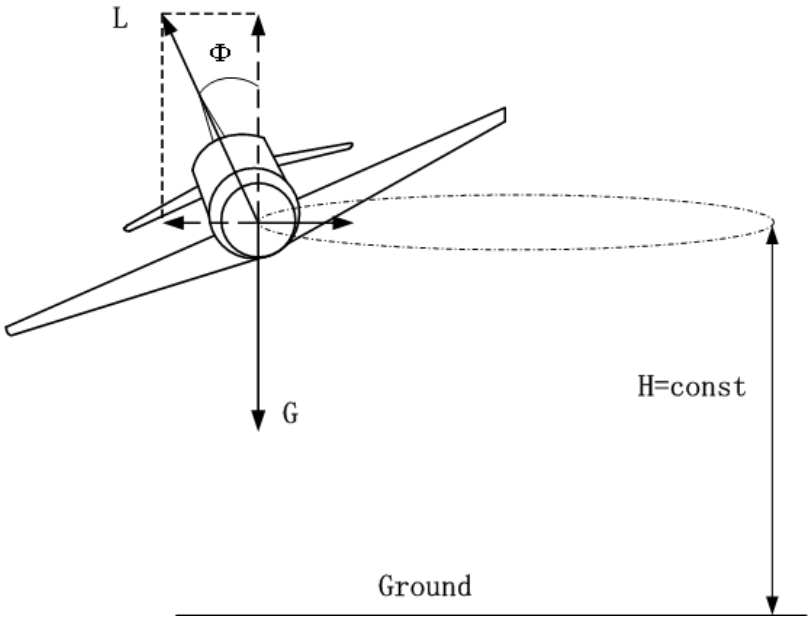

Figure 7-3 the forces on aircraft during coordinated turn

As which is illustrated in figure 7-3, the forces balanc during aircraft coordinated turn in horizontal and vertical direction are:

$$G = L\cos\Phi \tag{7-2}$$

$$m\dot{\psi}V = L\sin\Phi \tag{7-3}$$

Thus the equation for coordinated turn is:

$$\dot{\psi} = \frac{g}{V}\tan\Phi \tag{7-4}$$

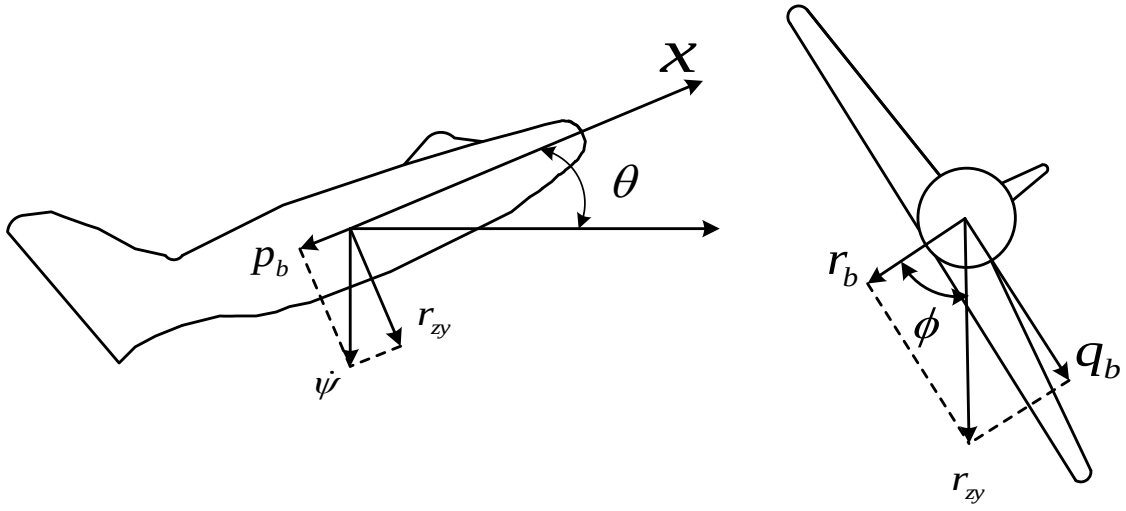

Figure 7-4 the components of $\dot{\psi}$ in aircraft body axes

When control aircraft co-ordinately turn, yaw angle rate is upright the ground. In order to holding altitude and maintaining constant yaw angle rate $\dot{\psi}$, aircraft would exists pitch angle θ and roll angle ϕ . Roll angle rate $p_b = \dot{\psi}\sin\theta$ and $r_{zy} = \dot{\psi}\cos\theta$ can be gotten when analyzing the components of yaw angle rate $\dot{\psi}$ in x and y axes of aircraft body. In generally, the θ and ϕ are small, so roll angle rate $p_b = \dot{\psi}\sin\theta \approx 0$, its effects to coordinated turn can be neglected; Yaw angle rate $r_b = \dot{\psi}\cos\theta\cos\phi$ and pitch angle rate $q_b = \dot{\psi}\cos\theta\sin\phi$ can be gotten when analyzing the component of yaw angle rate $r_{zy} = \dot{\psi}\cos\theta$ in z and y axes of aircraft body.

After combined with the coordinated turn equation (7-4), yaw angle rate r_b and pitch angle rate q_b are as follows.

$$r_b = \dot{\psi}\cos\theta\cos\phi = \frac{g}{V}\tan\phi \qquad \textbf{(7-5)}$$

$$q_b = \dot{\psi}\cos\theta\sin\phi = \frac{g}{V}\cos\theta\sin\phi\tan\phi \qquad \textbf{(7-6)}$$

Therefore, to complete constant altitude coordinated turning, aircraft should be controlled by aileron, elevator and rudder and the same time.

Control scheme

Coordinated turn control law is designed in this thesis as follows:

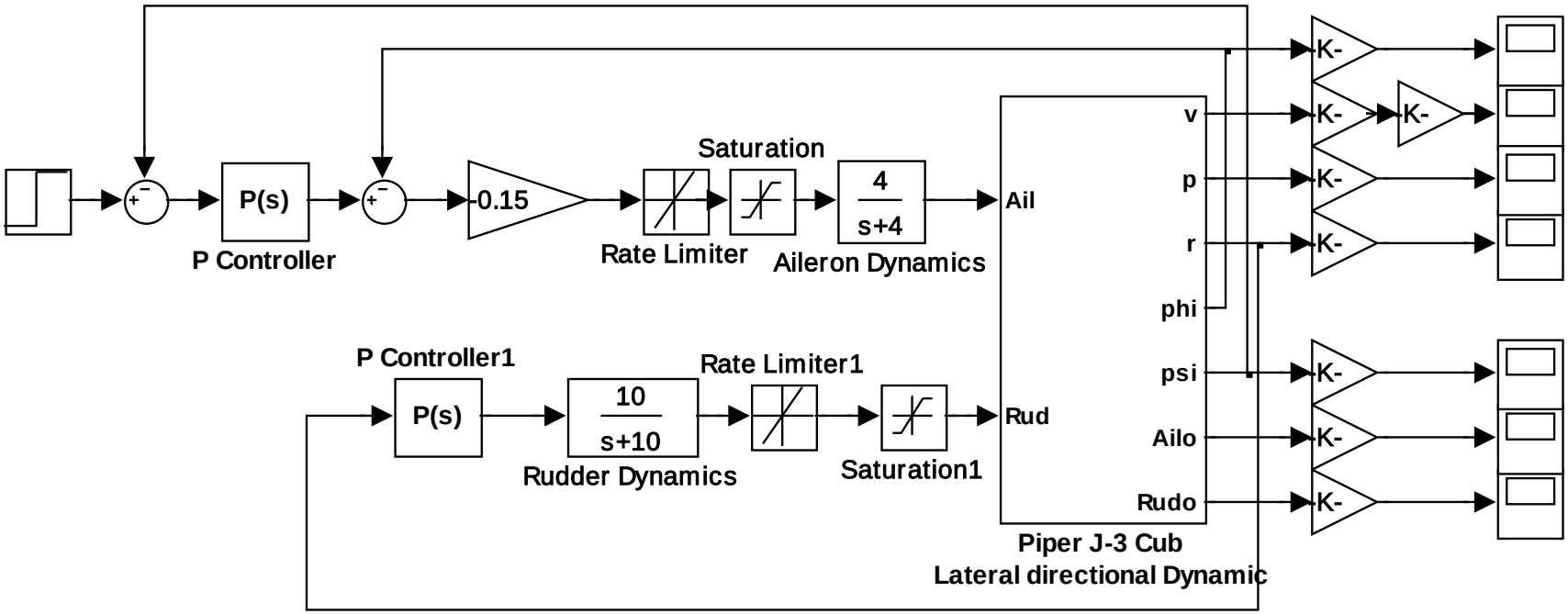

Figure 7-5 wing level lateral control block diagram

In order to achieve constant altitude during coordinated turn, roll angle ϕ can be brought as a feedback to altitude hold feedback to compensate lift loss. It would not be discussed in details in this thesis.

Wing level lateral controller parameters are as follows: P controller Kp is selected as 1.23. P controller 1 Kp is selected as -1.32. The lateral responses for 20 degrees coordinated turn are shown in figure 7-6.

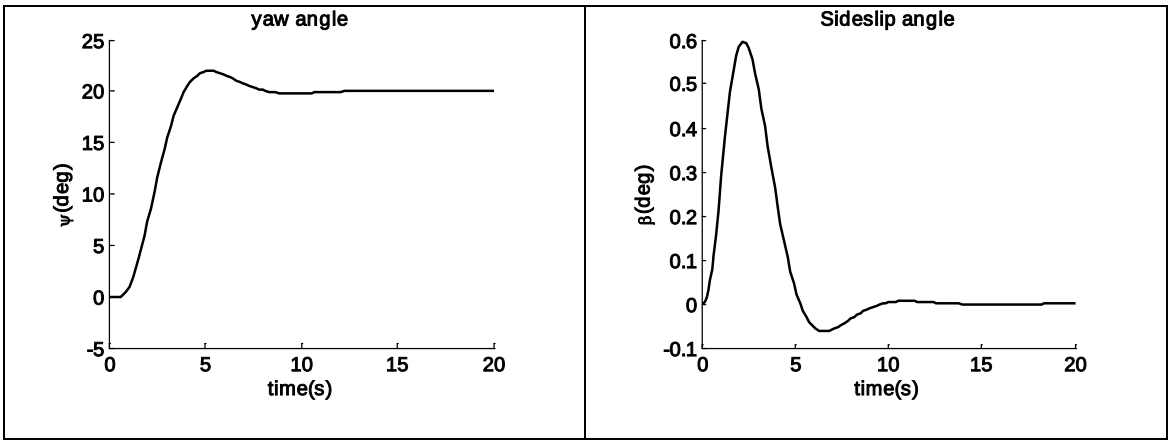

Figure 7-6 wing level lateral control response

7.3.2 Decrab control

Decrab control method 1

The lateral-directional axis has to control aileron and rudder. They are coupled with each other, the aileron is used to roll control is studied first, to which the control block is shown in figure 7-7. The parameters are selected by the root locus method with the help of the SISO toolbox of MATLAB. The Kp is selected as -0.15 and the forward gain is chosen as 0.9091. The maximum of the aileron deflection plus-minus 20 degrees and with the maximum deflection rate 60 degrees per second is selected in this block. The responses for 15 degrees roll angle step input are shown in figure 7-8. It illustrates that the roll response very quick with the setting time of less than 5 seconds and at the same time the aircraft has a constant yaw rate. Therefore, this phenomenon is used to design the Decrab control at the next step.

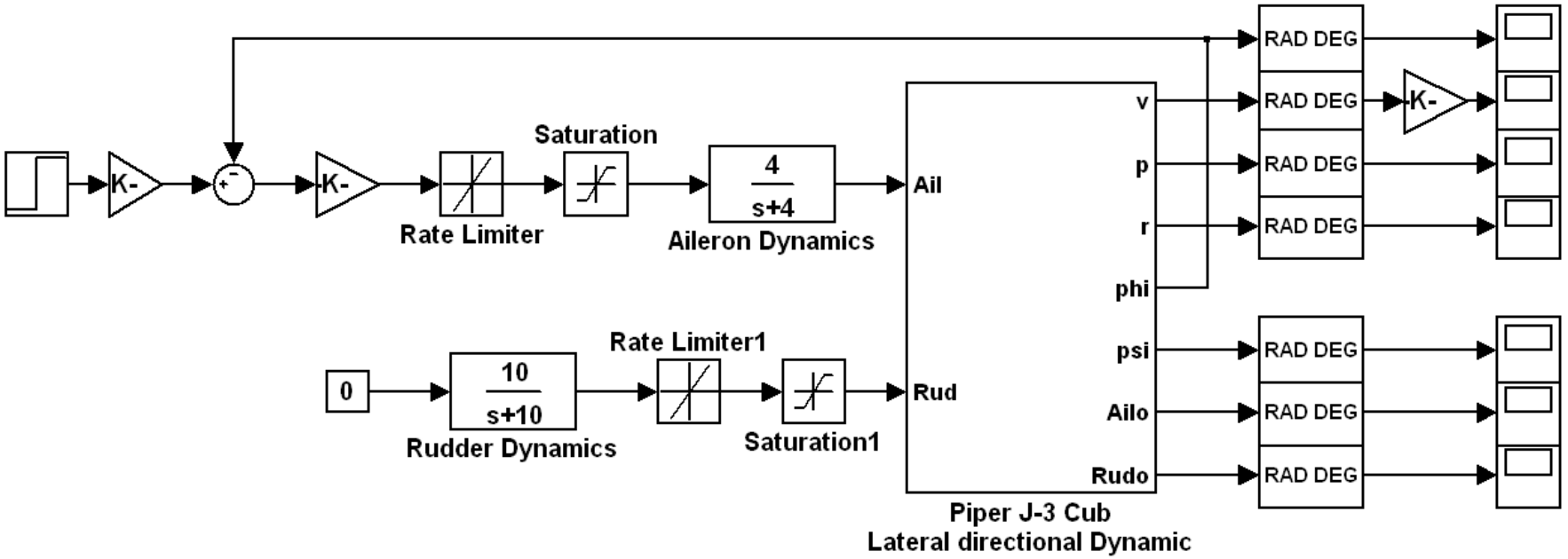

Figure 7-7 Roll controller block diagram

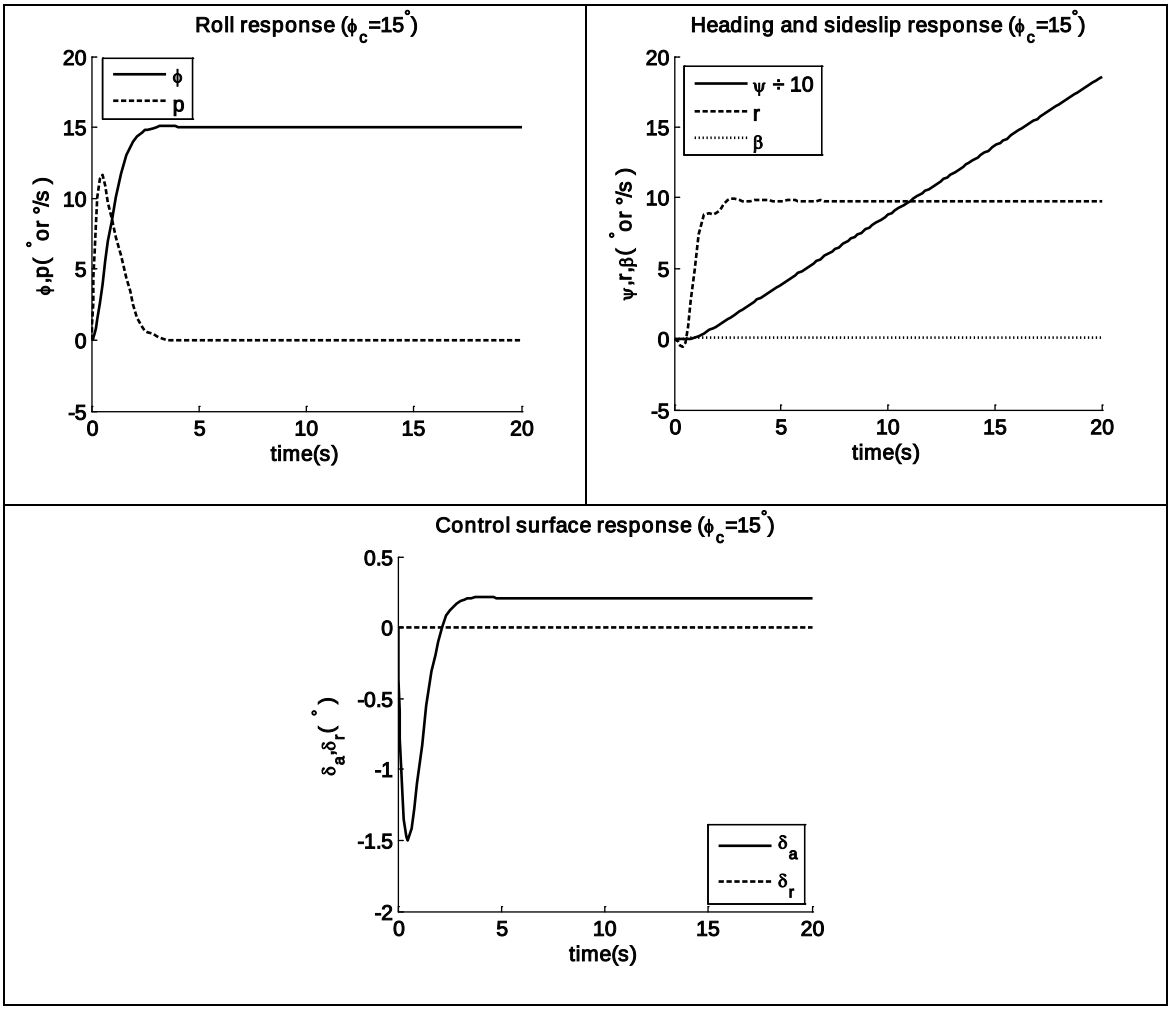

Figure 7-8 Roll control response

Using the roll controller as the inner loop, a Decrab controller is designed in Figure 7-9 using P algorithm. The parameter for Kp is 0.6487. The responses for 15 degrees yaw step input is given in figure 7-10. With the aileron deflection and without the movement of the rudder, aircraft Decrab control has good performance.

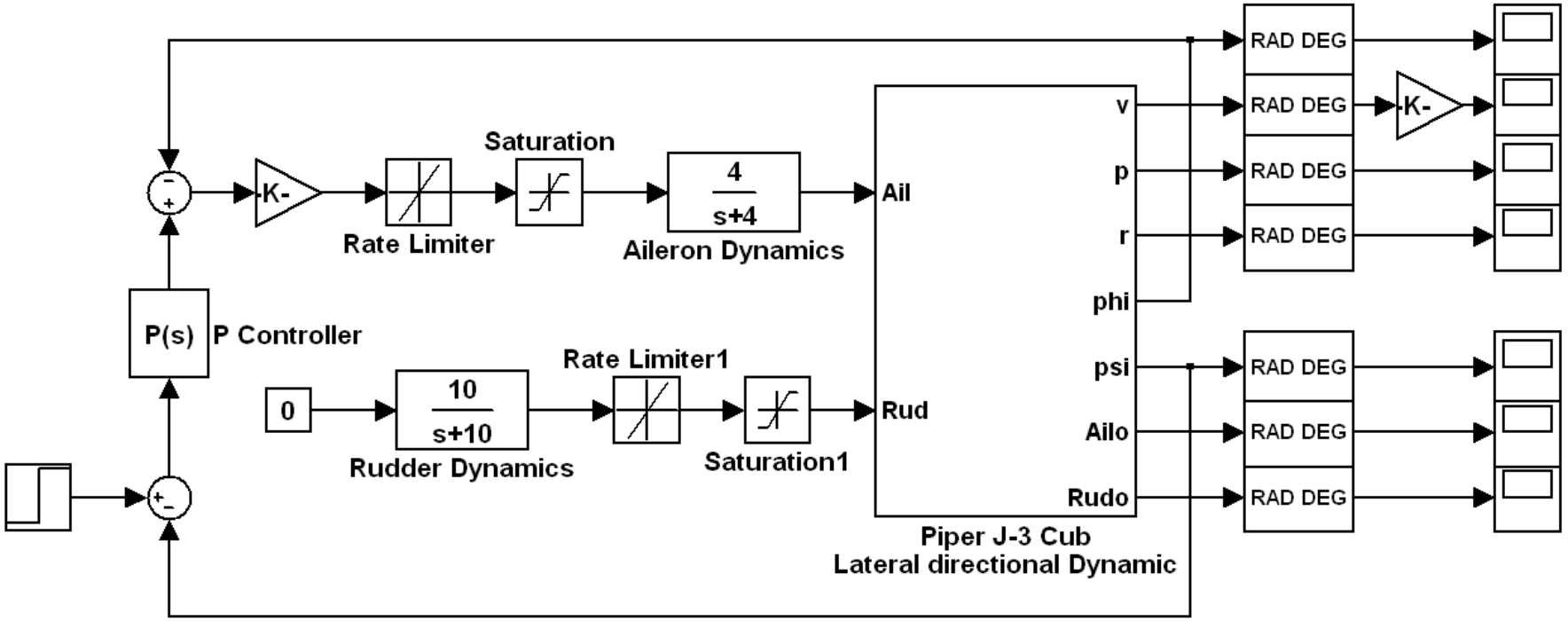

Figure 7-9 Decrab control law block diagram (controlled by aileron)

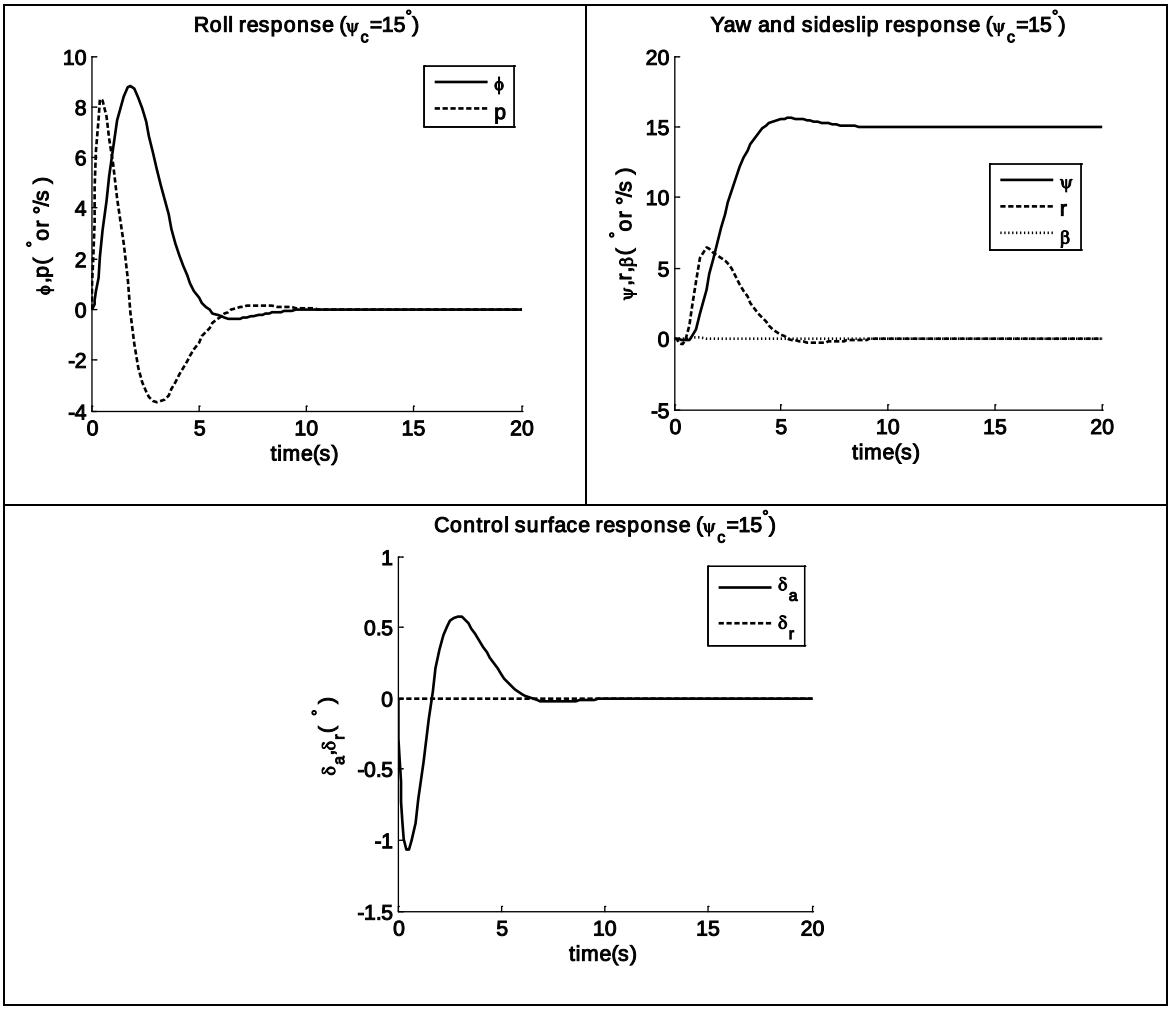

Figure 7-10 Decrab control response (controlled by aileron)

Decrab control method 2

An alternative way for Decrab control is designed in this thesis and is shown in figure 7-11. Thee roll controller to the rudder that is designed above but with zero input, the yaw control uses the rudder with the heading feedback. The controller design uses the PID algorithm; the Kp, Ki and Kd are 0.6487, 0.0021 and -1.2679 respectively. Using this control law, the aileron is also deflected together to assist the rudder to achieve the yaw control. The yaw command response can be accomplished in about 15 seconds.

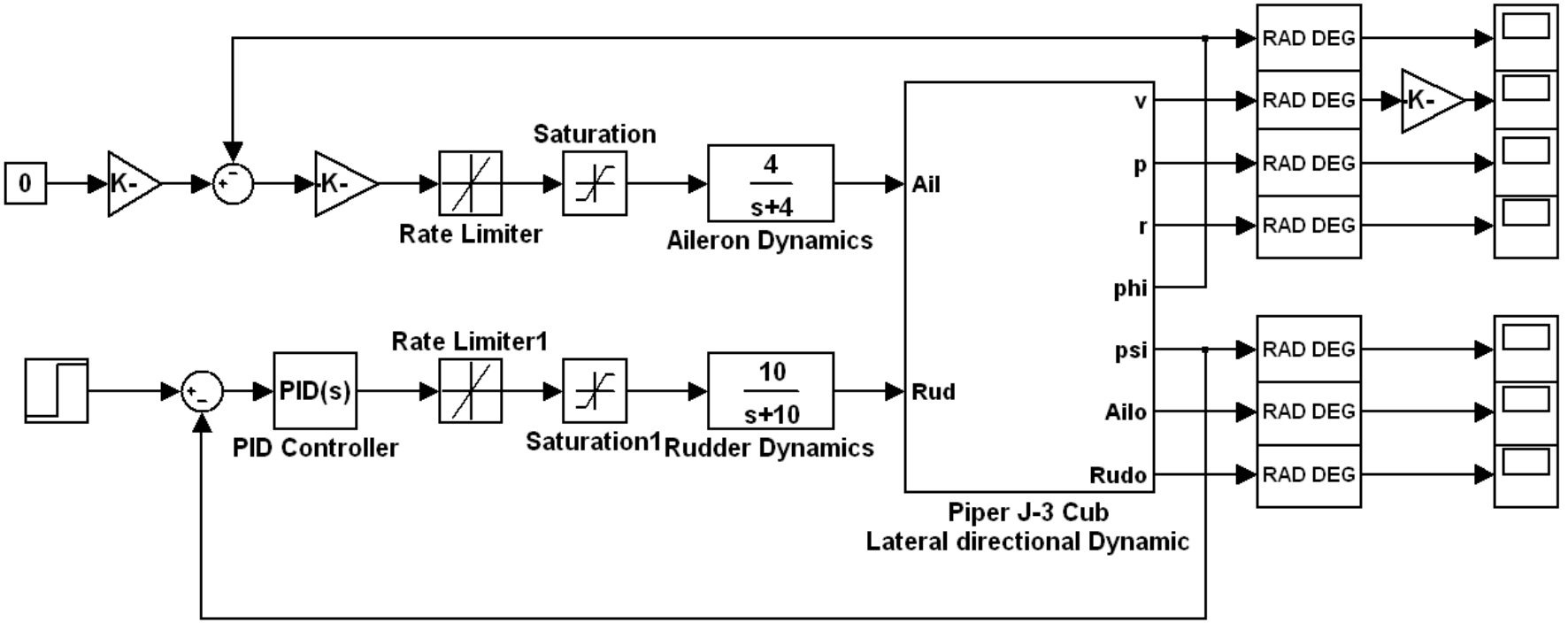

Figure 7-11 Decrab control law block (controlled by rudder)

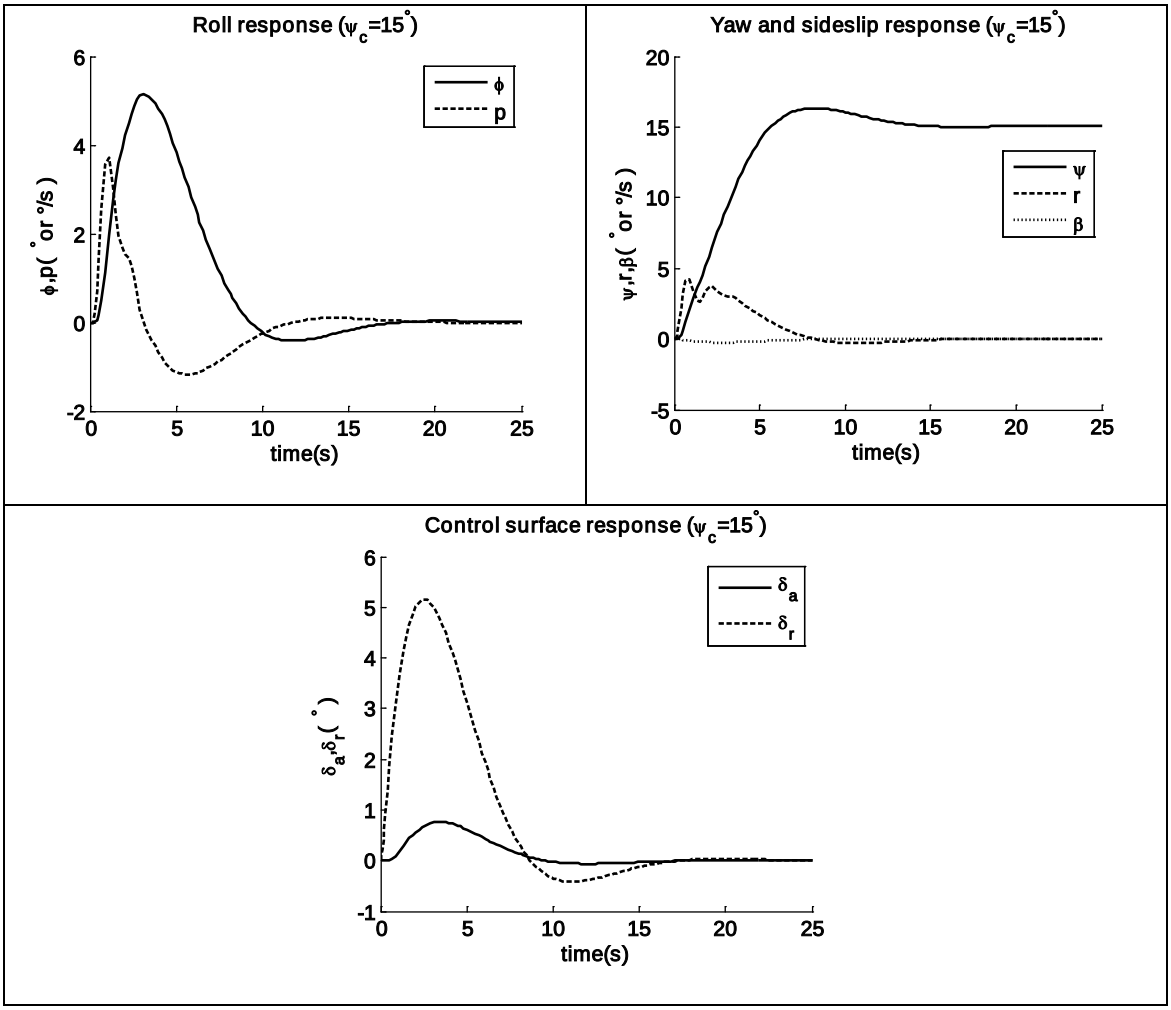

Figure 7-12 Decrab control response (controlled by rudder)

Comparison

The first method can achieve an aircraft change heading direction very quickly with only the deflection of the aileron, but it needs more rolling movement than the second, which means that the second method can keep more wings level than the first one.

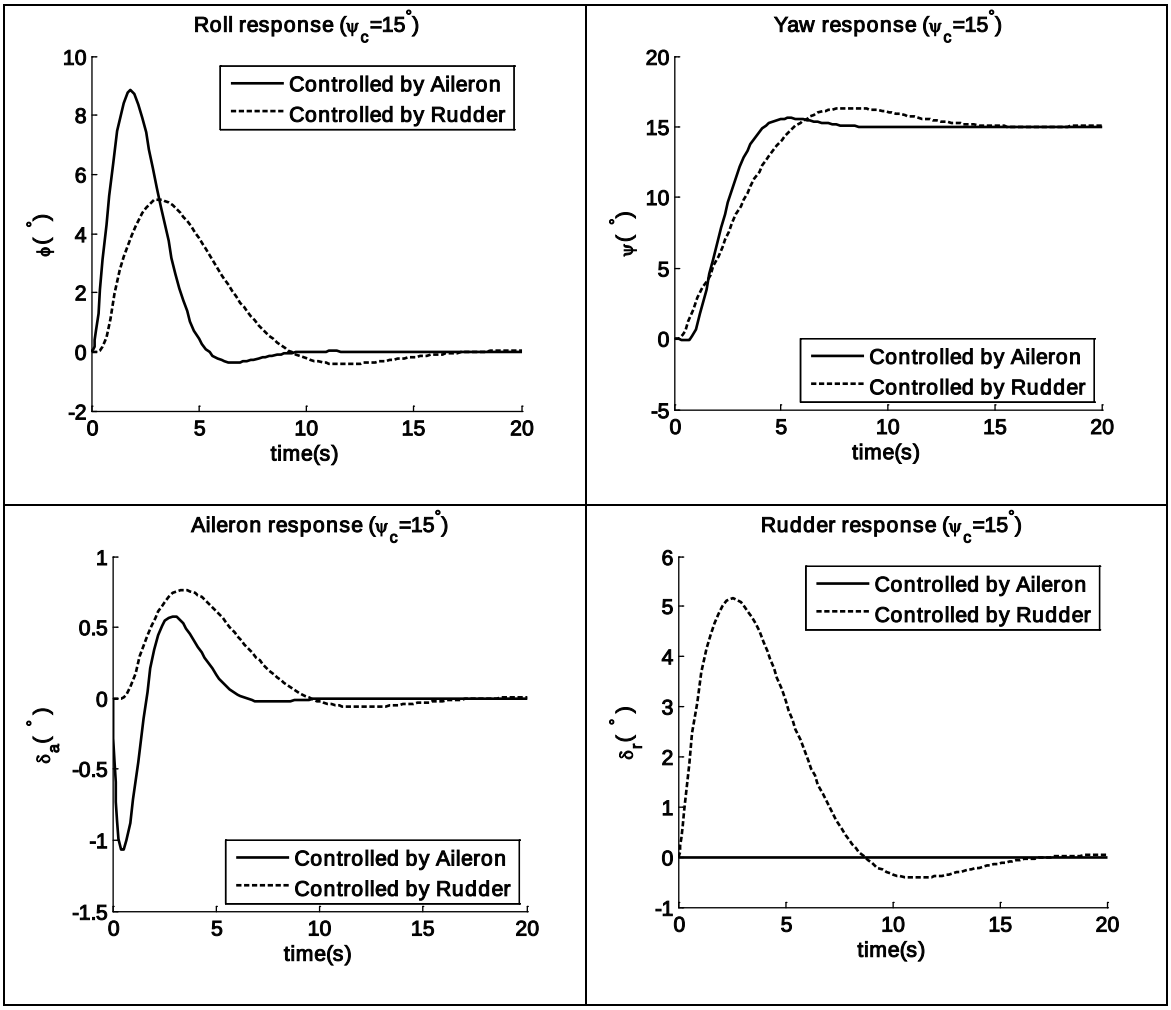

Figure 7-13 two methods of Decrab control compare

7.4 Chapter summary

At first, the ground trajectory guidance algorithm is designed from ideas previously suggested on paper. Then crosswind landing, the toughest manipulation, is discussed with a control strategy suggested for ultra-light aircraft. Lastly, control law about coordinated turn and Decrab control are investigated. The simulation curves reveal that the controllers satisfy the PI requirements.

8 FLIGHT SIMULATION INTEGRATION

8.1 Introduction

Simulation is a useful and quick approach to evaluate the design without the need to build and experiment on a real system, which generally is very expensive and time consuming, and sometimes is impractical.

The potential objective of Flight simulation is to throw a flood of light on the possible mechanisms of the control behaviour of the Piper J-3 Cub. It means practical simulation can be applied to forecast the coming response of FCS and the airplane, and clarify what can be done to improve the actual performance.

More detailed simulation is discussed in this chapter to check the robustness of the controller, including the model shift. At first the simulation is performed according longitudinal axis and lateral-directional axis respectively, then by combining them together gives a comprehensive simulation which including the whole flight phases from aircraft takeoff to landing, it also contains the vision simulation based on FLIGHT GEAR software.

8.2 Longitudinal simulation

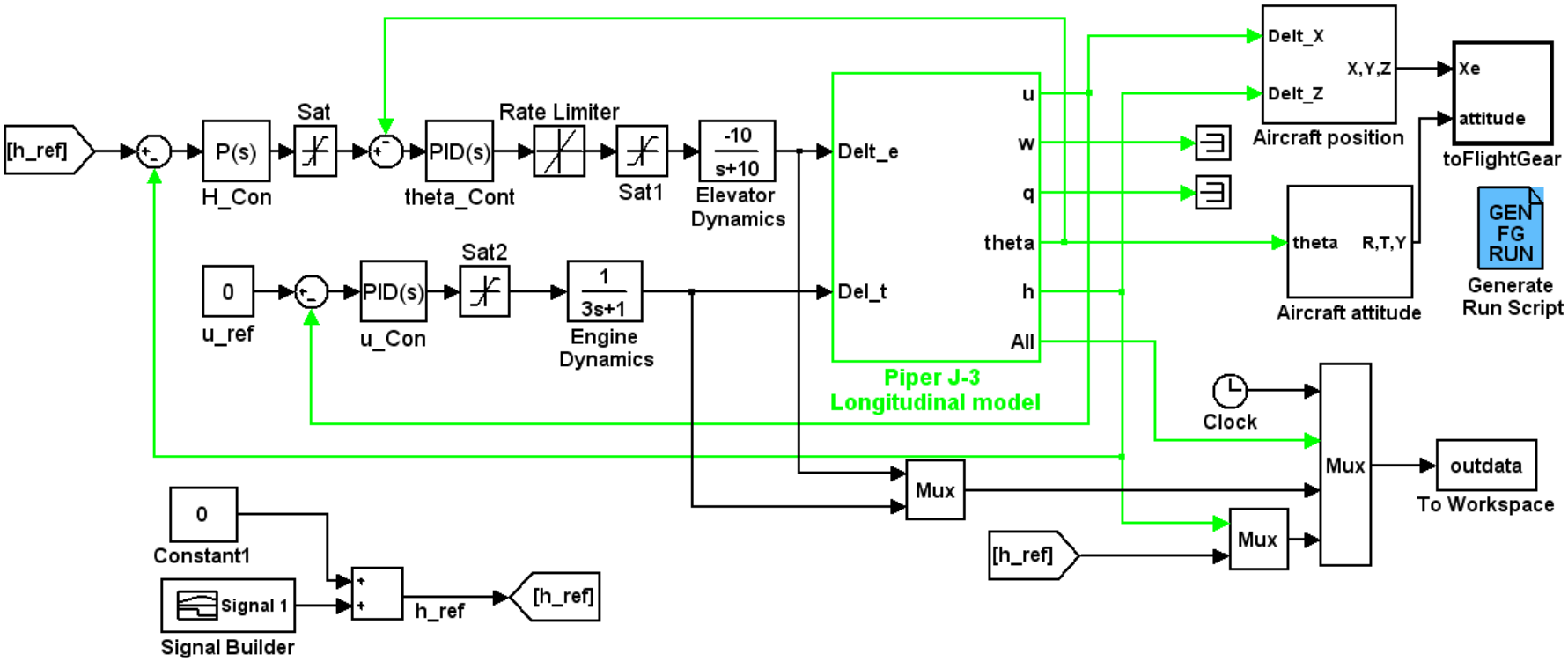

Figure 8-1 Longitudinal simulation block

As previously discussed, the need is to design different controllers for different flight conditions, but it can only select a limited number of design points, so with the slight changes to the model, the controller should also satisfy the control requirement. Very stringent terms are used here, the controller designed for 15m/s flight condition is used to check the response of 20m/s flight condition, the result being shown in figure 8-2. Based on the pre-text calculation, the theta limit used for 15m/s is [-3 15] degrees, 20m/s is [-4 15] degrees. Figure 8-2 (a) and (b) is the response for flight condition of 15m/s, (c) and (d) is for the flight condition of 20m/s, it illustrates than the controller has a good robustness with the model changes.

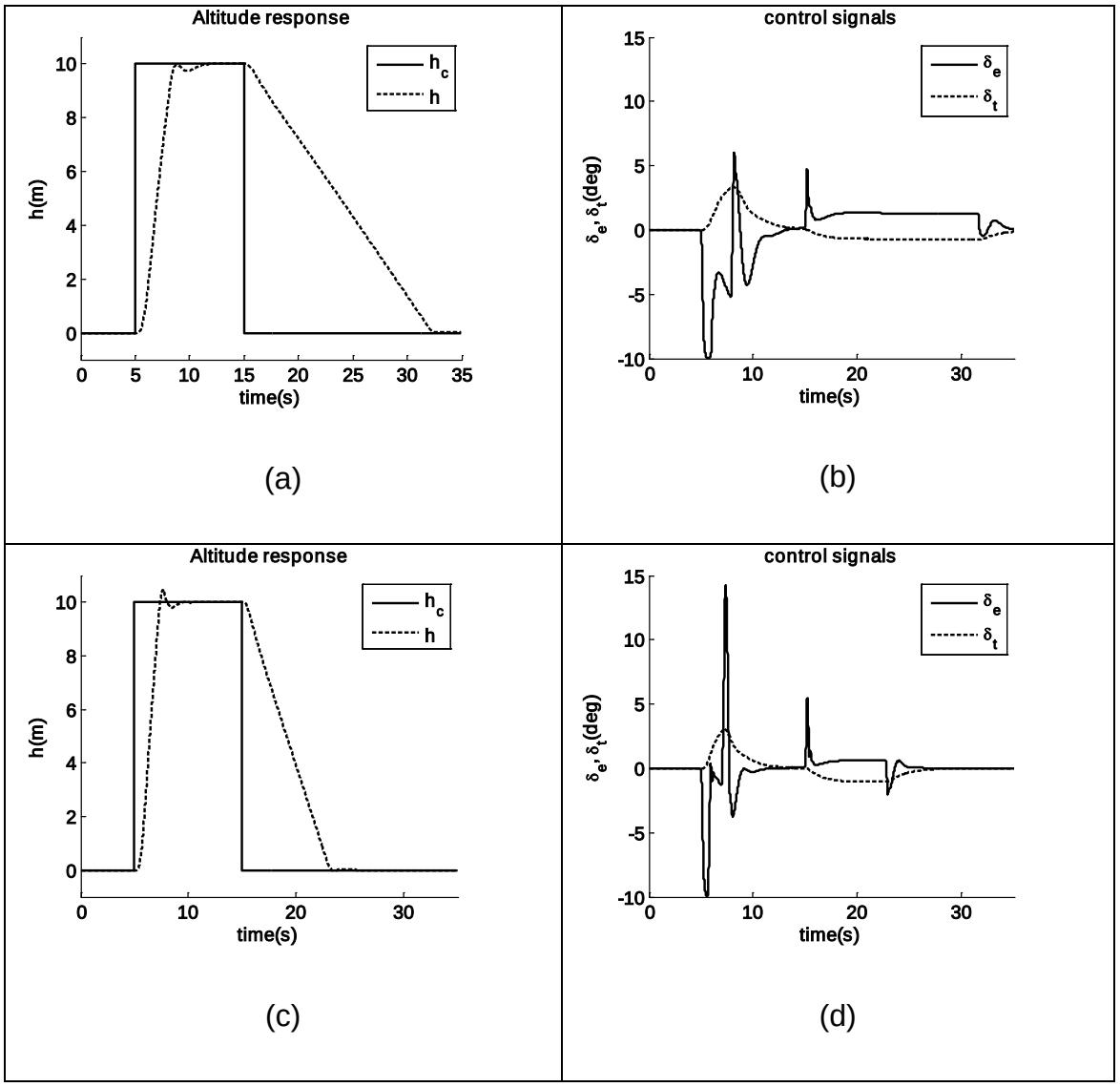

Figure 8-2 Longitudinal simulation with model shift

Again, the landing control is simulated at flight condition of 20m/s with the controller designed for 15m/s. As is shown in figure 8-3, the auto-landing is a fairly smooth process.

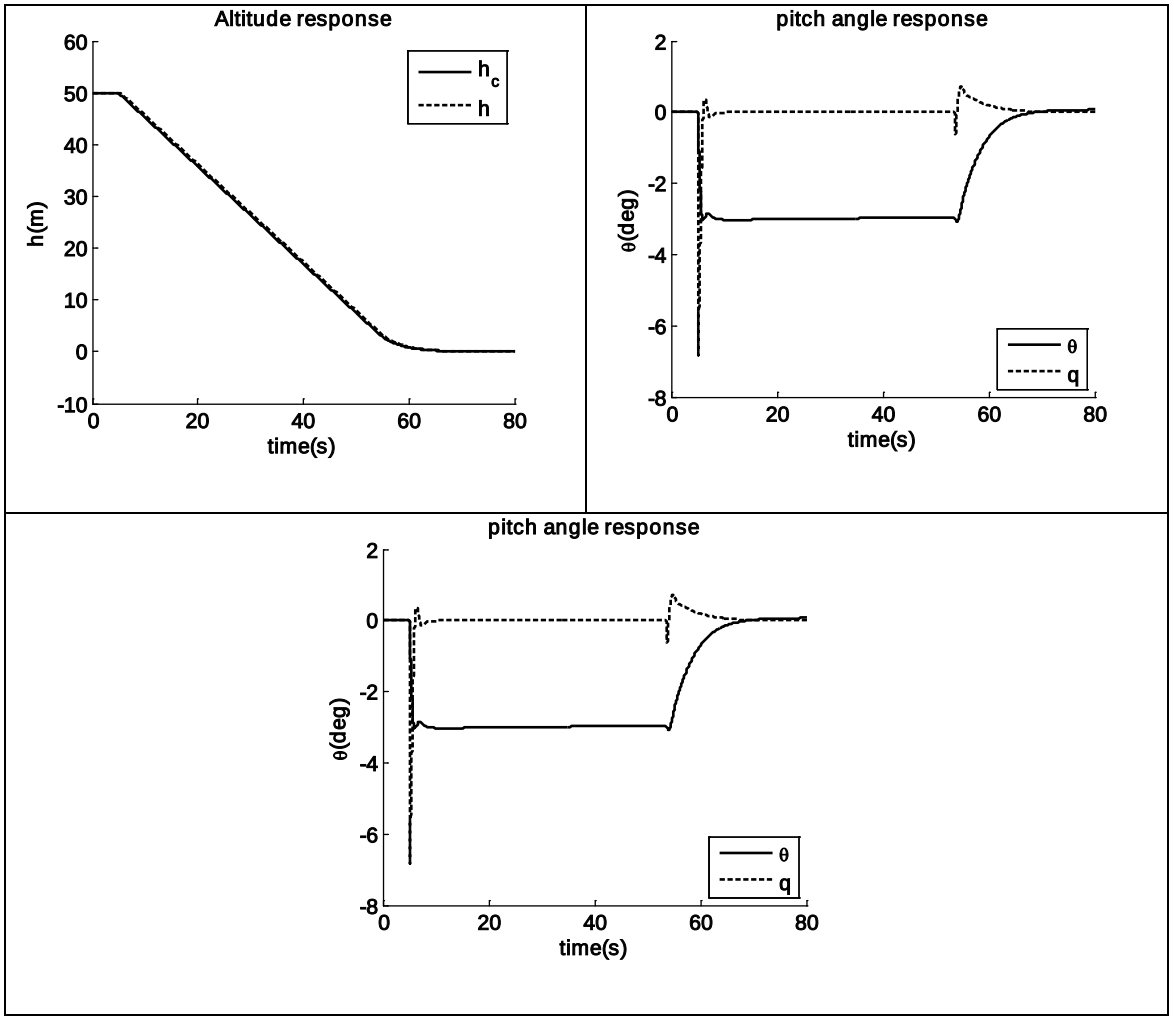

Figure 8-3 Automatic Landing simulation

With a high thrust to weight ratio, the Piper J-3 Cub has a good takeoff performance, the steady state automatic takeoff for 15m/s with 25 degree flight path angle is shown in figure 8-4 (a). The takeoff command is in altitude input format, which is followed quite well with a fairly smooth response.

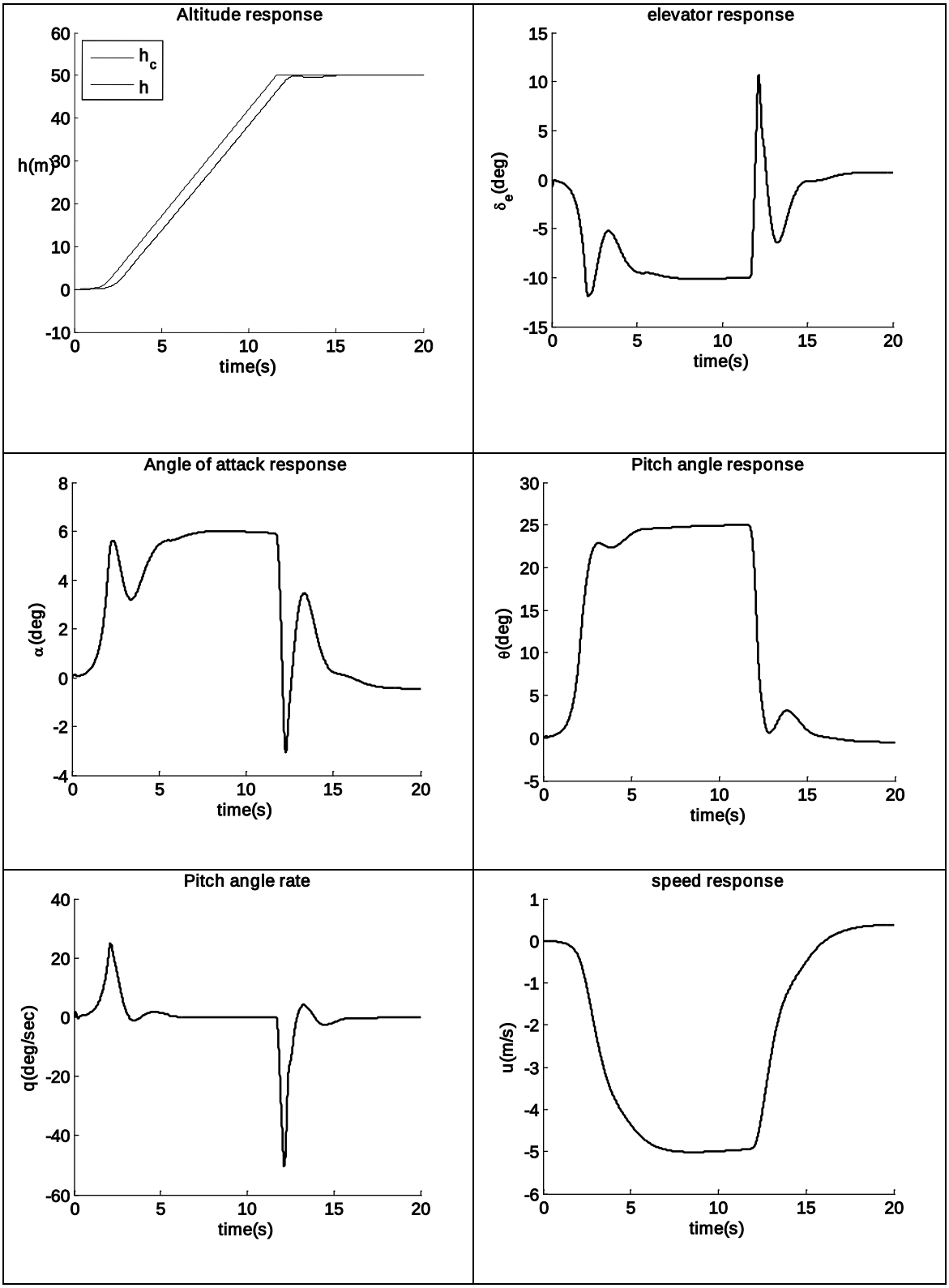
Altitude response
h_c
h
h(m)
time(s)
elevator response
δe(deg)
time(s)
Angle of attack response
α(deg)
time(s)
Pitch angle response
θ(deg)
time(s)
Pitch angle rate
q(deg/sec)
time(s)
speed response
u(m/s)
time(s)

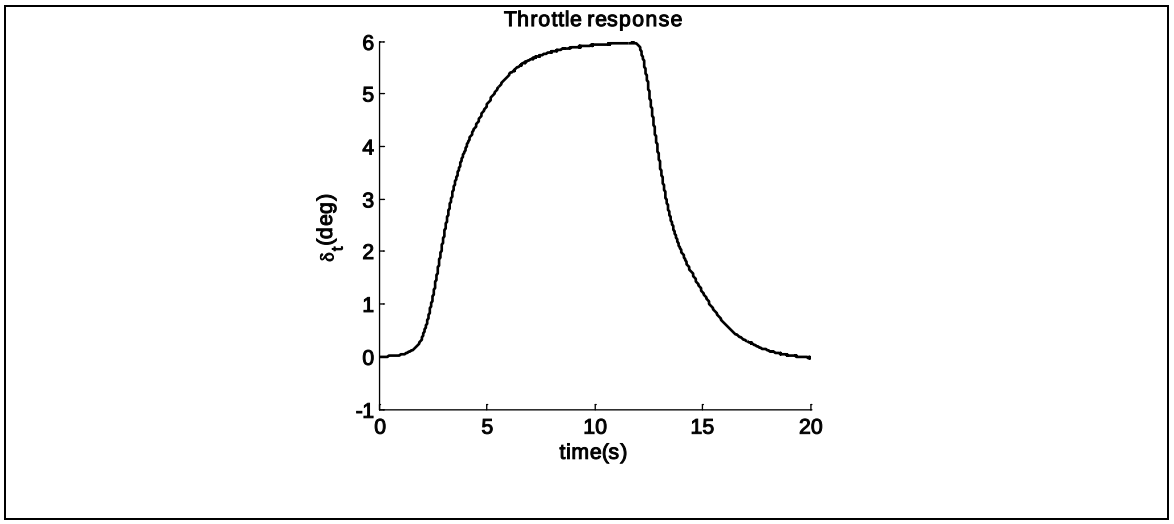

Figure 8-4 Automatic takeoff simulation

8.3 Lateral-directional control simulation

Lateral-directional controller is shown in figure 8-5. A 1000m lateral deviation is given to check the ground track following response. In order to get to the desired flight path quickly, the trajectory guidance algorithm which is discussed in the previous chapter is not used here. The constant heading control method is used. As shown in figure 8-6, the response is very quick and the transition is fairly smooth.

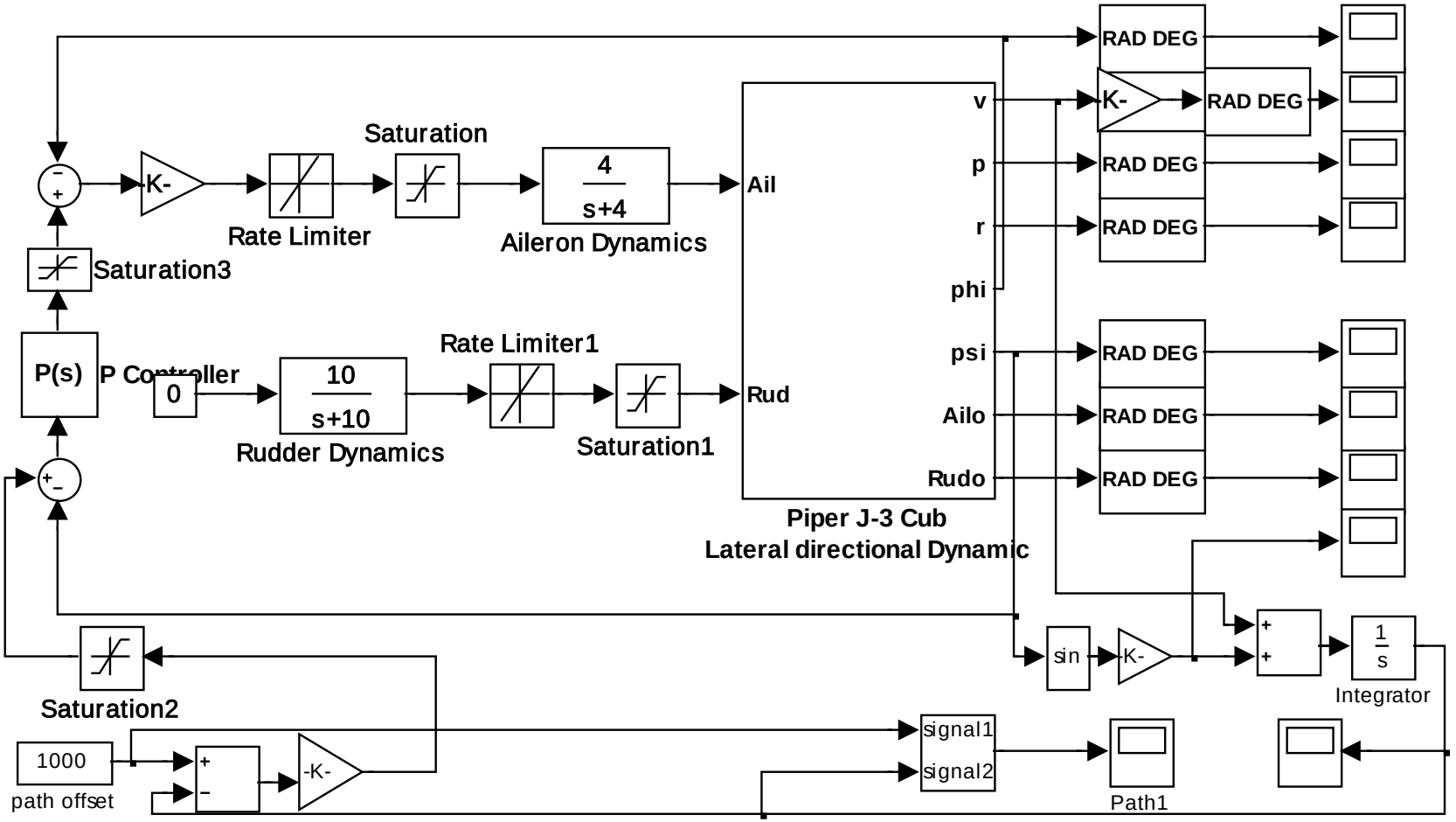

Figure 8-5 Heading control simulation

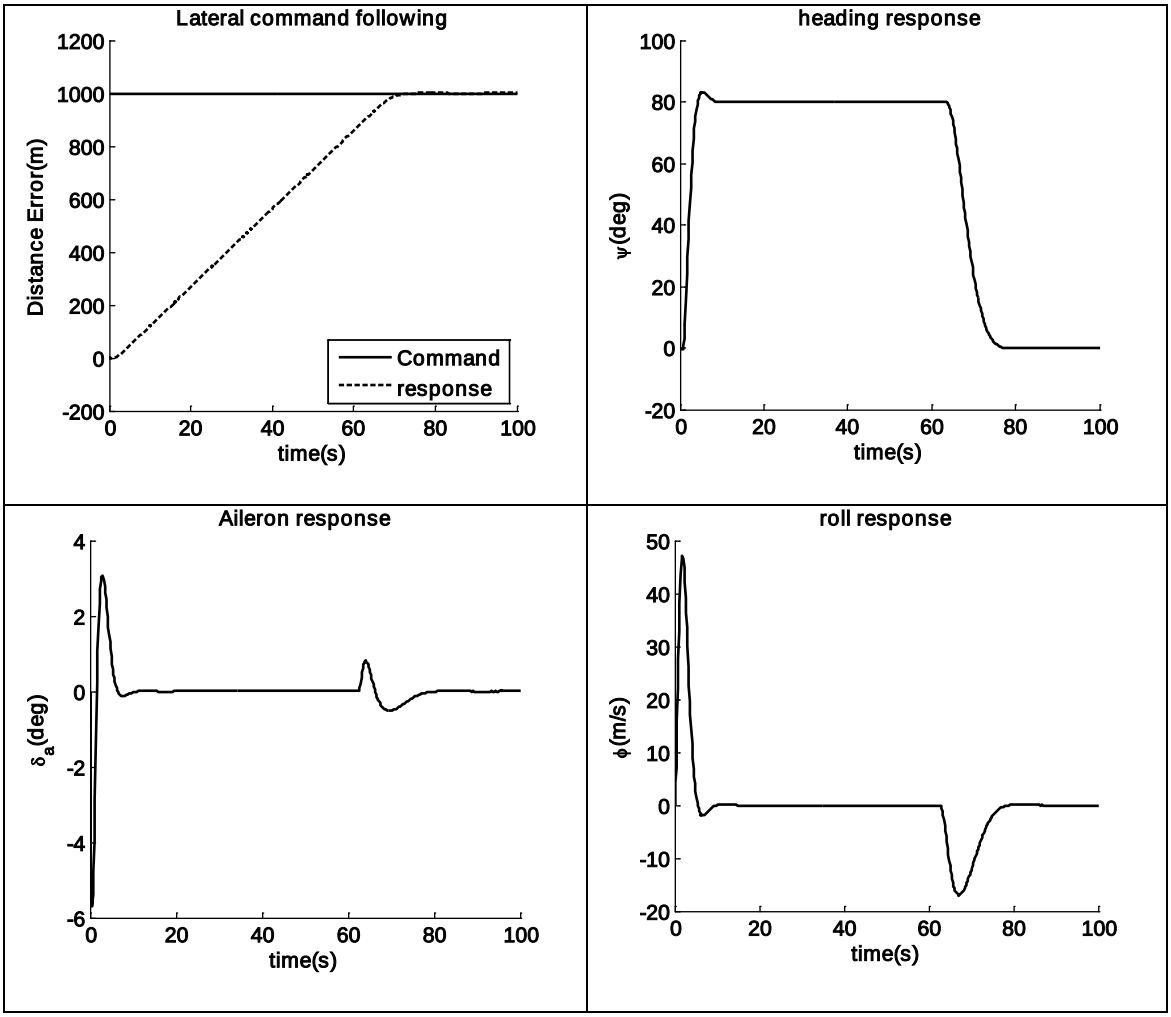

Figure 8-6 Heading control simulation response

8.4 Integrated simulation

The objective of this thesis is to give an overview of automatic control for the low cost airplane, so the whole flight profile simulation is performed in this part to check the methodology previously studied. The flight trajectory from takeoff to landing is given in figure 8-7, the ground track is shown in figure 8-8. The aircraft dynamics model is built in MATLAB, which is shown in figure 8-9. The simulation is executed based on the model and through the visualization block to send the kinetic parameters to FLIGHT GEAR to give a visual result. Combined with the curve output from MATLAB, the simulation shows that the Piper J-3 Cub has a good performance with the designed control laws.

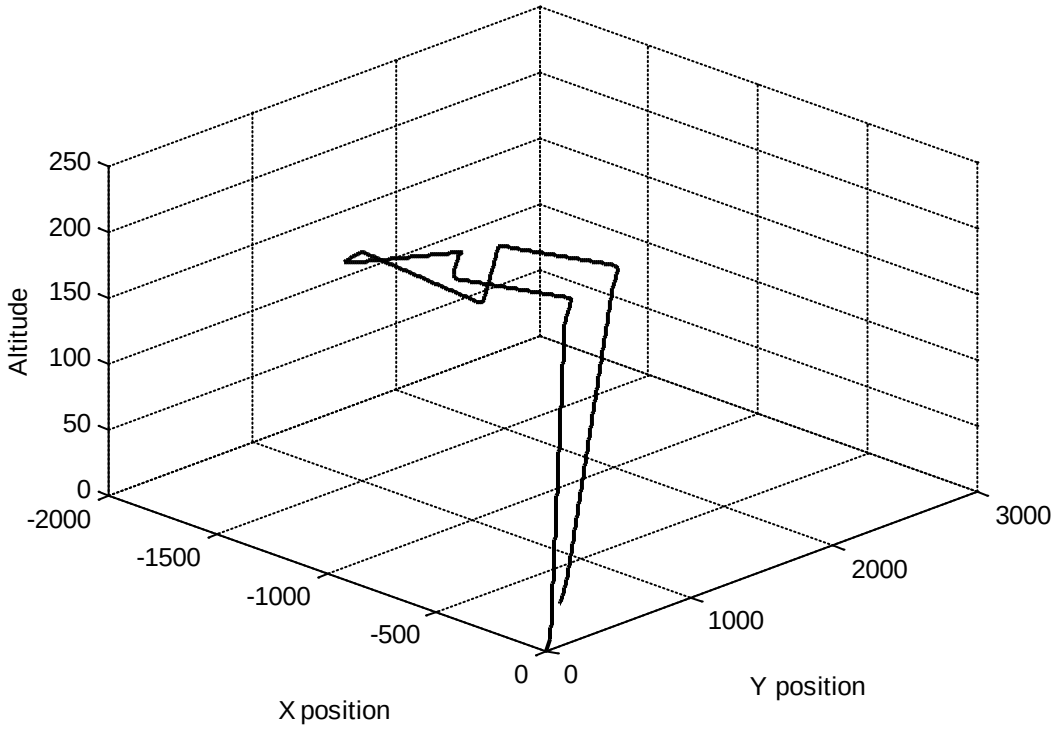

Figure 8-7 Flight trajectory

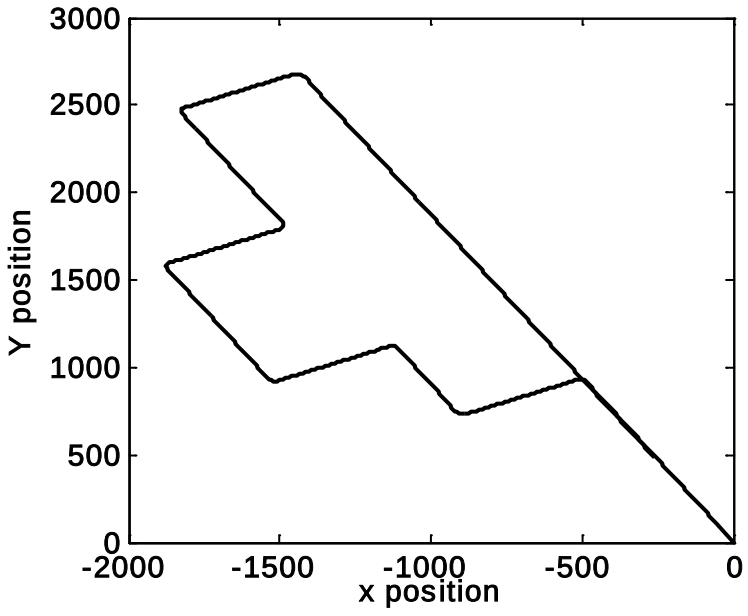

Figure 8-8 Ground track

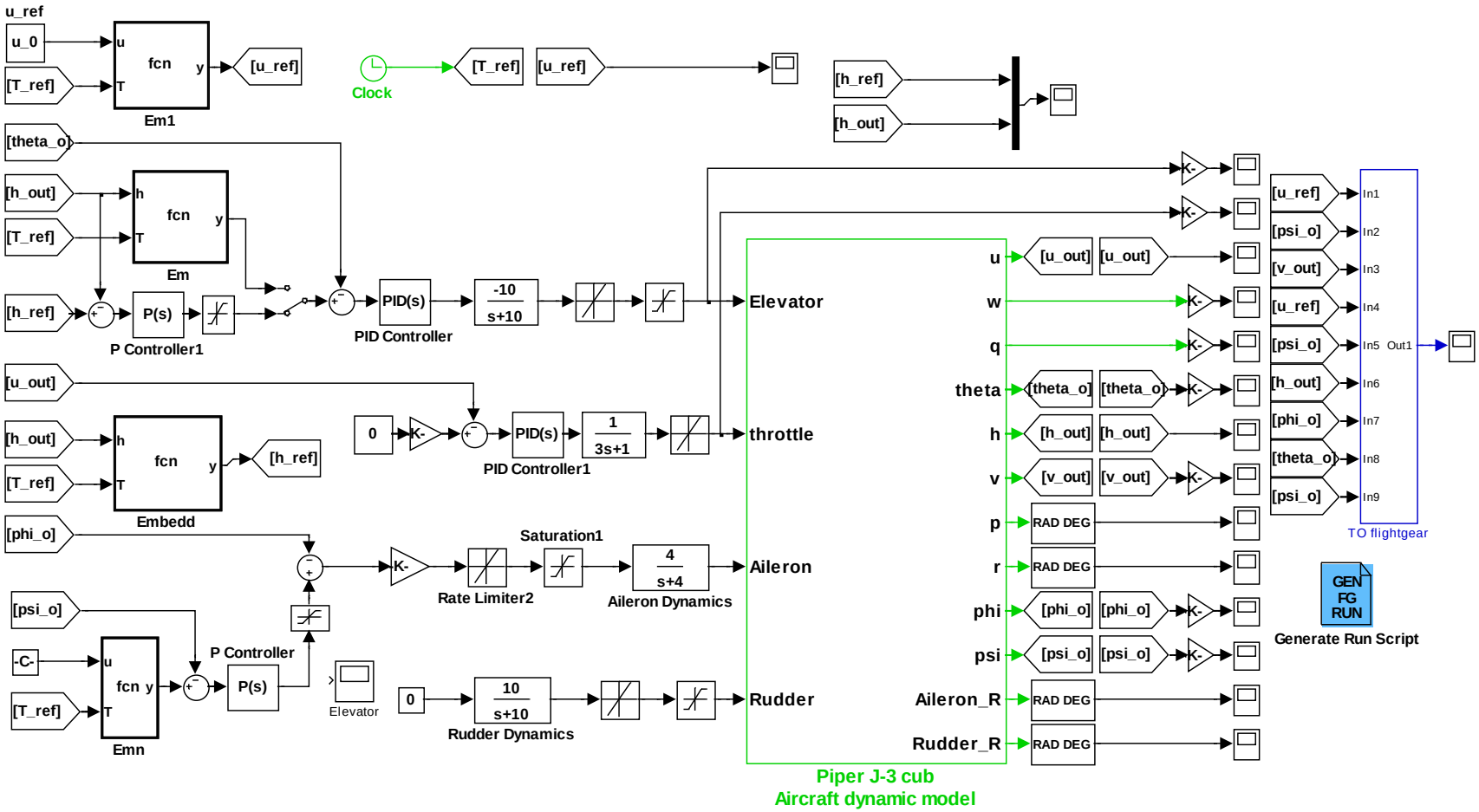

Figure 8-9 Piper J-3 full model simulation block

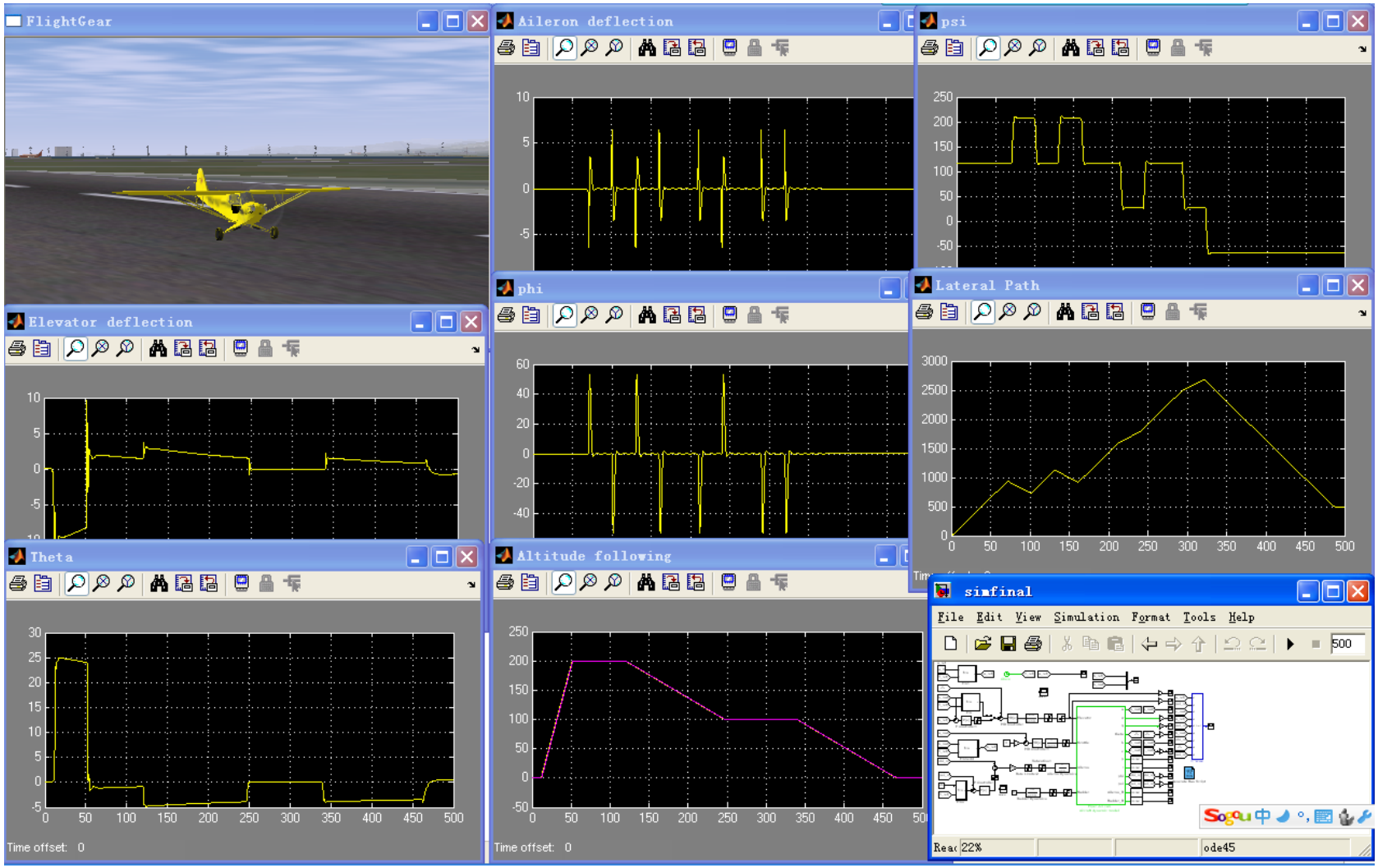

Figure 8-10 Integrated simulation overview

8.5 Chapter Summary

Although individual simulation is performed independently in Chapter 6 and Chapter 7, the more integrated simulation is executed in this chapter to give a more comprehensive evaluation of the work. Except for the traditional simulation methods, the modelling errors are also evaluated here to test the robustness of the designed controller. Especially, at the last step, the whole model integrated simulation is made by MATLAB and FLIGHT GEAR to get more intuitive simulation results, and which shows that the aircraft has good performance with the designed control law.

9 CONCLUSIONS AND FUTURE WORK

9.1 Work Summary

A DATCOM and an AVL program are built based on the Piper J-3 Cub model to calculate the aerodynamics coefficients, and then the analyzed flight conditions are selected. At the same time a trim program is built in MATLAB to get the aerodynamics coefficients of trim status for those flight conditions. With this data in hand, the aircraft aerodynamics characteristics are analyzed.

For an unsatisfied longitudinal flying quality, longitudinal SAS with gain scheduling method was designed for all selected flight conditions to improve the aircraft longitudinal flying qualities. With the longitudinal SAS, the longitudinal flying qualities of the aircraft had obviously improved.

The Autopilot is designed with the hope of reducing the workload of the pilot and even possibly flying the aircraft following a certain predesigned flight path without a pilot.

At first, a full flight profile is designed for automatic flying the aircraft.

Then, a more detailed investigation is made for the more complex takeoff and landing flight phases. Compared with nose wheel aircraft, the operation strategy for tail wheel like the Piper J-3 Cub is depicted. In order to get the operational boundary of the Piper J-3 Cub, takeoff performance is calculated from the data come from DATCOM. The work content is almost the same as the landing phase.

Thirdly, the guidance law for every special flight phase is studied.

After that, control law is designed for longitudinal axis and lateral-directional axis respectively. Several methods are studied for altitude hold and pitch attitude autopilot design. At the same time, auto-throttle is designed to control and hold the velocity. To lateral-directional axis, two methods are designed to control the aircraft heading. The merits and demerits of the different control methods are analyzed for comparison.

Finally, digital simulation is applied to verify the design results and check the system robustness. MATLAB simulation is used to check the longitudinal and lateral-directional performance individually, and the performance of the controller for modelling errors is also used to check in longitudinal by using 15 m/s flight condition controller to control the aircraft at 20 m/s flight condition. A whole profile flight simulation is illustrated in the second part of the simulation, which is based on the MATLAB model and the FLIGHT GEAR visual effect to illustrate the results of the designed autopilot.

9.2 Further work

But with limited time and knowledge, much work still needs to be done.

- A modern flight control system needs to design a wide flight envelopment controller, the full selected condition control law for longitudinal SAS is designed and the gain scheduling method is also discussed. For time reason, in spite of the design methods that are all given, many other controllers are designed just for special flight conditions. So the controller parameters for the rest of flight conditions still need to be designed.

- This thesis does not covering the landing gear control, which including the steering control and the brake control when aircraft is on the ground. It is important when there is a need to automatically park an aircraft on a desired place.

- In order to check the robustness of the controller, only the modelling errors is performed in the simulation experiment, in the later design process, the wind gusts and sensor noise should also be simulated.

- The design method is mainly focused on classical root locus and traditional PID algorithm. The afterward research should also including robust control, adaptive control, fuzzy control and Neural Network Control.

REFERENCES

[1] available at: http://air-and-space.com/20070818-19%20Camarillo%20flying%201.htm (accessed 3 September 2010).

[2] Arkadiy Turevskiy, Stacey Gage and Craig Buhr (2007), "Model-Based Design of a New Light-weight Aircraft", *AIAA Modeling and Simulation Technologies Conference and Exhibit,* no. Hilton Head, South Carolina.

[3] Tanner Austin Sims (May 2009), *Design and Control Considerations for a Skid-to-Turn Unmanned Aerial Vehicle*.

[4] Johnson, K. L. and Awni, K. A. (2002), "A roll autopilot for autonomous air refueling", vol. AIAA Paper 2002-4752.

[5] Branimir Stojiljkovic, Ljubiša Vasov, Časlav Mitrovic and Dragan Cvetkovic (2009), "The Application of the Root Locus Method for the Design of Pitch Controller of an F-104A Aircraft", *Journal of Mechanical Engineering 55(2009)*.

[6] S. H. Sadati, M. Sabzeh Parvar and M. B. Menhaj (December 2007), "COMPARISON OF FLIGHT CONTROL SYSTEM DESIGN METHODS IN LANDING", *Asian Journal of Control, Vol. 9, No. 4,* pp. 491-496.

[7] Andry, A. N., Shapiro, E. Y. and Chung, J. C. (1983), "Eigenstructure Assignment for Linear Systems", *Aerospace and Electronic Systems, IEEE Transactions on,* vol. AES-19, no. 5, pp. 711-729.

[8] Dogan, A. and Sato, S. (2006), "Flight control and simulation for aerial refueling", *STAR,* vol. 44, no. 13.

[9] Alsuwaidan, B. N. and Crassidis, J. L. (2006), "Robust Aircraft Longitudinal Control Using Model-Error Control Synthesis", *AIAA Guidance,* vol. AIAA Paper 2006-6050.

[10] Sghairi, M., Aubert, J., Brot, P., de Bonneval, A., Crouzet, Y. and Laarouchi, Y. (2009), "Distributed and reconfigurable architecture for flight control system", *Digital Avionics Systems Conference, 2009. DASC'09. IEEE/AIAA 28th,* pp. 6.B.2-1.

[11] HALL, O. and STIGALL, P. (1992), "Distributed flight control system using fiber distributed data interface (FDDI)", *IEEE Aerospace and Electronic Systems Magazine,* vol. 7, no. 6, pp. 21-33.

[12] Ahlstrom, K. and Torin, J. (2002), "Future architecture of flight control systems", *Aerospace and Electronic Systems Magazine, IEEE,* vol. 17, no. 12, pp. 21-27.

[13] Zhang Zengan, Chen Xin and Zhou Yueping (2010), "Implementation of a Distributed Fault-Tolerant Computer for UAV", *Electrical and Control Engineering (ICECE), 2010 International Conference on,* pp. 5266.

[14] Hammett, R. C. (1999), "Ultra-reliable real-time control systems-future trends", *Aerospace and Electronic Systems Magazine, IEEE,* vol. 14, no. 8, pp. 31-36.

[15] DENNIS, R. W. and HILLS, A. D. (1990), "A fault tolerant fly by wire system for maintenance free applications", *IEEE/AIAA/NASA Digital Avionics Systems Conference, 9th, Virginia Beach, VA; UNITED STATES; 15-18 Oct. 1990,* New York, Institute of Electrical and Electronics Engineers, Inc.

[16] Popp, D. J. and Kahler, R. L. (1992), "C-17 flight control systems software design", *IEEE/AIAA Digital Avionics Systems Conference, 11th, Seattle, WA, Proceedings; UNITED STATES; 5-8 Oct. 1992,* New York: Institute of Electrical and Electronics Engineers, Inc.

[17] David Jensen, Michael Roberts, Joseph Alifano, Thomas Szumczyk and William Cheung (May, 2004), "Development of PolyUAV: Polytechnic University's Unmanned Aerial Vehicle".

[18] McDonnell Douglas Astronautics Company, *THE USAF STABILITY AND CONTROL DATCOM* (accessed April).

[19] Nelson, R. C. (1998), *Flight stability and automatic control,* 2nd ed, WCB/McGraw-Hill, Boston.

[20] ESDU International (June 2010), "Estimation of take-off distance", *ESDU PERF EG 5/1,* [Online], no. With Amendments A to C.

[21] available at: http://www.jperkinsdistribution.co.uk/downloads/5500905a.pdf (accessed 15 December 2010).

[22] Jih-Gau Juang and Hao-Hsiang Chang (2002), "Application of time delay neural network to automatic landing control", *Control Applications, 2002. Proceedings of the 2002 International Conference on,* Vol. 1, pp. 150.

[23] Niculescu, M. (2001), "Lateral track control law for aerosonde UAV", vol. AIAA Paper 2001-0016.

[24] Biju prasad B., Dr. S. Pradeep.(2007),"Automatic Landing System Design using Feedback Linearization Method", AIAA Aerospace 2007 Conference and Exhibit,7-10 May 2007, Rohnert Park, California.

APPENDICES

Appendix A Program for estimate aerodynamic coefficients

A.1 AVL input data

```
Piper J-3 Cub
#Mach
 0.0
#IYsym   IZsym   Zsym
 0       0       0.0
#Sref        Cref     Bref
 0.816894     0.3491    2.34
#Xref    Yref    Zref
0.46     0.0     -0.18
# CDp
0.0215
#--------------------------------------------------
SURFACE
Wing
#Nchord   Cspace   Nspan  Sspace
8          3.0     8          3.0
# reflect image wing about y=0 plane
YDUPLICATE
0.0
```

```
#
# twist angle bias for whole surface
ANGLE
    0.0000

#
SCALE
 1.0   1.0   1.0
#
# x,y,z bias for whole surface
TRANSLATE
   0.00000     0.00000     0.00000
#------------------------------------------------------------
SECTION
#Xle    Yle    Zle     Chord   Ainc  Nspanwise  Sspace
0.4     0     0.1      0.3491    0   0          0

NACA
2314
#------------------------------------------------------------
SECTION
#Xle    Yle    Zle     Chord   Ainc  Nspanwise  Sspace
0.4    0.41   0.1      0.3491    0   0          0
CONTROL
```

aileron 57.29578 0.75 0.0 0.0 0.0 -1.0

NACA

2314

#--

SECTION

#Xle Yle Zle Chord Ainc Nspanwise Sspace

0.4 1.02 0.1 0.3491 0 0 0

CONTROL

aileron 57.29578 0.75 0.0 0.0 0.0 -1.0

NACA

2314

#--

SECTION

#Xle Yle Zle Chord Ainc Nspanwise Sspace

0.4 1.17 0.1 0.3491 0 0 0

NACA

2314

#==

SURFACE

Horizontal tail

#Nchordwise Cspace Nspanwise Sspace

8 3.0 20 3.0

#

YDUPLICATE

0.0

#

ANGLE

0.0

#--

SECTION

#Xle Yle Zle Chord Ainc Nspanwise Sspace

1.57 0.03 0.07 0.35 0.0 0 0

CONTROL

elevator 57.29578 0.7 0.0 1.0 0.0 1.0

NACA

0002

#--

SECTION

#Xle Yle Zle Chord Ainc Nspanwise Sspace

1.68 0.35 0.07 0.25 0.0 0 0

CONTROL

elevator 57.29578 0.7 0.0 1.0 0.0 1.0

NACA

0002

#==========

===

SURFACE

Fin

#Nchordwise Cspace   Nspanwise   Sspace

8   3.0   8   3.0

ANGLE

0.0

#----------

SECTION

#Xle   Yle   Zle   Chord   Ainc Nspanwise Sspace

1.57   0   0.07   0.45   0.0   0   0

CONTROL

rudder 57.29578 0.7   0.0 0.0 1.0   1.0

NACA

0002

#----------

```
SECTION
#Xle    Yle    Zle     Chord    Ainc  Nspanwise  Sspace
1.70    0      0.3      0.30     0.0   0          0

CONTROL
rudder  57.29578  0.7    0.0 0.0 1.0    1.0

NACA
0002
#-------------------------------------------------------------
```

A.2 DATCOM input data

```
************************
*   List of Command Card
************************
TRIM
DAMP
PART
DERIV RAD
**********************
*  Flight Conditions *
**********************
 $FLTCON LOOP=2.0, TR=1.0,
    NMACH=1.0,MACH(1)=0.0441,
```

```
    NALPHA=9.0,ALSCHD(1)=-2.0,-1.0,0.0,
      2.0,4.0,6.0,8.0,10.0,11.0,
    NALT=1.0,ALT(1)=0.0,
    GAMMA=0.0$
************************
*  Reference Parameters *
************************
 $OPTINS SREF=0.816894,CBARR=0.3491,BLREF=2.34$
****************************************
* Group II     Synthesis Parameters
****************************************
 $SYNTHS XCG=0.46,ZCG=-0.18,XW=0.5,ZW=0.1,ALIW=0.0,XH=1.57,
    ZV=0.07,XV=1.47,
    ZH=0.07,ALIH=0.0,VERTUP=.TRUE.$
 $BODY    NX = 5.0,
          X = 0.00, 0.35, 0.5, 0.800, 1.90,
          S = 0.020, 0.08, 0.1, 0.1, 0.015,
          ZU = -0.02, 0.02, 0.02, 0.02, 0.08,
          ZL = 0.1, 0.14, 0.18, 0.18, -0.02$


NACA W 4 2314
NACA V 4 0002
NACA H 4 0002
********************************
```

```
*        Wing planform variables
*********************************
 $WGPLNF CHRDTP=0.3491,SSPNE=1.17,SSPN=1.17,CHRDR=0.3491,SAVSI=0.0,
        CHSTAT=0.0,TWISTA=0.0,DHDADI=0.0,DHDADO=0.0,TYPE=1.0$
*****************************************
*        Vertical Tail planform variables
*****************************************
 $VTPLNF CHRDTP=0.30,SSPNE=0.23,SSPN=0.30,CHRDR=0.45,SAVSI=13.5,
    CHSTAT=.25,TYPE=1.0$
*********************************************
*        Horizontal Tail planform variables    pg 37-38
*********************************************
 $HTPLNF CHRDTP=0.25,SSPNE=0.35,SSPN=0.35,CHRDR=0.35,SAVSI=6.0,
    CHSTAT=0.25,TWISTA=0.0,DHDADI=0.0,DHDADO=0.0,TYPE=1.0$
***********************************
*    Elevator Deflection parameters
***********************************
 $SYMFLP FTYPE=1.0,
    NDELTA=9.0,DELTA(1)=-40.,-30.,-20.,-10.,0.,10.,20.,30.,40.,
    SPANFI=.400,SPANFO=6.586,CHRDFI=1.882,CHRDFO=.706,NTYPE=1.0,
    CB=.357,TC=.220,PHETE=.003,PHETEP=.002$
CASEID Piper J-3 cub
```

Appendix B Aerodynamic coefficients

B.1 Aerodynamic for level flight

Flight condition: sea level (15m/s)

AOA	-2.0	-1.0	0.0	2.0	4.0	6.0	8.0	10.0
δ_e	0.35651	-0.64405	-1.72725	-4.14132	-6.88692	-9.96794	-13.39092	-17.16521
C_L	-0.01529	0.06328	0.14135	0.29578	0.44760	0.59644	0.74190	0.88361
C_D	0.02167	0.02189	0.02269	0.02597	0.03146	0.03911	0.04884	0.06058
$C_{L\alpha}$	4.828680	4.828806	4.825709	4.809975	4.781771	4.741454	4.689438	4.626200
$C_{D\alpha}$	0.0126	0.0458	0.0940	0.1573	0.2192	0.2787	0.3363	0.3782
$C_{m\alpha}$	-1.145873	-1.249572	-1.352434	-1.555510	-1.754829	-1.950125	-2.141135	-2.327606
$C_{L\dot{\alpha}}$	2.014	2.062	2.154	2.326	2.359	2.35	2.318	2.263
$C_{m\dot{\alpha}}$	-6.978	-7.146	-7.465	-8.06	-8.176	-8.143	-8.032	-7.841
C_{Lq}	8.507438	8.383569	8.258701	8.006501	7.751908	7.496001	7.239868	6.984593
C_{mq}	-12.309361	-12.388563	-12.466298	-12.617212	-12.761776	-12.899679	-13.030644	-13.154417
C_{m_u}	-0.0026	-0.0026	-0.0031	-0.0040	-0.0031	-0.0035	-0.0035	-0.0031
$C_{L_{\delta e}}$	0.326908	0.327263	0.327401	0.327060	0.325948	0.324131	0.321678	0.318660
$C_{m_{\delta e}}$	-1.195736	-1.198480	-1.200601	-1.202962	-1.202798	-1.200103	-1.194880	-1.187147
C_{y_β}	-0.133869	-0.134426	-0.134939	-0.135833	-0.136551	-0.137092	-0.137456	-0.137643
$C_{l\beta}$	-0.010147	-0.018092	-0.025991	-0.041620	-0.056959	-0.071939	-0.086491	-0.100549
$C_{n\beta}$	0.058681	0.059022	0.05963	0.061666	0.064755	0.068876	0.073997	0.080084
C_{yp}	-0.037250	-0.016627	0.003995	0.045133	0.085962	0.126281	0.165893	0.204604
C_{lp}	-0.526020	-0.525436	-0.524517	-0.521689	-0.517569	-0.512196	-0.505618	-0.497890
C_{np}	0.013593	0.006168	-0.001268	-0.016201	-0.031258	-0.046486	-0.061928	-0.077621

AOA	-2.0	-1.0	0.0	2.0	4.0	6.0	8.0	10.0
C_{yr}	0.142189	0.143792	0.144662	0.144208	0.140847	0.134616	0.125564	0.113752
C_{lr}	0.021874	0.042119	0.062272	0.102249	0.141690	0.180486	0.218531	0.255726
C_{nr}	-0.075643	-0.076730	-0.077958	-0.080829	-0.084226	-0.088108	-0.092432	-0.097144
$C_{l\delta a}$	-0.349277	-0.349300	-0.349111	-0.348094	-0.346232	-0.343533	-0.340012	-0.335685
$C_{n\delta a}$	0.001706	-0.000067	-0.001836	-0.005358	-0.008842	-0.012272	-0.015630	-0.018900
$C_{y\delta r}$	-0.092765	-0.093006	-0.093181	-0.093331	-0.093218	-0.092842	-0.092205	-0.091311
$C_{l\delta r}$	-0.013787	-0.013733	-0.013670	-0.013512	-0.013316	-0.013083	-0.012813	-0.012509
$C_{n\delta r}$	0.056189	0.056346	0.056464	0.056579	0.056536	0.056334	0.055974	0.055460

Flight condition: sea level (20m/s)

AOA	-2.0	-1.0	0.0	2.0	4.0	6.0	8.0	10.0
δ_e	0.35522	-0.64502	-1.72791	-4.14139	-6.88643	-9.96693	-13.38942	-17.16327
C_L	-0.01529	0.06332	0.14143	0.29594	0.44785	0.59676	0.74230	0.88409
C_D	0.02167	0.02189	0.02269	0.02597	0.03147	0.03913	0.04887	0.06062
$C_{L\alpha}$	4.831077	4.831203	4.828104	4.812356	4.784130	4.743781	4.691724	4.628437
$C_{D\alpha}$	0.0126	0.0458	0.0940	0.1576	0.2194	0.2790	0.3366	0.3782
$C_{m\alpha}$	-1.145827	-1.249565	-1.352466	-1.555620	-1.755017	-1.950390	-2.141478	-2.328027
$C_{L\dot{\alpha}}$	2.022	2.071	2.164	2.332	2.360	2.350	2.318	2.263
$C_{m\dot{\alpha}}$	-7.006	-7.177	-7.500	-8.082	-8.178	-8.145	-8.034	-7.842
C_{Lq}	8.510620	8.386687	8.261753	8.009414	7.754676	7.498621	7.242335	6.986906
C_{mq}	-12.311625	-12.390825	-12.468564	-12.619485	-12.764055	-12.901971	-13.032950	-13.156738

AOA	-2.0	-1.0	0.0	2.0	4.0	6.0	8.0	10.0
C_{m_u}	-0.0024	-0.0024	-0.0029	-0.0041	-0.0035	-0.0041	-0.0041	-0.0041
$C_{L_{\delta e}}$	0.326987	0.327341	0.327479	0.327138	0.326026	0.324209	0.321755	0.318736
$C_{m_{\delta e}}$	-1.196087	-1.198832	-1.200953	-1.203313	-1.203149	-1.200452	-1.195227	-1.187491
C_{y_β}	-0.133875	-0.134432	-0.134946	-0.135840	-0.136558	-0.137100	-0.137464	-0.137651
$C_{l\beta}$	-0.010142	-0.018092	-0.025997	-0.041635	-0.056984	-0.071973	-0.086535	-0.100602
$C_{n\beta}$	0.058684	0.059024	0.059637	0.061669	0.064760	0.068882	0.074007	0.080097
C_{yp}	-0.037254	-0.016621	0.004010	0.045168	0.086017	0.126356	0.165988	0.204718
C_{lp}	-0.526195	-0.525611	-0.524692	-0.521863	-0.517741	-0.512365	-0.505784	-0.498052
C_{np}	0.013591	0.006165	-0.001272	-0.016208	-0.031267	-0.046498	-0.061943	-0.077639
C_{yr}	0.142199	0.143803	0.144673	0.144217	0.140855	0.134620	0.125563	0.113745
C_{lr}	0.021877	0.042130	0.062293	0.102288	0.141747	0.180560	0.218622	0.255834
C_{nr}	-0.075648	-0.076735	-0.077964	-0.080836	-0.084234	-0.088119	-0.092445	-0.097161
$C_{l\delta a}$	-0.349430	-0.349453	-0.349263	-0.348246	-0.346383	-0.343683	-0.340161	-0.335832
$C_{n\delta a}$	0.001708	-0.000065	-0.001835	-0.005356	-0.008840	-0.012269	-0.015627	-0.018898
$C_{y\delta r}$	-0.092783	-0.093023	-0.093198	-0.093349	-0.093235	-0.092859	-0.092221	-0.091328
$C_{l\delta r}$	-0.013790	-0.013736	-0.013672	-0.013515	-0.013319	-0.013086	-0.012816	-0.012512
$C_{n\delta r}$	0.056200	0.056358	0.056475	0.056591	0.056547	0.056345	0.055985	0.055471

Flight condition: sea level (25m/s)

AOA	-2.0	-1.0	0.0	2.0	4.0	6.0	8.0	10.0

AOA	-2.0	-1.0	0.0	2.0	4.0	6.0	8.0	10.0
δ_e	0.35356	-0.64627	-1.72876	-4.14147	-6.88581	-9.96563	-13.38751	-17.16077
C_L	-0.01530	0.06337	0.14153	0.29615	0.44816	0.59718	0.74282	0.88471
C_D	0.02167	0.02189	0.02269	0.02598	0.03149	0.03915	0.04891	0.06067
$C_{L\alpha}$	4.834163	4.834290	4.831187	4.815424	4.787169	4.746778	4.694669	4.631318
$C_{D\alpha}$	0.0126	0.0458	0.0943	0.1578	0.2194	0.2796	0.3369	0.3787
$C_{m\alpha}$	-1.145765	-1.249554	-1.352505	-1.555760	-1.755259	-1.950733	-2.141921	-2.328571
$C_{L\dot{\alpha}}$	2.029	2.079	2.173	2.338	2.362	2.352	2.320	2.264
$C_{m\dot{\alpha}}$	-7.031	-7.205	-7.531	-8.100	-8.183	-8.150	-8.038	-7.846
C_{Lq}	8.514720	8.390702	8.265679	8.013163	7.758239	7.501997	7.245518	6.989892
C_{mq}	-12.314519	-12.393726	-12.471474	-12.622409	-12.766999	-12.904935	-13.035941	-13.159755
C_{m_u}	-0.0022	-0.0022	-0.0029	-0.0037	-0.0037	-0.0044	-0.0044	-0.0044
$C_{L_{\delta e}}$	0.327088	0.327442	0.327581	0.327240	0.326127	0.324309	0.321855	0.318835
$C_{m_{\delta e}}$	-1.196540	-1.199285	-1.201406	-1.203766	-1.203600	-1.200901	-1.195674	-1.187935
C_{y_β}	-0.133883	-0.134441	-0.134954	-0.135849	-0.136568	-0.137110	-0.137475	-0.137662
$C_{l\beta}$	-0.010137	-0.018093	-0.026004	-0.041654	-0.057016	-0.072018	-0.086591	-0.100670
$C_{n\beta}$	0.058687	0.059027	0.059640	0.061673	0.064766	0.068891	0.074019	0.080113
C_{yp}	-0.037260	-0.016614	0.004030	0.045214	0.086089	0.126453	0.166110	0.204864
C_{lp}	-0.526421	-0.525837	-0.524918	-0.522088	-0.517963	-0.512584	-0.505998	-0.498260
C_{np}	0.013589	0.006162	-0.001277	-0.016216	-0.031279	-0.046513	-0.061962	-0.077662
C_{yr}	0.142212	0.143816	0.144686	0.144230	0.140864	0.134625	0.125561	0.113735
C_{lr}	0.021880	0.042146	0.062320	0.102338	0.141820	0.180656	0.218740	0.255973

AOA	-2.0	-1.0	0.0	2.0	4.0	6.0	8.0	10.0
C_{nr}	-0.075654	-0.076741	-0.077970	-0.080844	-0.084245	-0.088133	-0.092463	-0.097184
$C_{l\delta a}$	-0.349626	-0.349649	-0.349459	-0.348441	-0.346577	-0.343876	-0.340352	-0.336020
$C_{n\delta a}$	0.001709	-0.000063	-0.001833	-0.005354	-0.008837	-0.012266	-0.015624	-0.018894
$C_{y\delta r}$	-0.092805	-0.093046	-0.093221	-0.093371	-0.093257	-0.092880	-0.092243	-0.091348
$C_{l\delta r}$	-0.013793	-0.013739	-0.013676	-0.013518	-0.013322	-0.013089	-0.012819	-0.012515
$C_{n\delta r}$	0.056215	0.056373	0.056490	0.056606	0.056562	0.056360	0.056000	0.055485

Flight condition: sea level (30m/s)

AOA	-2.0	-1.0	0.0	2.0	4.0	6.0	8.0	10.0
δ_e	0.35153	-0.64780	-1.72980	-4.14158	-6.88504	-9.96405	-13.38516	-17.15772
C_L	-0.01531	0.06342	0.14165	0.29640	0.44855	0.59769	0.74346	0.88547
C_D	0.02167	0.02189	0.02269	0.02599	0.03150	0.03918	0.04895	0.06074
$C_{L\alpha}$	4.837944	4.838070	4.834963	4.819181	4.790892	4.750450	4.698277	4.634846
$C_{D\alpha}$	0.0126	0.0458	0.0945	0.1578	0.2200	0.2799	0.3378	0.3793
$C_{m\alpha}$	-1.145688	-1.249539	-1.352552	-1.555931	-1.755554	-1.951152	-2.142464	-2.329237
$C_{L\dot{\alpha}}$	2.035	2.086	2.181	2.342	2.363	2.353	2.321	2.266
$C_{m\dot{\alpha}}$	-7.053	-7.229	-7.558	-8.116	-8.190	-8.155	-8.044	-7.851
C_{Lq}	8.519737	8.395617	8.270488	8.017752	7.762602	7.506127	7.249413	6.993549
C_{mq}	-12.318055	-12.397272	-12.475027	-12.625987	-12.770601	-12.908569	-13.039606	-13.163457
C_{m_u}	-0.0018	-0.0026	-0.0026	-0.0035	-0.0035	-0.0035	-0.0044	-0.0044
$C_{L_{\delta e}}$	0.327211	0.327566	0.327704	0.327363	0.326250	0.324431	0.321976	0.318955

AOA	-2.0	-1.0	0.0	2.0	4.0	6.0	8.0	10.0
$C_{m_{\delta e}}$	-1.197093	-1.199839	-1.201960	-1.204320	-1.204153	-1.201452	-1.196222	-1.188478
C_{y_β}	-0.133893	-0.134451	-0.134965	-0.135861	-0.136580	-0.137122	-0.137488	-0.137676
$C_{l\beta}$	-0.010130	-0.018094	-0.026013	-0.041678	-0.057055	-0.072072	-0.086660	-0.100753
$C_{n\beta}$	0.058691	0.059031	0.059644	0.061679	0.064773	0.068902	0.074034	0.080134
C_{yp}	-0.037267	-0.016606	0.004055	0.045270	0.086176	0.126572	0.166259	0.205043
C_{lp}	-0.526698	-0.526113	-0.525194	-0.522362	-0.518235	-0.512851	-0.506259	-0.498515
C_{np}	0.013587	0.006158	-0.001283	-0.016226	-0.031293	-0.046532	-0.061985	-0.077690
C_{yr}	0.142227	0.143832	0.144702	0.144245	0.140876	0.134631	0.125559	0.113722
C_{lr}	0.021884	0.042164	0.062353	0.102399	0.141909	0.180773	0.218884	0.256144
C_{nr}	-0.075662	-0.076749	-0.077979	-0.080854	-0.084258	-0.088150	-0.092485	-0.097211
$C_{l\delta a}$	-0.349867	-0.349890	-0.349700	-0.348681	-0.346816	-0.344113	-0.340586	-0.336252
$C_{n\delta a}$	0.001712	-0.000061	-0.001830	-0.005351	-0.008834	-0.012262	-0.015620	-0.018889
$C_{y\delta r}$	-0.092833	-0.093074	-0.093248	-0.093399	-0.093284	-0.092907	-0.092269	-0.091374
$C_{l\delta r}$	-0.013798	-0.013744	-0.013680	-0.013522	-0.013326	-0.013093	-0.012823	-0.012519
$C_{n\delta r}$	0.056234	0.056391	0.056509	0.056624	0.056580	0.056377	0.056017	0.055502

Flight condition: sea level (120km/h，33.33m/s)

AOA	-2.0	-1.0	0.0	2.0	4.0	6.0	8.0	10.0
δ_e	0.34996	-0.64898	-1.73060	-4.14166	-6.88445	-9.96282	-13.38335	-17.15536
C_L	-0.01532	0.06347	0.14175	0.29660	0.44884	0.59809	0.74395	0.88605
C_D	0.02167	0.02189	0.02269	0.02599	0.03152	0.03921	0.04899	0.06079

AOA	-2.0	-1.0	0.0	2.0	4.0	6.0	8.0	10.0
$C_{L\alpha}$	4.840854	4.840981	4.837871	4.822074	4.793757	4.753278	4.701055	4.637563
$C_{D\alpha}$	0.0126	0.0458	0.0945	0.1584	0.2203	0.2802	0.3380	0.3799
$C_{m\alpha}$	-1.145628	-1.249527	-1.352587	-1.556062	-1.755780	-1.951473	-2.142880	-2.329748
$C_{L\dot{\alpha}}$	2.039	2.090	2.186	2.345	2.365	2.355	2.322	2.267
$C_{m\dot{\alpha}}$	-7.066	-7.244	-7.574	-8.126	-8.194	-8.159	-8.047	-7.855
C_{Lq}	8.523602	8.399400	8.274190	8.021285	7.765963	7.509308	7.252413	6.996364
C_{mq}	-12.320779	-12.400001	-12.477763	-12.628736	-12.773371	-12.911357	-13.042416	-13.166294
C_{m_u}	-0.0020	-0.0020	-0.0020	-0.0029	-0.0029	-0.0039	-0.0039	-0.0049
$C_{L_{\delta e}}$	0.327307	0.327662	0.327800	0.327459	0.326346	0.324526	0.322070	0.319048
$C_{m_{\delta e}}$	-1.197520	-1.200265	-1.202387	-1.204746	-1.204578	-1.201875	-1.196643	-1.188896
C_{y_β}	-0.133901	-0.134459	-0.134973	-0.135869	-0.136589	-0.137132	-0.137498	-0.137686
$C_{l\beta}$	-0.010125	-0.018094	-0.026019	-0.041697	-0.057085	-0.072114	-0.086713	-0.100818
$C_{n\beta}$	0.058694	0.059034	0.059647	0.061683	0.064779	0.068910	0.074046	0.080149
C_{yp}	-0.037273	-0.016599	0.004074	0.045314	0.086244	0.126663	0.166374	0.205181
C_{lp}	-0.526910	-0.526326	-0.525407	-0.522574	-0.518444	-0.513057	-0.506461	-0.498711
C_{np}	0.013585	0.006155	-0.001288	-0.016234	-0.031304	-0.046546	-0.062003	-0.077712
C_{yr}	0.142239	0.143845	0.144715	0.144256	0.140885	0.134635	0.125557	0.113713
C_{lr}	0.021888	0.042179	0.062378	0.102447	0.141978	0.180863	0.218995	0.256275
C_{nr}	-0.075668	-0.076755	-0.077985	-0.080862	-0.084268	-0.088163	-0.092502	-0.097233
$C_{l\delta a}$	-0.350052	-0.350075	-0.349885	-0.348865	-0.346999	-0.344295	-0.340766	-0.336429
$C_{n\delta a}$	0.001713	-0.000059	-0.001828	-0.005349	-0.008831	-0.012260	-0.015617	-0.018886

AOA	-2.0	-1.0	0.0	2.0	4.0	6.0	8.0	10.0
$C_{y\delta r}$	-0.092854	-0.093095	-0.093269	-0.093420	-0.093305	-0.092927	-0.092289	-0.091393
$C_{l\delta r}$	-0.013801	-0.013747	-0.013683	-0.013525	-0.013329	-0.013096	-0.012826	-0.012521
$C_{n\delta r}$	0.056248	0.056405	0.056523	0.056638	0.056594	0.056391	0.056030	0.055515

Appendix C Matlab programs

C.1 Trim condition calculation (15m/s)

```
%data from AVL & Datcom
%sea level,0.098 Mach
alphaset=[ -2.0 -1.0    0.0 2.0 4.0 6.0 8.0 10.0];
CL_out=[-0.01529 0.06328 0.14135 0.29578 0.44760 0.59644 0.74190 0.88361];
CD_out=[0.02167 0.02189 0.02269 0.02597 0.03146 0.03911 0.04884 0.06058];
CLa_out=[4.828680  4.828806  4.825709  4.809975  4.781771  4.741454  4.689438
4.626200];
CDa_out=[0.0126 0.0458 0.0940 0.1573 0.2192 0.2787 0.3363 0.3782];
Cma_out=[-1.145873  -1.249572  -1.352434  -1.555510  -1.754829  -1.950125  -
2.141135 -2.327606];
CLadot_out=[2.014 2.062 2.154 2.326 2.359 2.35 2.318 2.263];
Cmadot_out=[-6.978 -7.146 -7.465 -8.06 -8.176 -8.143 -8.032 -7.841];
CLq_out=[8.507438  8.383569  8.258701  8.006501  7.751908  7.496001  7.239868
6.984593];
Cmq_out=[-12.309361 -12.388563 -12.466298 -12.617212 -12.761776 -12.899679 -
13.030644 -13.154417];
Cmu_out=[-0.0026 -0.0026 -0.0031 -0.0040 -0.0031 -0.0035 -0.0035 -0.0031];
CLde_out=[0.326908  0.327263  0.327401  0.327060  0.325948  0.324131  0.321678
0.318660];
Cmde_out=[-1.195736  -1.198480  -1.200601  -1.202962  -1.202798  -1.200103  -
1.194880 -1.187147];
CyB_out=[-0.133869  -0.134426  -0.134939  -0.135833  -0.136551  -0.137092  -
0.137456 -0.137643];
ClB_out=[-0.010147  -0.018092  -0.025991  -0.041620  -0.056959  -0.071939  -
```

```
0.086491 -0.100549];
CnB_out=[0.058681  0.059022  0.05963  0.061666  0.064755  0.068876  0.073997
0.080084];
Cyp_out=[-0.037250  -0.016627  0.003995  0.045133  0.085962  0.126281  0.165893
0.204604];
Clp_out=[-0.526020  -0.525436  -0.524517  -0.521689  -0.517569  -0.512196  -
0.505618 -0.497890];
Cnp_out=[0.013593 0.006168 -0.001268 -0.016201 -0.031258 -0.046486 -0.061928
-0.077621];
Cyr_out=[0.142189  0.143792  0.144662  0.144208  0.140847  0.134616  0.125564
0.113752];
Clr_out=[0.021874 0.042119 0.062272 0.102249 0.141690 0.180486 0.218531
0.255726];
Cnr_out=[-0.075643  -0.076730  -0.077958  -0.080829  -0.084226  -0.088108  -
0.092432 -0.097144];
Clda_out=[-0.349277  -0.349300  -0.349111  -0.348094  -0.346232  -0.343533  -
0.340012 -0.335685];
Cnda_out=[0.001706  -0.000067  -0.001836  -0.005358  -0.008842  -0.012272  -
0.015630 -0.018900];
Cydr_out=[-0.092765  -0.093006  -0.093181  -0.093331  -0.093218  -0.092842  -
0.092205 -0.091311];
Cldr_out=[-0.013787  -0.013733  -0.013670  -0.013512  -0.013316  -0.013083  -
0.012813 -0.012509];
Cndr_out=[0.056189  0.056346  0.056464  0.056579  0.056536  0.056334  0.055974
0.055460];

%Wing area
S=0.816894;%m2
m=7.62; %kg
g=9.81; %m/s^2
G=m*g; %N
%G:gravity
%sea level
rou=1.2250;%air desity
a=340;%m/s speed of sound
M=0.0441;
```

```
u_0=M*a;
Q=0.5*rou*u_0*u_0;
QS=Q*S;
cbar=0.3491;

%Trim condition calculation
Iy=0.6335;%kg.m2
thrustang=0;%deg
L=G;% first hypothesis
CL=L/QS;
alp=spline(CL_out,alphaset,CL); %deg
CD=spline(alphaset,CD_out,alp);
D=CD*QS;

P=-L*sin(alp/180*pi)+D*cos(alp/180*pi)+G*sin(alp/180*pi);
Z=G*cos(alp/180*pi)-L*cos(alp/180*pi)-D*sin(alp/180*pi)-
P*sin(thrustang/180*pi);

while abs(Z)>=0.005
    if alp<1
        L=L+0.01;
    else
        L=L-0.01;
    end
    CL=L/QS;
    alp=spline(CL_out,alphaset,CL); %deg
    CD=spline(alphaset,CD_out,alp);
    D=CD*QS;
    P=-L*sin(alp/180*pi)+D*cos(alp/180*pi)+G*sin(alp/180*pi);
    Z=G*cos(alp/180*pi)-L*cos(alp/180*pi)-D*sin(alp/180*pi)-
P*sin(thrustang/180*pi);
end

%Aerodynamic coefficent of Cruise condition
C_L=spline(alphaset,CL_out,alp);
C_D=spline(alphaset,CD_out,alp);
```

```
C_La=spline(alphaset,CLa_out,alp);
C_Da=spline(alphaset,CDa_out,alp);
C_ma=spline(alphaset,Cma_out,alp);

C_Ladot=spline(alphaset,CLadot_out,alp);
C_madot=spline(alphaset,Cmadot_out,alp);

C_Lq=spline(alphaset,CLq_out,alp);
C_mq=spline(alphaset,Cmq_out,alp);
C_mu=spline(alphaset,Cmu_out,alp);

C_Lde=spline(alphaset,CLde_out,alp);
C_mde=spline(alphaset,Cmde_out,alp);

C_yB=spline(alphaset,CyB_out,alp);
C_lB=spline(alphaset,ClB_out,alp);
C_nB=spline(alphaset,CnB_out,alp);

C_yp=spline(alphaset,Cyp_out,alp);
C_lp=spline(alphaset,Clp_out,alp);
C_np=spline(alphaset,Cnp_out,alp);

C_yr=spline(alphaset,Cyr_out,alp);
C_lr=spline(alphaset,Clr_out,alp);
C_nr=spline(alphaset,Cnr_out,alp);

C_lda=spline(alphaset,Clda_out,alp);
C_nda=spline(alphaset,Cnda_out,alp);

C_ydr=spline(alphaset,Cydr_out,alp);
C_ldr=spline(alphaset,Cldr_out,alp);
C_ndr=spline(alphaset,Cndr_out,alp);
```

C.2 Longitudinal Matrices (15m/s)

```
%Longitudinal state space calculate
%clear
clc
%Piper J-3 cub model Geometry
S=0.816894;
cbar=0.3491;
%Piper J-3 cub model mass
m=7.62;
g=9.81;
G=m*g;
%Piper J-3 cub model inertia
Iy=0.6335;
%**************Flight condition*********
simulationHft=0;
%M=0.0441;%

%standard term
HAft=[0,2500,5000,7500,10000,12500,15000,17500,20000,22500,25000,27500,30000,
32500,35000,37500,40000,42500,45000,47500,50000,52500,55000,57500,60000];
rouA=[2.3769E-3,2.2079E-3,2.0482E-3,1.8975E-3,1.7556E-3,1.6219E-3,1.4963E-
3,1.3781E-3,1.2673E-3,1.1634E-3,1.0663E-3,9.7544E-4,8.9068E-4,8.1169E-
4,7.3820E-4,6.6196E-4,5.8727E-4,5.2103E-4,4.6227E-4,4.1015E-4,3.6391E-
4,3.2290E-4,2.8652E-4,2.5424E-4,2.2561E-4];
soundspeedA=[1116.45,1106.81,1097.10,1087.29,1077.40,1067.43,1057.36,1047.19,
1036.93,1026.57,1016.10,1005.53,994.85,984.05,973.14,968.08,968.08,968.08,968
.08,968.08,968.08,968.08,968.08,968.08,968.08];
%--------------------------------
rou=interp1(HAft,rouA,simulationHft)*14.5939*35.3146667;
a=interp1(HAft,soundspeedA,simulationHft)*0.3048;
%--------------------------------
u_0=M*a;
Q=0.5*rou*u_0.*u_0;
QS=Q*S;
%************************************
%Longitudinal derivatives
X_u=-2*C_D.*QS./(m*u_0);
```

```
X_w=-(C_Da-C_L)*QS./(m*u_0);
X_de=0;
Z_u=-2*C_L*QS./(m*u_0);
Z_w=-(C_La+C_D).*QS./(m*u_0);
Z_wdot=-C_Ladot.*cbar.*QS./(2*u_0.*u_0*m);

Z_q=-C_Lq.*cbar.*QS./(2*m*u_0);
Z_de=-C_Lde*QS/(m);
M_u=C_mu.*QS*cbar./(u_0*Iy);
M_w=C_ma.*QS*cbar./(u_0*Iy);
M_wdot=C_madot.*QS*cbar*cbar./(2*u_0.*u_0*Iy);
M_q=C_mq.*QS*cbar*cbar./(2*u_0*Iy);
M_de=C_mde*QS*cbar/Iy;

X_dp=0.75*m*g/(100*pi/180)
%X_dp=D/m/g;
Z_dp=0;M_dp=0;

%Matrix
a11=X_u;
a12=X_w;
a13=0;
a14=-9.81;
a15=0;
a21=Z_u;
a22=Z_w;
a23=u_0;
a24=0;
a25=-0;
a31=M_u+M_wdot*Z_u;
a32=M_w+M_wdot*Z_w;
a33=M_q+M_wdot*u_0;
a34=0;
a35=0;
a41=0;
a42=0;
```

```
a43=1;
a44=0;
a45=0;
a51=0;
a52=-u_0;
a53=0;
a54=u_0;
a55=0;

b11=X_de;
b12=X_dp
b21=Z_de;
b22=Z_dp;
b31=M_de+M_wdot*Z_de;
b32=M_dp;
b41=0;
b42=0;
b51=0;
b52=0;

A=[a11 a12 a13 a14 0;
a21 a22 a23 a24 0;
a31 a32 a33 a34 0;
a41 a42 a43 a44 0;
0 -1 0 u_0 0];

B=[b11 b12;b21 b22; b31 b32;b41 b42;b52 b52];

C=[eye(5);];
D=[zeros(5,2)]; %last 2 outputs are the controls

Ar=[a22 a23;
    a32 a33;]
Br=[b21;b31];
Cr=[0 1];
Dr=0;
```

```
Gq=tf(ss(Ar,Br,Cr,Dr))
Gth=Gq*tf(1,[1 0])

eig(A)

U = ctrb(A, B);
n = length(A)
rang = rank(U)
if rang == n
display ('Object is controllable');
else
display ('Object is not controllable');
end
```

C.3 Lateral-directional Matrices (15m/s)

```
%Lateral Directional state space calculate
%clear
clc
%Piper J-3 cub model Geometry
S=0.816894;
b=2.34;
cbar=0.3491;

%Piper J-3 cub model mass
m=7.62;%slugs 64582kg
g=9.81;
G=m*g;

%Piper J-3 cub model inertia
Ix=0.5528;
Iy=0.6335;
Iz=1.0783;
%**************Flight condition*********
simulationHft=0;
%M=0.098;
```

```
%Standard term
HAft=[0,2500,5000,7500,10000,12500,15000,17500,20000,22500,25000,27500,30000,
32500,35000,37500,40000,42500,45000,47500,50000,52500,55000,57500,60000];
rouA=[2.3769E-3,2.2079E-3,2.0482E-3,1.8975E-3,1.7556E-3,1.6219E-3,1.4963E-
3,1.3781E-3,1.2673E-3,1.1634E-3,1.0663E-3,9.7544E-4,8.9068E-4,8.1169E-
4,7.3820E-4,6.6196E-4,5.8727E-4,5.2103E-4,4.6227E-4,4.1015E-4,3.6391E-
4,3.2290E-4,2.8652E-4,2.5424E-4,2.2561E-4];
soundspeedA=[1116.45,1106.81,1097.10,1087.29,1077.40,1067.43,1057.36,1047.19,
1036.93,1026.57,1016.10,1005.53,994.85,984.05,973.14,968.08,968.08,968.08,968
.08,968.08,968.08,968.08,968.08,968.08,968.08];
%-------------------------------
rou=interp1(HAft,rouA,simulationHft)*14.5939*35.3146667;
a=interp1(HAft,soundspeedA,simulationHft)*0.3048;
%-------------------------------
u_0=M*a;
Q=0.5*rou*u_0.*u_0;
QS=Q*S;
%************************************
%Lateral Directional derivatives
Y_B=QS.*C_yB/m;
Y_p=QS.*b.*C_yp./(2*m*u_0);
Y_r=QS.*b.*C_yr./(2*m*u_0);
L_B=QS*b.*C_lB/Ix;
L_p=QS*b*b.*C_lp./(2*Ix*u_0);
L_r=QS*b*b.*C_lr./(2*Ix*u_0);
N_B=QS*b.*C_nB./Iz;
N_p=QS*b*b.*C_np./(2*Iz*u_0);
N_r=QS*b*b.*C_nr./(2*Iz*u_0);

L_da=QS*b.*C_lda/Ix;
N_da=QS*b.*C_nda/Iz;

Y_dr=QS.*C_ydr/m;
L_dr=QS*b.*C_ldr/Ix;
N_dr=QS*b*C_ndr/Iz;
```

```
%
a11=Y_B./u_0;
a12=Y_p./u_0;
a13=-(1-Y_r/u_0);
a14=9.81/u_0; %
a21=L_B;
a22=L_p;
a23=L_r;
a24=0;
a31=N_B;
a32=N_p;
a33=N_r;
a34=0;
a41=0;
a42=1;
a43=0;
a44=0;

b11=0;
b12=Y_dr/u_0;
b21=L_da;
b22=L_dr;
b31=N_da;
b32=N_dr;
b41=0;
b42=0;

Alat=[a11 a12 a13 a14 0;
    a21 a22 a23 a24 0;
    a31 a32 a33 a34 0;
    a41 a42 a43 a44 0;
    0 0 1 0 0];
Blat=[b11 b12;
    b21 b22;
    b31 b32;
    b41 b42;
```

```
    0 0;];
eig(Alat)
Clat=eye(5);Dlat=zeros(5,2);

U = ctrb(Alat, Blat);
n = length(Alat)
rang = rank(U)
if rang == n
display ('Object is controllable');
else
display ('Object is not controllable');
end
```